

University of Windsor

Scholarship at UWindor

Electronic Theses and Dissertations

Theses, Dissertations, and Major Papers

2005

Estimation of volumetric flow rate in a square duct: Equal area versus log-Tchebycheff methods.

Changjie Zhou
University of Windsor

Follow this and additional works at: <https://scholar.uwindsor.ca/etd>

Recommended Citation

Zhou, Changjie, "Estimation of volumetric flow rate in a square duct: Equal area versus log-Tchebycheff methods." (2005). *Electronic Theses and Dissertations*. 1961.
<https://scholar.uwindsor.ca/etd/1961>

This online database contains the full-text of PhD dissertations and Masters' theses of University of Windsor students from 1954 forward. These documents are made available for personal study and research purposes only, in accordance with the Canadian Copyright Act and the Creative Commons license—CC BY-NC-ND (Attribution, Non-Commercial, No Derivative Works). Under this license, works must always be attributed to the copyright holder (original author), cannot be used for any commercial purposes, and may not be altered. Any other use would require the permission of the copyright holder. Students may inquire about withdrawing their dissertation and/or thesis from this database. For additional inquiries, please contact the repository administrator via email (scholarship@uwindsor.ca) or by telephone at 519-253-3000ext. 3208.

**Estimation of Volumetric Flow Rate Through a Circular Duct:
Equal Area Versus Log-Tchebycheff Method**

by

Md Ramiz Ahemad

A Thesis

Submitted to the Faculty of Graduate Studies and Research
through the Department of Mechanical, Automotive and Materials Engineering
in Partial Fulfillment of the Requirements for
the Degree of Master of Applied Science at the
University of Windsor

Windsor, Ontario, Canada

2005



Library and
Archives Canada

Bibliothèque et
Archives Canada

Published Heritage
Branch

Direction du
Patrimoine de l'édition

395 Wellington Street
Ottawa ON K1A 0N4
Canada

395, rue Wellington
Ottawa ON K1A 0N4
Canada

Your file *Votre référence*
ISBN: 0-494-09785-X
Our file *Notre référence*
ISBN: 0-494-09785-X

NOTICE:

The author has granted a non-exclusive license allowing Library and Archives Canada to reproduce, publish, archive, preserve, conserve, communicate to the public by telecommunication or on the Internet, loan, distribute and sell theses worldwide, for commercial or non-commercial purposes, in microform, paper, electronic and/or any other formats.

The author retains copyright ownership and moral rights in this thesis. Neither the thesis nor substantial extracts from it may be printed or otherwise reproduced without the author's permission.

AVIS:

L'auteur a accordé une licence non exclusive permettant à la Bibliothèque et Archives Canada de reproduire, publier, archiver, sauvegarder, conserver, transmettre au public par télécommunication ou par l'Internet, prêter, distribuer et vendre des thèses partout dans le monde, à des fins commerciales ou autres, sur support microforme, papier, électronique et/ou autres formats.

L'auteur conserve la propriété du droit d'auteur et des droits moraux qui protègent cette thèse. Ni la thèse ni des extraits substantiels de celle-ci ne doivent être imprimés ou autrement reproduits sans son autorisation.

In compliance with the Canadian Privacy Act some supporting forms may have been removed from this thesis.

Conformément à la loi canadienne sur la protection de la vie privée, quelques formulaires secondaires ont été enlevés de cette thèse.

While these forms may be included in the document page count, their removal does not represent any loss of content from the thesis.

Bien que ces formulaires aient inclus dans la pagination, il n'y aura aucun contenu manquant.


Canada

1027316

Copyright© 2005 Ramiz Ahemad

ABSTRACT

Proper control of airflow through a duct is critical in HVAC application. At present, the airflow rate is typically estimated by means of Equal Area and Log-Tchebycheff methods. Both methods deduce the flow rate based on velocities measured at discrete locations in a cross section; the difference is associated with the rules that prescribe the specific locations. This research aims at making a step towards resolving the existing debate as to which method is preferable for a given situation.

To achieve this, two-dimensional numerical simulations of air at a uniform velocity entering a straight circular duct of $60D$ length were performed over a range of Re from 200 to 54000. It was revealed that in the absence of imperfections that are encountered in a real environment, the Equal Area method estimates the volumetric flow rate better in the laminar flow regime, whereas the Log-Tchebycheff method provides greater accuracy in the turbulent regime. In addition, experiments were conducted for Re of 24400, 54800 and 99400 in a straight circular duct of $32D$ ($D = 0.266$ m) length. A Pitot-static tube and/or a velocity meter were utilized to determine the point velocities. The Equal Area method over-predicted the flow rate by 2 to 4%, whereas the Log-Tchebycheff's values fell within $\pm 1\%$ of the reference flow rate measured by a venturi meter. The experimental results appeared to confirm with simulations that the Log-Tchebycheff method could give more accurate flow rate in the tested turbulent flow regime.

Dedicated to my –

Wife Nusrat

Son Tanjeev Ahmad

and

Tasneem Ahmed

ACKNOWLEDGEMENTS

I would like to give my sincere thanks to my supervisors, Dr. D. Ting and Dr. A. Fartaj, for their excellent supervision, guidance, patience and encouragement throughout this research work. I would also like to thank Dr. Hu and Dr. Chen for participating on my thesis committee.

I would also like to give special thanks to Mr. P. Seguin and Mr. R. Tattersal for their technical assistance throughout this project. The impressive work conducted by the Technical support center at the University is also greatly valued.

The author gratefully thank to Ms. R. Gignac for providing very pleasant secretarial assistance throughout his studentship with the Department of Mechanical, Automotive, and Materials Engineering. The secretarial supports in regards to the graduate assistantship provided by Ms. B. Denomey are also appreciated acknowledged.

In addition to the support at the University I am eternally grateful to my family and friends for their encouragement and support. I'm forever grateful to my family for instilling the values of hard work and dedication and giving me every opportunity in life.

The financial assistance provided by the University of Windsor in the form of Graduate Assistantship is highly acknowledged. The author is very grateful to ASHRAE (American Society of Heating Ventilation and Air Condition Engineers) for supporting with a Grant-in-Aid scholarship. The financial supports from the Natural Sciences and Engineering Research Council of Canada (NSERC), the Canadian Associated Air Balance Council, the American Society of Heating Ventilation and Air Condition Engineers are gratefully acknowledged.

TABLE OF CONTENTS

ABSTRACT	iv
DEDICATION	v
ACKNOWLEDGEMENTS	vi
LIST OF FIGURES	xi
LIST OF TABLES	xv
NOMENCLATURE	xvi
CHAPTERS	
CHAPTER 1 INTRODUCTION	1
1.1 Motivation	2
1.2 Objectives	4
1.3 Thesis Outline	4
CHAPTER 2 LITERATURE REVIEW	5
2.1 Volumetric flow measurement techniques	6
2.2 Estimating the volumetric flow rate through a duct	9
CHAPTER 3 THE SIMULATION OF DUCT FLOW	12
3.1 Governing equations	13
3.2 Boundary conditions	14
3.3 Numerical methods	17
3.4 Numerical validation	21
CHAPTER 4 EXPERIMENTAL SET-UP AND PROCEDURE	26
4.1 Duct-blower and venturi meter assembly	27
4.1.1 Selection of venturi meter	29

4.1.2	Volumetric airflow rate using venturi meter	30
4.2	The measuring instrument for point velocity	33
4.3	Specifying the velocity measurement points	37
4.4	Experimental methods and procedures	39
4.5	Measurement and data collections	41
4.5.1	Measurement of approach air velocity upstream of the venturi meter	41
4.5.2	Reference flow rate deduced using the venturi meter	42
4.5.3	Flow rate estimation using Equal Area and Log- Tchebycheff methods	43
CHAPTER 5 RESULTS AND DISCUSSIONS		45
5.1	Numerical results	45
5.1.1	Flow development	45
5.1.2	U_{max}/U_{mean} at fully developed zone	48
5.1.3	Axial velocity distribution at outlet	50
5.1.4	Friction Coefficient	54
5.1.5	Effect of locations on accuracies of Equal Area and Log-Tchebycheff methods	55
5.1.6	Effect of number of measurement points	61
5.2	Experimental results	64
5.2.1	Flow profile	65

5.2.2	Accuracy of Equal Area and Log-Tchebycheff methods on mean velocity deduction	68
5.2.3	Accuracy of Equal Area and Log-Tchebycheff methods on airflow rate calculation.	76 78
5.3	Comparison of numerical results with experimental results	
CHAPTER 6 CONCLUSIONS AND RECOMMENDATIONS		83
6.1	Conclusions	84
6.2	Recommendations	86
REFERENCES		87
APPENDICES		
APPENDIX A UNCERTAINTY ANALYSIS AND ERROR ESTIMATION		98
A.1	Evaluating uncertainty	98
A.2	Instrumental and measurements uncertainty of independent parameters	101
A.2.1	Uncertainty of diameter (D) of the duct	102
A.2.2	Uncertainty of barometric pressure	103
A.2.3	Uncertainty of atmospheric temperature	104
A.2.4	Uncertainty of Δh along venturi meter	105
A.2.5	Uncertainty of point velocity using velocity meter.	107
A.3	Uncertainties of the thermo-physical property of fluid	108
A.4	Propagation of uncertainty from independent to dependent parameters.	109
A.4.1	Uncertainty in the area of the duct	110

A.4.2	Uncertainty associated with gravitational acceleration (g).	111
A.4.3	Uncertainty of Δp	111
A.4.4	Uncertainty of p_{sat}	112
A.4.5	Uncertainty of p_{par}	112
A.4.6	Uncertainty of ρ	113
A.4.7	Uncertainty in the volumetric flow rate using venturi meter	114
A.4.8	Uncertainty of Re	115
A.4.9	Uncertainty of U_{mean}	116
A.4.10	Uncertainty of μ	116
A.4.11	Uncertainty of measurement locations	117
A.4.12	Uncertainty of the point velocity	118
A.4.12.1	Uncertainty associated with velocity meter	118
A.4.12.2	Uncertainty associated with manometer	120
A.4.13	Uncertainties of Q_{EQ} and Q_{LT}	121
APPENDIX B	CALIBRATION OF A HOT WIRE PROBE	123
B.1	Calibration principle	124
B.2	Components of auto calibration	125
B.3	Auto calibration procedure	126
APPENDIX C	STANDARD κ - ϵ MODEL	130
APPENDIX D	COPYRIGHT RELEASES	133
VITA AUCTORS		136

LIST OF FIGURES

Figures	Descriptions	Page No.
3.1	Schematic diagram of the flow geometry.	12
3.2	A sketch of the boundary conditions for computational domain.	16
3.3	Subdivisions of the near-wall region.	19
3.4	A sample mesh of 600 grid points along the duct axis and 40 grid points along the duct radius.	22
3.5	The effect of mesh on the axial (streamwise) velocity along the duct axis (a) Laminar flow at $Re = 500$; (b) Turbulent flow at $Re = 5300$.	23
3.6	The effect of mesh on axial velocity across the duct radius at $x/D = 60$ (a) Laminar flow at $Re = 500$; (b) Turbulent flow at $Re = 5300$.	25
4.1	A schematic of the experimental apparatus.	26
4.2	Schematic of the duct with measuring grid (drawing not in scale).	28
4.3	Comparison of the pressure loss in a venturi meter with respect to other head devices.	29
4.4	Schematic of a venturi meter of model 2300.	30
4.5	Schematic of velocity meter connected in duct for measurement.	35
4.6	Schematic of the manometer connected with Pitot-static tube.	35
4.7	Pitot-static tube with stem diameter $D_p = 2.38$ mm (drawing not in scale).	36

4.8	Sample measurement points (six points per diameter) for circular duct flow. Circles (O) for the Equal Area method and pluses (+) for the Log-Tchebycheff method.	39
4.9	Schematic of the duct with 14 x 14 measuring grid at upstream of venturi meter (drawing not in scale).	40
5.1	Effect of Re on the axial, centerline velocity development along the duct (a) Laminar flow (b) Turbulent flow.	47
5.2	Comparison of U_{mean}/U_{max} for simulation to theoretical prediction for turbulent flow (Re = 2300 to 20000).	49
5.3	Effect of Re on the axial velocity development along the duct (a) Laminar flow (b) Turbulent flow.	51
5.4	Comparison of mean velocity profiles with available published data.	52
5.5	Effect of location ($x/D = 20, 40$ and 60) on the velocity profile and on the mean velocities via the Equal Area and Log-Tchebycheff methods for (a) Re = 500 (b) Re = 10000.	57
5.6	The influence of flow regime on the velocity profile and on the mean velocities estimated via the Equal Area and Log-Tchebycheff methods at Re = 2300 (a) Laminar flow (b) Turbulent flow.	60
5.7	The effects of measurement points and Re on the accuracies of Equal Area and Log-Tchebycheff methods in deducing the mean velocity at $x/D = 60$ (a) Six-point per diameter (b) Eight-point per diameter.	62

5.8	The effect of flow model, number of measurement points and Re on the deviations of U_{EA} and U_{LT} from U_{mean} at $x/D = 60$. (a) Laminar flow; (b) Turbulent flow.	64
5.9	Instantaneous velocity at $1.34D$ upstream of the venturi meter.	66
5.10	Axial mean velocity normalized by the centerline velocity as a function of the distance from one side of the duct	67
5.11	Instantaneous velocity at $4D$ upstream from the exit.	68
5.12	Air velocity contour for $Re = 54800$ using six-point traversing at $4D$ upstream from the exit (a) Equal Area (b) Log-Tchebycheff.	69
5.13	The effect of measurement points on the accuracies of Equal Area and Log-Tchebycheff methods ($Re = 54800$).	70
5.14	Air velocity contour for $Re = 99400$ using six-point traversing at $4D$ upstream from the exit (a) Equal Area (b) Log-Tchebycheff.	71
5.15	Velocity profile using Equal Area and Log-Tchebycheff six-point traversing (a) $Re = 24400$ (b) $Re = 54800$.	73
5.16	Effects of measurement points and Re on the accuracies of Equal Area and Log-Tchebycheff methods (a) Six-point per diameter (b) Eight-point per diameter.	75
5.17	Effects of measurement points and Re on the accuracies of Log-Tchebycheff methods.	76
5.18	Comparison of normalized axial mean velocity as a function of the distance from the center of the duct.	78

5.19	Comparison of numerical simulation at $Re = 20000$ and experimental investigation at $Re = 25000$ (a) Equal Area (b) Log-Tchebycheff.	80
5.20	The comparison of numerical simulation at $Re = 54000$ and experimental investigation at $Re = 54800$ (a) Equal Area (b) Log-Tchebycheff.	81
5.21	Effect of measurement points on the accuracies of Equal Area and Log-Tchebycheff methods for different Re .	82
B.1	Schematic of hot-wire calibration set-up.	123
B.2	Performance curve for calibration before experiment.	128
B.3	Performance curve for calibration after experiment.	129

LIST OF TABLES

Tables	Descriptions	Page No.
4.1	Locations of measurement points for the Equal Area and Log-Tchebycheff methods for circular duct flow.	38
5.1	The fully developed axial velocity along the duct centerline with respect to the mean velocity.	48
5.2	Comparison of the mean flow properties obtained from present numerical simulation with some past findings.	53
5.3	Comparison of simulated friction factors with those in the open literature.	55
5.4	The accuracies of the Equal Area and Log-Tchebycheff methods in deducting the mean velocity at $x/D = 20, 40$ and 60 (six-point per diameter).	58
5.5	The accuracies of the Equal Area and Log-Tchebycheff methods in estimating the volumetric airflow rate at $x/D = 60$.	63
5.6	The accuracies of the Equal Area and Log-Tchebycheff methods in estimating the volumetric airflow rate.	77
A.1	Mean point velocity and precision limit for the Equal Area traversing ($Re = 54800$).	119
A.2	Data for volumetric flow rate measurement with uncertainties.	122

NOMENCLATURE

Letter/Symbol

A	Area [m^2]
AABC	Associated Air Balance Council
ASHRAE	American Society of Heating, Refrigeration & Air Conditioning Engineers
ASME	American Society of Mechanical Engineers
B	Bias error
$B_{\bar{F}}$	Bias error for the parameter F
C_D	Discharge coefficient ($C_D = 0.995$)
C_f	Friction coefficient
C_1, C_2, C_3	Velocity constant
CFD	Computational Fluid Dynamics
C_{μ}	An empirical constant specified in the turbulence model (≈ 0.9)
d	Venturi meter throat diameter [m]
d_{wire}	The diameter of wire (μm)
\bar{D}	Mean diameter of the circular duct
D_{Ci}	Venturi meter inlet diameter [m]
D_p	Pitot-static tube stem diameter [m]
E	Variable to denote the uncertainty
$E_{\bar{F}}$	Overall absolute uncertainty in the measurement of parameter F
f_t	The friction factor for turbulent region
F	A generic variable to denote any parameters used in experiment.
\bar{F}	Mean value of parameter F
g	Gravitational acceleration [m/s^2]

h	The rate of heat loss per unit length of wire [cal/ μm]
H	Altitude [Km]
HVAC	Heating, Ventilation and Air Conditioning
i	Iteration number
I_{turb}	Relative turbulence intensity [%]
K	The thermal conductivity of air [w/m-K]
L	Length of the circular duct [m]
L_e	Entrance length for fully developed flow [m]
L_{ven}	Length of the venturi meter [m]; $L_{ven} = L_{veni} + L_{veno} + T_c$
n	Number of measurement locations
P	Precision error
$P_{\bar{F}}$	Precision error limit of the mean for the parameter F
p	Pressure [kPa]
Q	Volumetric flow rate [m^3/s]
Q_{ven}	Volumetric flow rate across venturi meter [m^3/s]
r	Distance in the radial direction (from the duct center) [m]
R	Gas constant [$R = 287.1 \text{ J/kgK}$]
Re	Reynolds number based mean velocity
Re_C	Reynolds number based on centerline velocity
Re_{τ}	Reynolds number based on wall shear velocity
S	The specific heat at constant volume of air [kJ/kg-K]
SEI	Swiss Electronic Committee
S_F	Standard deviation of parameter F

$S_{\bar{F}}$	Standard deviation of the mean for the parameter F
t	Time [s]
t_d	Distribution function
T	Temperature [$^{\circ}\text{C}$]
u	Velocity, axial component (in the x -direction) [m/s]
u_{τ}	Wall shear velocity [m/s]
U	Velocity in the axial direction [m/s]
U_C	Centerline velocity in the axial direction [m/s]
U_{EA}	Average axial velocity from the Equal Area method [m/s]
U_j	Axial velocity at different locations ($j = 1, 2, 3 \dots n$) [m/s]
U_{LT}	Average axial velocity from the Log-Tchebycheff method [m/s]
U_{max}	Axial velocity at the centerline of the duct at fully developed section [m/s]
U_{mean}	Mean (inlet) axial velocity [m/s]
U_o	Axial velocity at the duct outlet [m/s]
U_{vm}	Point velocity measured by velocity meter [m/s]
v	Velocity, radial component (in the r -direction) [m/s]
V	Anemometer output voltage [v]
w	Degree of freedom
x	Distance in the axial direction [m]
x_{tr}	Horizontal traverse distance from one side to the other side of the duct [m]
y	Distance from the wall of the duct (toward the duct center) [m]
y_{tr}	Vertical distance from one side to the other side of the duct [m]
y^+	Dimensionless sub-layer distance, $\rho u_{\tau} y / \mu$

z Total number of error sources

Greek letters

β Beta ratio, ratio of throat diameter to inlet diameter of venturi meter

ρ Density of the air [kg/m^3]

φ Latitude [$^\circ$]

κ Turbulent kinetic energy [m^2/s^2]

Δh Pressure difference [inch of H_2O]

v_{tur} Turbulent velocity scale [m/s]

ρ_{water} Density of the water [kg/m^3]

∇ Divergence of the velocity field

δ_{ij} Kronecker delta

ε Turbulent dissipation rate [m^2/s^3]

Λ Turbulent length scale [m]

Φ Dependent variable

τ_{ij} Wall shear stress [kPa]

τ_w Wall shear stress [kPa]

μ Viscosity [$\text{N}\cdot\text{s}/\text{m}^2$]

μ_τ Turbulent viscosity [$\text{N}\cdot\text{s}/\text{m}^2$]

Subscripts/Exponents

b Barometric

br Bridge voltage

<i>B</i>	Binormal
<i>c</i>	Calibration
<i>con</i>	Condition voltage
<i>corr</i>	Correction
<i>count</i>	Binary count
<i>dry</i>	Dry bulb
<i>e</i>	A subscript used during hotwire experiment
<i>eff</i>	Effective
<i>EA</i>	Equal Area
<i>LT</i>	Log-Tchebycheff
<i>m</i>	index
<i>N</i>	Normal
<i>par</i>	Partial
<i>static</i>	Static
<i>sat</i>	Saturated
<i>st</i>	Stagnation
<i>total</i>	Total
<i>T</i>	Tangential
<i>throat</i>	Throat of venturi meter
<i>upst</i>	Upstream of venturi meter
<i>v</i>	Dynamic
<i>wet</i>	Wet bulb

CHAPTER 1

INTRODUCTION TO THE ESTIMATION OF VOLUMETRIC FLOW RATE

The Heating, Ventilation and Air Conditioning (HVAC) system is an essential part of human's everyday life and has a major impact on health and economy of our society. The HVAC systems are designed based on heating and cooling load with critical attention on the required airflow pattern in the air distribution system. Consequently, the estimation of the volumetric airflow rates through ducts has been the focus of HVAC engineers for a long time.

Today, most people spend 90 percent of their time indoor [Kosonen and Tan, 2004; Health Canada, 2004; EPA and CPSC, 1995], often in shared spaces. So, indoor air quality is very important. To maintain good indoor air quality, extensive research has been conducted on the optimization of the HVAC system, considering energy conservation [Lu et al., 2005; Chow et al., 2002; Austin, 1993].

Supply and return ducts are designed to be in balance, meaning that the amount of air supplied to a building is the same as the amount returned to the AHU (Air Handler Unit), keeping the pressure inside a building neutral. If either of the ducts (the supply or

return duct) has higher or lower air flow, balance will be disrupted and the pressure through the entire conditioned space can be skewed. In the case of less air supply, a negative pressure is created inside the building. Hence, the outside air, which is hotter in summer and colder in winter, is drawn into the building, so dropping comfort and wasting energy. For the case of higher supply, a positive pressure is created inside the building. So conditioned air escapes the building, and this can cause an enormous waste of energy [Srinivasan, 2005]. In case of hospital, space-to-space pressure unbalance is a violation of health code, causing germs and viruses to spread. Poor indoor climate due to unbalance pressure can create a negative effect on the performance of the occupant [Wyon, 1993; Jaakkola et al., 1989], and even hampers the Gross National Product [Fisk and Rosenfeld, 1997].

It is anticipated that the better estimation of the volumetric airflow rate through a duct, a critical factor in HVAC, can produce a better HVAC system design. An estimation of the velocity profile in the duct system can be very exigent due to the complex duct geometry and non-uniform flow distributions, along with real life disturbances. To ensure proper air distribution, a periodic air balancing is required. So the flow profile followed by volumetric airflow rate estimation through a duct is the main concern of the current study.

1.1 Motivation

In HVAC applications, initial setting and periodic monitoring of the airflow in the duct are necessary to ensure proper amount of fresh air is being supplied to specific areas and to provide optimum conditioned space. The volumetric airflow rate is typically based on a series of velocity readings taken at specific points across a centerline of the cross

section of the air-distributing duct. Accuracy of the volumetric airflow rate estimation depends on the number of measurement points, velocity distribution and shape and size of the duct. In practice, ASHRAE (American Society of Heating, Refrigeration & Air Conditioning Engineers) recommends the use of the Log-Tchebycheff method. However, for ducts of diameter or width less than 46 cm (18 inch), ASHRAE has no preference of the Log-Tchebycheff method over the Equal Area method, presumably due to the loss of physical differentiation (resolution) between consecutive measurement locations [Schwenk, 1997; ASHRAE, 1988]. On the other hand, AABC (Associated Air Balance Council) approves the use of the Equal Area method for all applications irrespective of the size of the duct [AABC, 2002].

The question about which method is more appropriate for a particular application has existed since the introduction of these (and other) methods. In recent years, there has been a re-emergence of interest in resolving this decades-old question. Unfortunately, some of the recent attempts [such as Klaassen and House, 2001; Richardson, 2001; MacFerran, 1999] have been casual, or to use Joseph's term in describing one of these studies [MacFerran, 1999], erroneous [Joseph, 2001]. It is clear that any attempt in resolving the dispute concerning the superiority of one method over the other requires a series of well-thought-out systematic investigations. In this study, a circular duct was chosen to investigate the accuracies of Equal Area and Log-Tchebycheff methods for volumetric flow rate estimation in a relative ideal environment.

1.2 Objective

The objective of this study is to numerically and experimentally evaluate the Equal-Area and Log-Tchebycheff methods for estimating the volumetric flow rate through a circular duct. This has been carried out for the following conditions

- Numerical simulations; $Re = 200$ to 54000 and $L/D = 60$ ($D = 0.2$ m)
- Experimental investigations; $Re = 20000$ to 100000 and $L/D = 35$ ($D = 0.266$ m)

1.3 Thesis outline

A historical review on volumetric flow measurement is documented in Chapter 2. Chapter 3 focuses on the simulation techniques. Chapter 4 presents a description of the experimental set-up and the measurement tools and procedure. In Chapter 5, the numerical results, experimental results and comparison of experimental results with simulations are presented and discussed. The conclusions from this study are summarized in Chapter 6. Furthermore, possible future developments are also proposed.

CHAPTER 2

LITERATURE REVIEW

Flow profiles have been extensively studied in HVAC and other engineering applications [Browne and Dinkelacker, 1995; Eggels et al., 1994; Kim et al., 1987; Laufer, 1954]. The accurate measurement of the flow profile in the duct system can be very challenging due to the complex, non-uniform flow distributions, along with unavoidable disturbances in the actual HVAC systems. An acceptable estimation of the volumetric flow rate depends on the number of measurement points [Ower and Pankhurst, 1977; Salami, 1971], which is in turn determined by the flow pattern [Winternitz and Fischl, 1957; Aichelen, 1947].

Although a number of ways have been designed for estimating the volumetric flow rate, the integration techniques are generally used. The volumetric flow rate (Q), can be calculated by integrating the velocity U over the duct cross-sectional area A [White, 1999], that is,

$$Q = \int_A \vec{U} \cdot d\vec{A} \approx U_{mean} A, \quad (2.1)$$

where the mean velocity (U_{mean}) can be approximated from a finite number of measurement points via

$$U_{mean} = \frac{1}{n} \sum_{j=1}^n U_j. \quad (2.2)$$

Obviously, the accuracy depends on the number of measuring points being used in deducing the volumetric flow rate through a duct [Ower and Pankhurst, 1977; Salami, 1971]. For practical reason, one would like to minimize the number of measurement points with required resolutions and accuracies as per measurement locations. It is therefore necessary to optimize a small number of measurement locations. Nevertheless, the velocity distribution, Reynolds number and roughness factor can be the decisive factor in the selection of the number and location of the measurement points. The following sections deal with the different types of flow measurement techniques evolved chronologically for estimating the volumetric flow rate in a duct.

2.1 Volumetric flow measurement techniques

There are numerous methods for estimating the volumetric flow measurement. However, the graphical integration is one of the accurate techniques for flow measurement according to ASME, SEI [ASME, 1949; SEI, 1947]. In this method numerical data is presented graphically and the flow rate can be determined using planimeter or “counting squares”. The method is slow and each stage of the process of evaluation is a possible source of error.

Another approach is based on equal area elements, in which, to locate the velocity-measurement points the cross section of the duct is divided into zones of equal areas with the specific locations corresponding to the centers of equal-area elements. Many authors have generalized this approach as the Equal Area method, which has different names depending on the shape of the duct. For example, when this approach is applied to a circular duct flow, this Equal Area method has been referred to as the Tangential method.

This is the most widely used method for the determination of the duct flow from velocity traverse measurement [Perry and Green, 1997; ASME, 1983; Ower and Pankhurst, 1977; Winternitz and Fischl, 1957; BSI 1042, 1943]. However, the velocity gradient and boundary effects are not considered in this technique.

Aichelen [1947] devised a simple ‘two-measurement-point’ method for estimating the mean velocity for fully developed circular duct flow. It was estimated that the mean velocity in fully developed circular duct flow occurs at a radius of $0.381D$ [Nikuradse, 1932]. Accordingly, Aichelen specified the traversing locations at $0.119D$ and $0.881D$ from any side of the circular duct at fully developed region. This technique takes minimal time for only two measurements are needed. However, experiments have shown that the mean velocity obtained by this method is overestimated and thus for good accuracy it is not recommended [Ower and Pankhurst, 1977; Winternitz and Fischl, 1957].

Ten years later, Winternitz’s invented an alternate method called the Log Linear method [Winternitz and Fischl, 1957] in which, just like the Equal-Area method, the cross section of the duct is divided into a number of equal-area zone. The traversing location for each zone is, however, based on knowing the measurement locations (traversing points), each of which correspond to the local velocity that is supposed to represent the mean velocity of that zone. In doing so, the Log Linear curve fit attempts to take the velocity gradient and boundary effects into account, the priori is that the velocity profile is known.

In 1966, Coffin devised a method called the “Method of Cubics” [Coffin, 1966]. In this method, a series of cubic curves replaced the actual velocity profile. The curves are

fitted between adjacent pairs of measured velocities, including the known zero velocity at the wall, so that the gradients of successive curves are equal at the common boundaries. Integrating the area under the curve will then give the mean flow velocity for estimating the volumetric flow rate [Ower and Pankhurst, 1977; Kinghorn et al., 1973]. This method involves a significant computational effort [Salami, 1971]; nevertheless, the accuracy is similar to the Log Linear method. The main advantage of the Method of Cubics is that the traversing points for this method do not need to be predetermined, whereas, those are predefined for the Log Linear method. Some of the researchers concluded that the Method of Cubics could be an alternative to the well-established Log Linear method in special cases. For example, when the required points cannot be estimated beforehand and/or is expected to alter significantly within the duct system and when extra computational effort is not a concern [Kinghorn et al., 1973].

A mathematician, Tchebycheff developed a method for duct flow measurement in 1977 by considering the wall law of the internal flow distribution, which is referred as the Log-Tchebycheff method [ISO, 1988; ASHRAE, 1988]. In this method, the cross sectional area of the duct is divided into a number of zones of equal area, with the traversing points at positions which subdivide the zones into two equal-volume flow elements. In such, Log-Tchebycheff method also requires the knowledge of the velocity profile prior to measurements. Note that in this method the overall mean velocity is simply the average of the local (point wise) values, and multiplying this overall mean velocity by the cross sectional area gives the volume flow rate, whereas in the Log Linear method, curve fitting and integration are required to deduce the volume flow rate. Nevertheless, some previous

studies claimed that the flow rates estimated via these two methods are almost the same [ASHRAE, 1988].

2.2 Estimating the volumetric flow rate through a duct

Salami [1971] estimated the errors associated with different types of velocity-area methods of flow measurement in a circular duct/pipe, where the Tangential, Log-Linear, Simpson's Rule and Method of Cubics were used. The point velocity was measured using 6 – 40 traversing points per diameter for each method. The investigated range of Reynolds number was not mentioned in this paper. His findings shows that the measured flow rate using the Log-Linear and the Method of Cubics have less error than that of other methods for the same number of traversing points. The author recommended that the errors could also be reduced gradually by making the measuring grid fine along the circumference of the circular duct across the measuring cross section.

Klassen and House [2001] also investigated the Equal Area and Log-Tchebycheff methods for the rectangular duct flow. A commercial-scale HVAC system was used in this study, in which air is supplied from the air-handling unit to the main supply duct, which later turns into a 90⁰ elbow with turning vanes. They tested the duct flow at 3 different planes; two of them were at 50% and 100% effective duct length from the outlet of the fan respectively and another was at one equivalent duct diameter from the elbow; the effective duct length is defined as a duct length corresponding to a uniform velocity profile, which would be expected 2.5-equivalent duct diameter from the fan outlet. They used 25 measurement points for the Log-Tchebycheff method and 20 measurement points for the Equal Area methods through a 28 by 20 inch airway. The flow rate obtained using both

methods were compared with the flow rate obtained by means of high resolution Equal Area method, where 140 measuring points were used. The calculated relative errors at aforementioned three planes were -0.04% , -2.48% and -1.46% for the Log-Tchebycheff method, and -6.73% , 5.91% and 0.31% for the Equal Area method.

Richardson [2001] studied the accuracy of the traversing methods for the volumetric flow measurement in rectangular duct sizes of 122×30 cm and 61×61 cm respectively, where a flow nozzle measured the reference flow rate. In this investigation 18 and 32 points were used in Equal Area method, whereas 25, 36 and 49 points were used in Log-Tchebycheff method for the duct size of 122×30 cm. For the duct size of 61×61 cm, 18 and 25 points were used in Equal Area and Log-Tchebycheff methods respectively. The experiment was performed at velocity of 5.08, 7.62, 10.16 and 12.7 m/s. The author gave no clear explanations about the measuring plane in the fully developed zone. For the duct size of 122×30 cm, the error increased from 0.25% to 3.95% for the Equal Area method and decreased from -1.25% to 0.5% for the Log-Tchebycheff method as the inlet velocity increases from 5.08 m/s to 12.7 m/s. The author also noticed that the rectangular duct had less error than the square duct and the error decreases due to the increase in measurement points. He also mentioned that the Equal Area method was easier to use.

Lee et al. [2001] investigated the flow distributions in complex duct systems. They predicted the flow distribution at each duct section using different techniques such as the Log-Tchebycheff method, the computational fluid dynamics (CFD) technique and the so-called T-method simulation. The T-method simulation can be defined as a simulation program to estimate the flow rate of a duct by obtaining pressure balancing; see Ref.

[Tsal and Behls, 1990] for details. Lee et al. [2001] observed that the converged solution took only 10s for T-method simulation, whereas it took 52h for CFD technique, but the result from CFD method agreed well with that of Log-Tchebycheff method. They also concluded that the uniformity of the upstream flow is a crucial factor for the better volumetric flow rate estimation.

CHAPTER 3**THE SIMULATION OF DUCT FLOW**

A two-dimensional simulation was performed for airflow through a circular duct of diameter, D and length, L ($60D$) at standard temperature (300 K) and pressure (101.3 kPa) using with the CFD software Fluent; see Figure 3.1. The flow fields were simulated over a range of Reynolds number, Re from 200 to 54000, where the Re is defined as

$$Re = \frac{\rho U_{mean} D}{\mu}, \quad (3.1)$$

where μ is the dynamic viscosity and ρ is the density of the air.

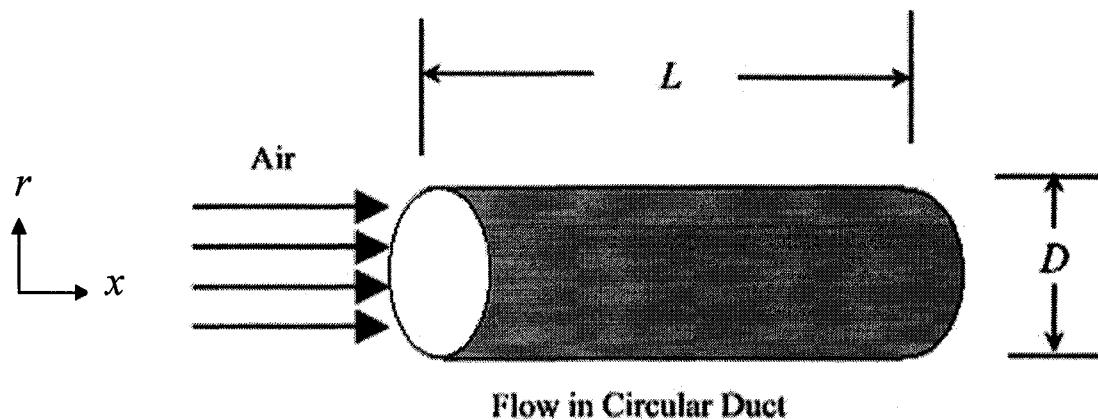


Figure 3.1 Schematic diagram of the flow geometry ($L = 60D$).

3.1 Governing equations

Since the flow investigated in the present study has relatively low Mach number ($M \leq 0.02$), the compressibility effects were neglected and the flow was considered incompressible. Hence, in the case of two-dimensional axisymmetric, steady flow in a cylindrical co-ordinate system, the continuity and momentum equations are

Continuity:

$$\frac{\partial u}{\partial x} + \frac{1}{r} \frac{\partial(rv)}{\partial r} = 0, \quad (3.2)$$

x-momentum:

$$u \frac{\partial u}{\partial x} + v \frac{\partial u}{\partial r} = -\frac{1}{\rho} \frac{\partial p}{\partial x} + \nu \left[\frac{1}{r} \frac{\partial}{\partial r} \left(r \frac{\partial u}{\partial r} \right) + \frac{\partial^2 u}{\partial x^2} \right], \quad (3.3)$$

r-momentum:

$$u \frac{\partial v}{\partial x} + v \frac{\partial v}{\partial r} = -\frac{1}{\rho} \frac{\partial p}{\partial r} + \nu \left[\frac{\partial^2 v}{\partial x^2} + \frac{1}{r} \frac{\partial}{\partial r} \left(r \frac{\partial v}{\partial r} \right) - \frac{v}{r^2} \right], \quad (3.4)$$

where p is the pressure, u is the velocity component in the x-direction, t is the time and v is the velocity component in the r -direction (where r is distance from the centerline/axis of the duct), which shown in Figure 3.1.

In this investigation, the flow for $Re \geq 2300$ are considered as turbulent flow. The continuity and momentum equations for turbulent flow in a cylindrical coordinate system become

Continuity:

$$\frac{\partial u}{\partial x} + \frac{1}{r} \frac{\partial(rv)}{\partial r} = 0, \quad (3.5)$$

Momentum:

$$\rho \left[u \frac{\partial u}{\partial x} + v \frac{\partial u}{\partial r} \right] = -\frac{\partial p}{\partial x} - \rho \left\{ \frac{\partial \overline{u'^2}}{\partial x} + \frac{1}{r} \frac{\partial}{\partial r} (r \overline{u'v'}) \right\} + \mu \nabla^2 u, \quad (3.6)$$

$$\rho \left[u \frac{\partial v}{\partial x} + v \frac{\partial v}{\partial r} \right] = -\frac{\partial p}{\partial r} - \rho \left\{ \frac{\partial \overline{u'v'}}{\partial x} + \frac{1}{r} \frac{\partial}{\partial r} (r \overline{v'^2}) \right\} + \mu \left\{ \nabla^2 v - \frac{v}{r^2} \right\}, \quad (3.7)$$

where u' , v' are the instantaneous velocity components. The divergence of the velocity field in cylindrical co-ordinate is given by

$$\nabla^2 = \frac{\partial^2}{\partial x^2} + \frac{\partial^2}{\partial r^2} + \frac{1}{r} \frac{\partial}{\partial r}. \quad (3.8)$$

The continuity and momentum equations are adequate for solving the laminar flow fields. In case of turbulent flow, however, the determination of the Reynolds stress terms needs extra equations to be solved; see Appendix C. The correlation of the Reynolds stress terms to the mean flow field was defined, such that the turbulent stresses are proportional to the mean velocity gradients [Boussinesq, 1877]. The standard k- ϵ model was used to solve the correlation [Chen, 1995; Launder and Spalding, 1974]; see Appendix C.

3.2 Boundary conditions

The boundary conditions were applied for solving the flow fields from the continuity and Navier-stokes equations in the computational domain. These included the inlet, centerline, wall surface and outlet. With reference to Figure 3.2, the four boundaries of the computational domain were treated as follows

(a) Inlet boundary

The uniform flow entering the duct was parallel to the longitudinal axis (x) of the duct, that is,

$$u = 1 \text{ and } v = 0 \text{ at } x = 0, 0 \leq r < D/2. \quad (3.9)$$

(b) Wall boundary

No slip wall boundary conditions were adopted in the present numerical analysis. Since no fluid crosses the duct wall, we can write

$$u = 0 \text{ and } v = 0 \text{ at } r = D/2, 0 \leq x \leq L. \quad (3.10)$$

(c) Centerline boundary

Symmetry of reflection boundary condition was applied along the centerline of the duct, that is,

$$\frac{\partial u}{\partial r} = 0 \text{ and } v = 0 \text{ at } r = 0, 0 \leq x \leq L. \quad (3.11)$$

(d) Outlet Boundary

The values of the variables at the duct outlet can be extrapolated from the interior cells adjacent to the outlet, while unsteady disturbances were allowed to travel out of the domain [Patankar, 1980]. Hence, the outflow boundary condition was applied at the outlet of the duct. For fully developed flow the velocity gradients in the stream wise (x) direction at the downstream must tend to be zero, that is,

$$\frac{\partial u}{\partial x} = 0 \text{ and } \frac{\partial v}{\partial x} = 0 \text{ at } x = L, 0 \leq r < D/2. \quad (3.12)$$

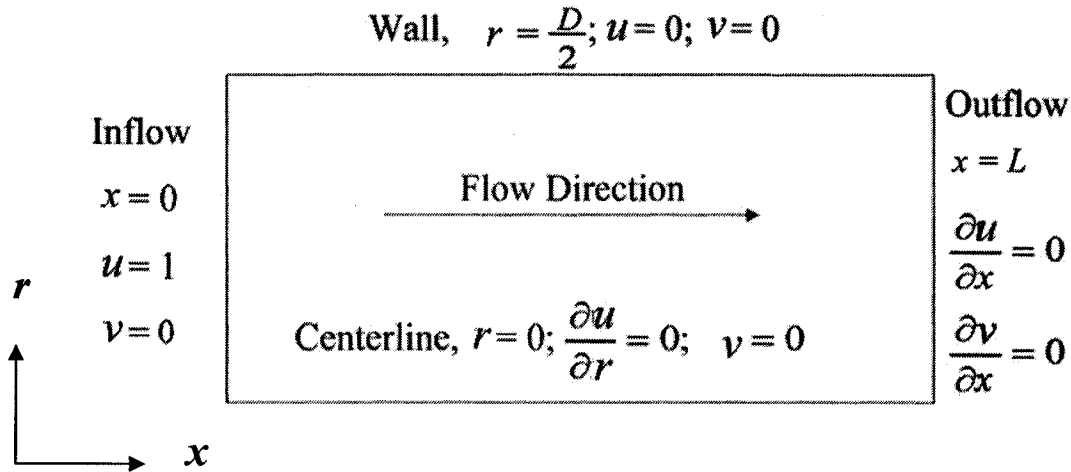


Figure 3.2 A sketch of the boundary conditions for the computational domain.

In case of turbulent flow, the standard κ - ϵ turbulence model was utilized; see Appendix C for κ - ϵ model. Accordingly, the additional inputs required are the relative turbulence intensity (I_{turb}), turbulent length scale (Λ), turbulent kinetic energy (κ), and turbulent dissipation rate (ϵ). The relative turbulence intensity (I_{turb}), is defined as the ratio of the root-mean-square of the velocity fluctuations to the mean flow velocity. Cheremisinoff [1990] recommended that for circular duct flows the turbulence intensity should be between 1 and 10% depending on the Reynolds number (i.e., $I_{turb} = 6\%$ for $Re = 5300$). The relative turbulence intensity values given by Cheremisinoff [1990] are in agreement with those provided by Fluent [2003], where the relative turbulence intensity is deduced as

$$I_{turb} = 0.16(Re)^{-1/8} . \quad (3.13)$$

The turbulent length scale (Λ), is a physical quantity related to the size of eddies that contain the energy in turbulent flows, which can be defined as

$$\Lambda = 0.07D . \quad (3.14)$$

The turbulent kinetic energy (κ), is the kinetic energy per unit mass of the turbulent fluctuations. Turbulent dissipation rate, ε , is defined as the rate of conversion of turbulence into heat by molecular viscosity. They were estimated according to the following relations [Fluent, 2003]

$$\kappa = \sqrt{\frac{3}{2}}(U_{mean}I_{turb})^2 \quad (3.15)$$

and

$$\varepsilon = C_{\mu}^{3/4} \frac{\kappa^{3/2}}{\Lambda}. \quad (3.16)$$

For the inlet and solid walls, kinetic energy and dissipation rate were given according to Equations (3.15) and (3.16). In symmetry axis, they are defined as

$$\frac{\partial \kappa}{\partial n_i} = 0; \quad \frac{\partial \varepsilon}{\partial n_i} = 0, \quad (3.17)$$

where n_i is the local co-ordinate normal to the wall and at free stream both κ and ε were set zero.

3.3 Numerical methods

A total length of $60D$ was chosen to ensure a reasonable length for the flow to become fully developed [Fox and McDonald, 1998; Schlichting, 1960]. With the increase of Reynolds number (i.e., Laminar flow at $Re = 2300$), this $L = 60D$ may become considerably larger than $60D$ as discussed later.

The control volume method was carried out as formulated by Patankar [1980]. In this procedure, the domain is discretized by a series of control volume each containing a

grid point. The differential equations for solving the flow fields are expressed in an integral form over the control volume. It should be pointed out that the exact solution of the differential equations depends on the number of grid points. Although, the higher order schemes (i.e., first-order, second-order, power law etc.) show a less stable solution, the simulation was performed based on second-order variation in each coordinate direction for better accuracy.

In the spatial discretization of viscous terms the simple pressure-velocity coupling as described by Patankar was employed. The computation was started by guessing the pressure field and subsequently, solving the momentum equations to obtain the velocity field. A pressure correction was obtained from the revised continuity equation and the velocity component values were corrected subsequently. After calculation of the coupled flow field variables, the corrected pressure was taken as the new pressure field and the operation was repeated until a converged solution was obtained. Note that the viscous terms were treated by a fully implicit scheme. The residuals of the dependent variables and the invariance of spot-checked values were examined to see if the solution at the end of the iteration had converged. The convergence criterion utilized was

$$\left| \frac{\varphi^{i+1} - \varphi^i}{\varphi^i} \right| \leq 10^{-6} , \quad (3.18)$$

where φ is the dependent variables.

Due to no-slip boundary condition at the wall, different layers are observed from the wall to the outer flow velocity. They can be largely subdivided into three layers; which are

viscous sub-layer, buffer layer and fully turbulent layer. The “viscous sub-layer” is the innermost layer in which viscosity plays a dominant role. The outermost layer called the “fully-turbulent layer” in which turbulent plays a major role. The intermediate region between the viscous sub-layer and fully turbulent layer is called the buffer layer, where Reynolds stresses and viscous stresses are equally important. Figure 3.3 illustrates the different layers, plotted in semi-log coordinates [Fluent, 2003].

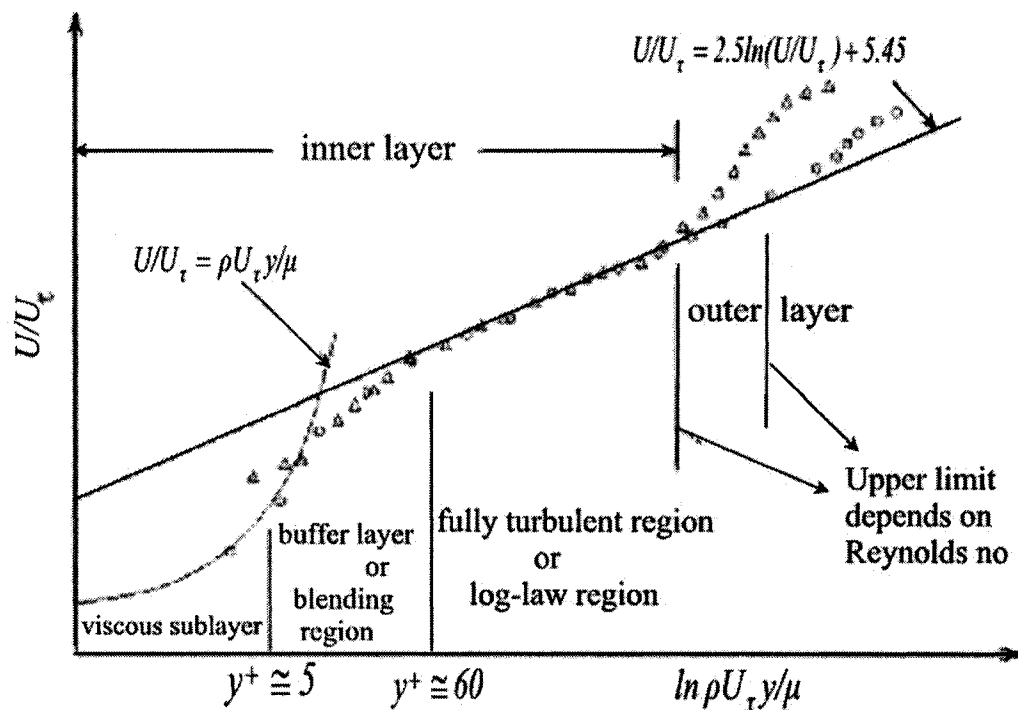


Figure 3.3 Subdivisions of the near-wall region [Fluent, 2003].

The standard κ - ϵ model (see Appendix C); however is only valid for flow regions where turbulent transport is dominating the flow. The flow near-wall region i.e., viscosity-affected region (viscous sub-layer and buffer layer) can be solved with the semi-empirical wall functions, so-called law of the wall [Fluent, 2003; Tennekes and Lumley, 1972]. These

are used to bridge the viscosity-affected region between wall and turbulent dominant region, which also obviated the necessity to modify the turbulence models to account for the presence of the wall. In this investigation, for turbulent flow cases ($2300 < \text{Re} < 20000$), the enhanced wall treatment was applied to extend the validity of near wall modeling beyond the viscous sub-layer; that is, the generated mesh should resolve the viscosity effect of the near wall region as discussed above. The grid points were distributed in a non-uniform manner with denser mesh closer to the wall after computing the dimensionless sub-layer distance, y^+ , which is defined as

$$y^+ \equiv \frac{\rho u \tau y}{\mu}, \quad (3.19)$$

where y is the normal distance from the wall at the cell centers. In Fluent y is interpreted as the distance from the nearest wall

$$y \equiv \left\| \vec{r} - \vec{r}_w \right\|, \quad (3.20)$$

where \vec{r} is the position vector at the field point and \vec{r}_w is the position vector on the wall boundary. The recommended y^+ value is no more than 4 or 5 [Fluent, 2003]. Experimentally observed the viscous sub layer up to the range of $y^+ = 4$ or 5, in which the Reynolds stresses remain small. The Reynolds stresses dominate the internal sub-layer [Versteeg and Malalasekera, 1995]. The relaxation factors for pressure, density, momentum, and turbulent quantities were readjusted during the iterative calculation process to avoid divergence in the simulations.

In short, the laminar model was used for the laminar cases ($200 < Re < 2300$), while the turbulent model was invoked when the flow is turbulent ($2300 < Re < 20000$). Both laminar and turbulent models were utilized for the $Re = 2300$ case.

3.4 Numerical validation

Preliminary validation was accomplished by checking the density of the mesh and then the simulated profiles were compared with analytical velocity profiles. A two-dimensional mesh was used to simulate the flow in the circular duct. To assess the potential dependency of the result on the mesh size, different structured meshes of 600×40 (i.e. 600 divisions in the axial direction and 40 divisions in the radial direction), 600×50 , 600×30 , 600×20 , and 600×10 were tested. Accordingly, a sample of 600×40 grid is shown in Figure 3.4. Finer mesh was utilized near the wall to account for the higher gradients of solution variables (velocity and pressure), while coarser mesh was used near the centerline to save computational costs. Further, in case of turbulent flow, the mesh should be constructed to resolve the viscosity effected near-wall region. As discussed earlier, the enhanced wall treatment was used in this study; which requires fine grid along the wall boundary. All simulations relied upon the implicit flow symmetry about the centerline.

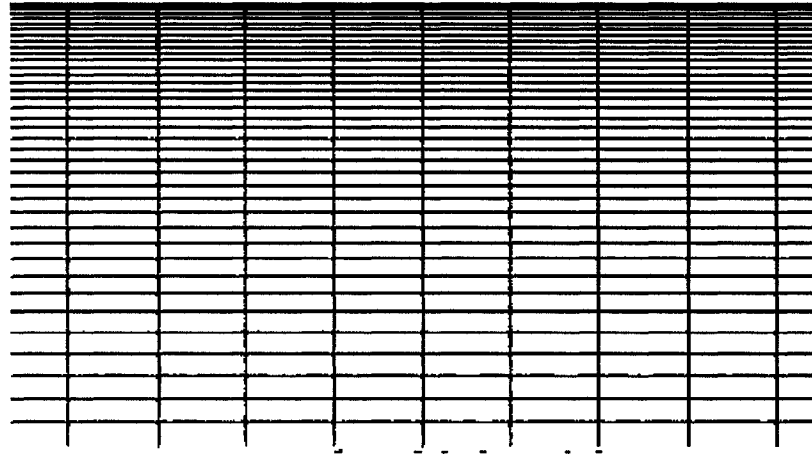


Figure 3.4 A sample mesh of 600 grid points along the duct axis and 40 grid points along the duct radius.

The effects of mesh on the axial velocity along the axis (duct centerline) for a laminar ($Re = 500$) case and a turbulent ($Re = 5300$) case are shown in Figure 3.5, which depicts the variation of normalized centerline velocity (U_C/U_{mean}) along the duct axis (x/L). For the laminar case ($Re = 500$), the fully developed axial velocities along the duct centerline (U_{max}) for the 600×40 and 600×50 meshes are almost identical, $U_{max} = 0.0778$ m/s ($U_{max}/U_{mean} = 2$); see Figure 3.5(a). It is noted that the centerline velocity (U_C) is assumed to be maximum velocity (U_{max}) at fully developed zone. Similarly, the fully developed axial, centerline velocities for the 600×40 and 600×50 meshes are the same i.e., $U_{max} = 0.51$ m/s ($U_{max}/U_{mean} = 1.26$) for the $Re = 5300$ (turbulent) case; see Figure 3.5(b). In other words, the prescribed meshes are sufficiently fine.

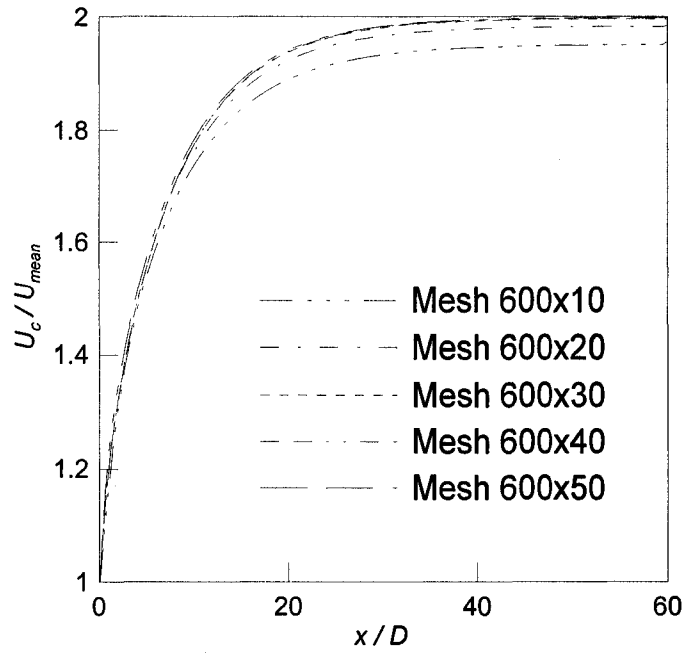
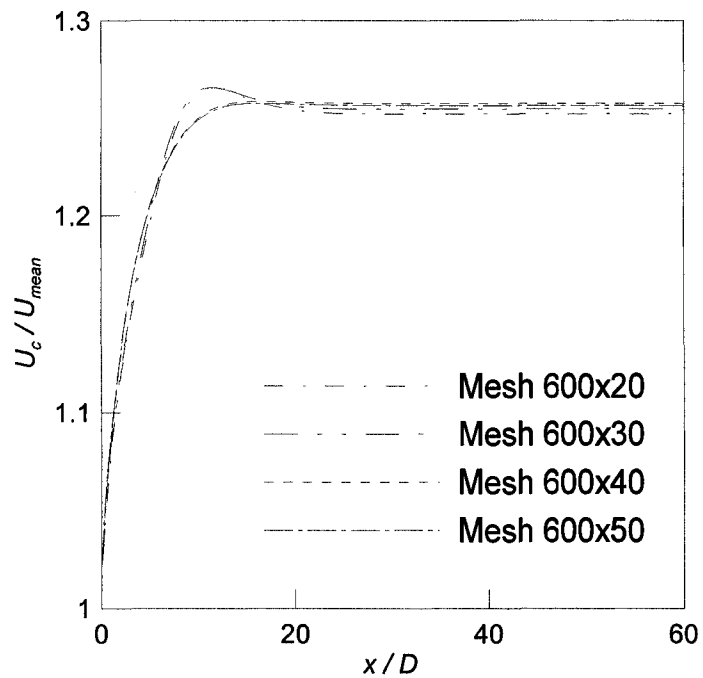
(a) Laminar flow ($Re = 500$)(b) Turbulent flow ($Re = 5300$)

Figure 3.5 Effect of mesh on the axial (streamwise) velocity along the duct axis (a) Laminar flow at $Re = 500$; and (b) Turbulent flow at $Re = 5300$.

The $Re = 500$ simulation as shown in the Figure 3.5(a) agreed well with the theory [Flow Kinetics, 2002] that the maximum axial velocity, which occurs at the duct center when the flow is fully developed, is twice the average velocity, i.e., $U_{max}/U_{mean} = 2$. The corresponding parabolic laminar velocity profile in the radial direction is shown in Figure 3.6(a); so is the flattened velocity profile for the turbulent ($Re = 5300$) case. Note that the velocity profile in the radial direction (Figure 3.6) is less mesh dependent, as compared to the centerline velocity along the duct axis (Figure 3.5). To save computation time while obtaining adequately accurate results, the 600×40 mesh was chosen for all the cases considered in this study.

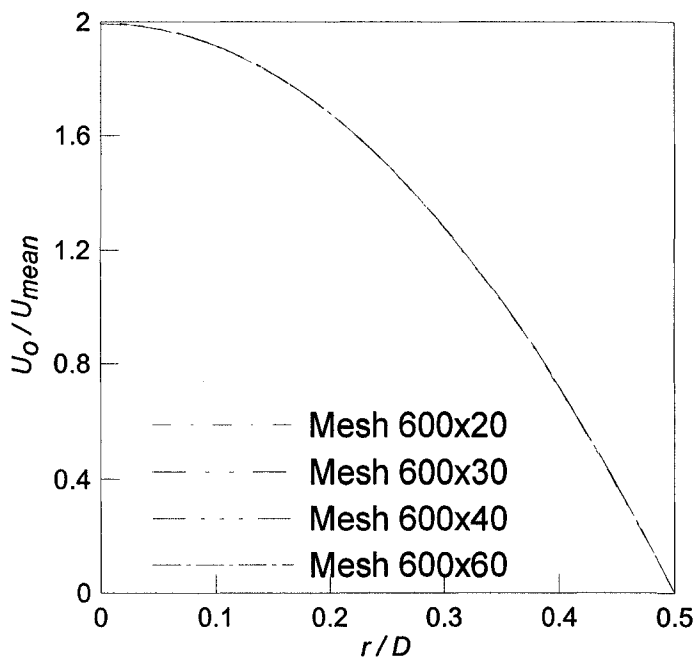
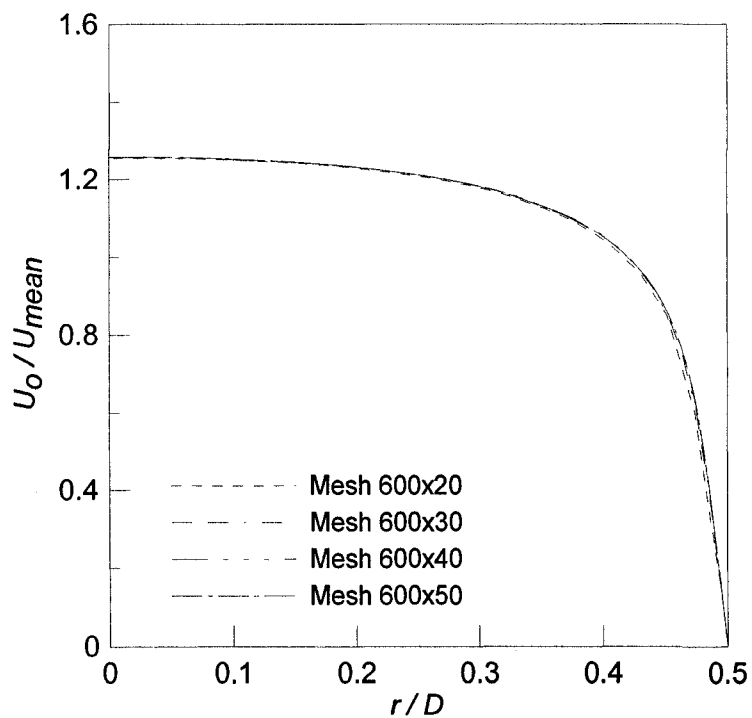
(a) Laminar flow at $Re = 500$ (b) Turbulent flow at $Re = 5300$

Figure 3.6 Effect of mesh on axial velocity across the duct radius at $x/D = 60$ (a) Laminar flow at $Re = 500$; and (b) Turbulent flow at $Re = 5300$.

CHAPTER 4
EXPERIMENTAL SETUP AND PROCEDURE

Figure 4.1 shows an overall picture of the experimental setup. In brief, an invariable speed blower was utilized to blow the air through a circular duct. A venturi meter was used to measure the volumetric flow rate, while a digital air velocity meter was used to get the point velocity for the traversing technique. A secondary check for the measured velocity was realized via the use of a Pitot-static tube connected to a manometer. The temperature and barometric pressure were recorded during the experiment as well. The instantaneous velocity was measured using the constant temperature anemometer system. The details of the experimental setup and procedures are described in following sections.

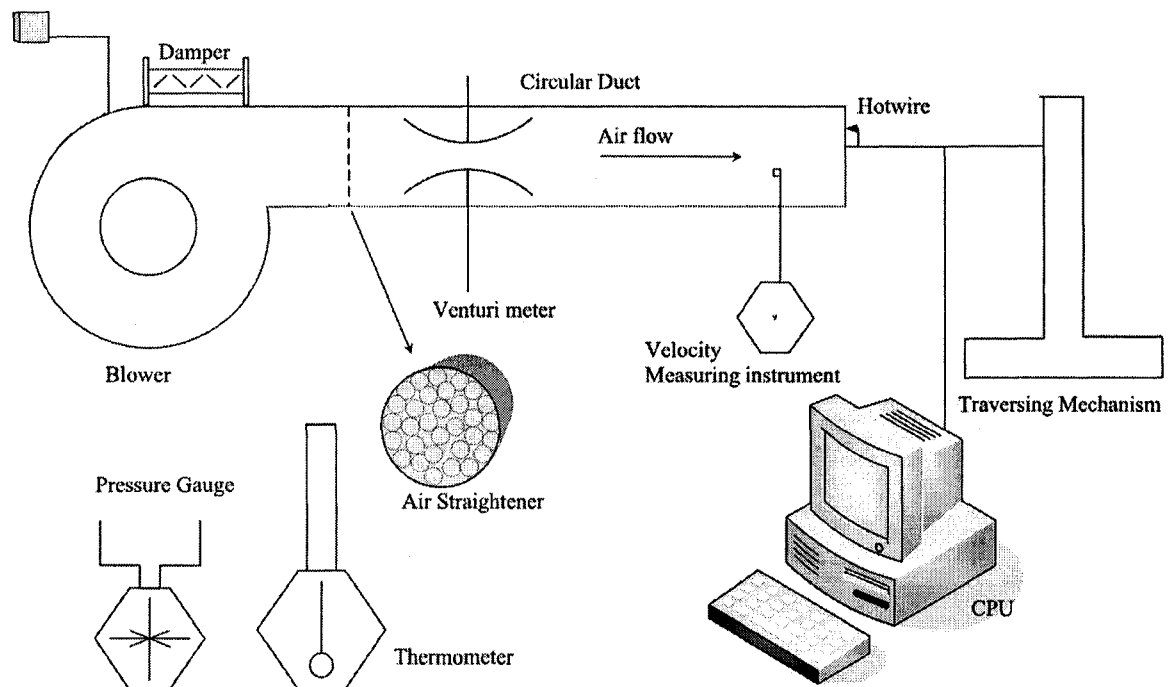


Figure 4.1 A schematic of the experimental apparatus

4.1 Duct-blower and venturi-meter assembly

The experiments were performed for the estimation of the volumetric flow rate through a circular duct using both the Equal Area and Log-Tchebycheff velocity traversing techniques. In the current study, a blower of 5 hp, 1750-rpm was utilized to blow the air through a circular duct. A continuous control gate damper, at the entrance of the blower, was used to control the airflow rate. The uniform velocity was accomplished by filling the circular duct with a bundle of flow straighteners made of plastic tube; these were installed at 50 cm (approximately $2D$) downstream from the blower exit as shown in Figures 4.1 and 4.2. Each piece of flow straightener is 130 mm long with an inner diameter of 18 mm. The geometry of the flow straighteners was chosen to improve the flow uniformity out of the flow straightener. Wire screens were placed at inlet and exit of the flow straightener. The screen acted as a barrier to keep the tubes inside the flow straightener, and also aided in the process of maintaining steady airflow. The combination of small plastic tube and wire screens made the flow steady and uniform [ANSI/ASHRAE, 1999; Akashi, et al., 1978; ASME, 1971].

A venturi-meter of Lambda Square model 2300 (range 0-25 m³/s, accuracy $\pm 0.75\%$ of actual flow, beta ratio (β), defined as the ratio of throat diameter to inlet diameter of the venturi meter is 0.7) was installed at 315 cm ($12D$) after the blower as shown in Figures 4.1 and 4.2; see Ref. [Lambda, 2005] for details of the venturi meter. It is specified that the recommended upstream minimum distance of the venturi meter should be $4.5D$ for minimizing the upstream disturbances [ISO 5167, 2003; ASME, 1971]. In this study, a length of approximately $12D$ from the blower ($10D$ after the flow straightener) was chosen

to ensure a reasonable length to follow the ISO and ASME standard. The flow at the upstream of the venturi meter was tested and the results will be discussed later. The venturi meter is a device in which the flow rate is determined by the pressure drop due to a restriction in a conduit. As fluid passes through the reduced area of the venturi meter (i.e., throat area), its velocity increases, result in a pressure differential between the inlet and throat regions. Again at the downstream, the flow area gradually increases and the fluid velocity decreases, allowing the pressure to recover. This pressure difference between inlet and throat of the venturi meter was measured using a digital manometer of Meriam Instrument model E200I (accuracy of $\pm 0.25\%$ of the reading, resolution 0.01 inch of H_2O , range 0-200 inch of H_2O). The following sub-sections deal with the selection of venturi meter and volumetric flow rate measured by venturi meter.

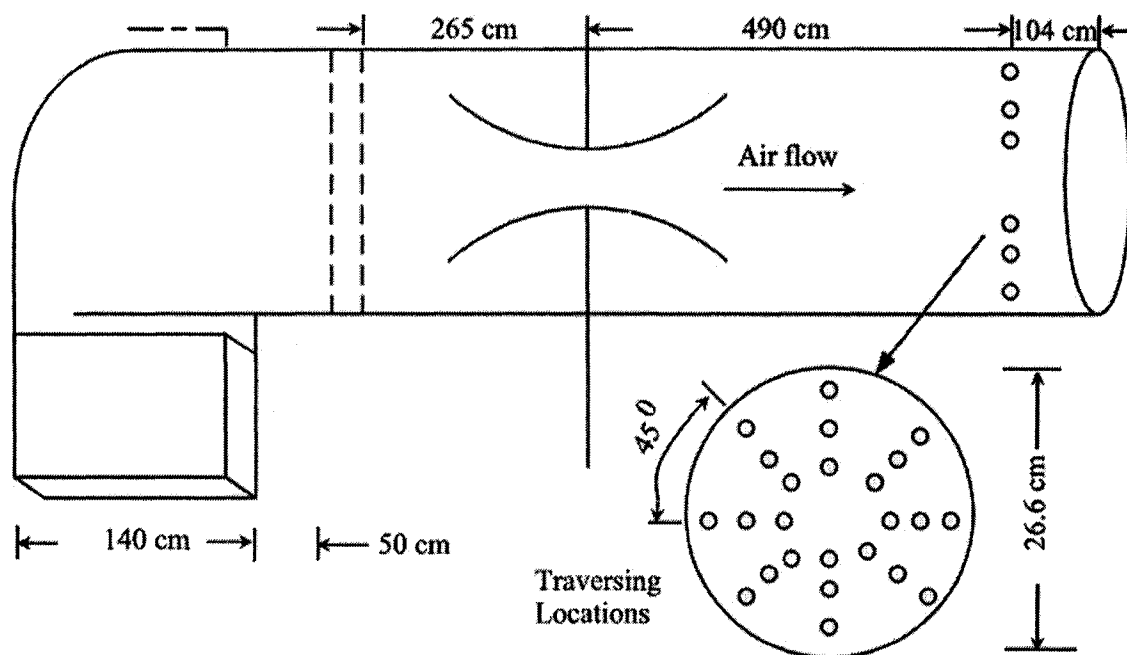


Figure 4.2 Schematic of the duct with measuring grid (drawing not in scale)

4.1.1 Selection of venturi meter

There are numerous types of flow meter available to obtain the flow rate based on pressure differential. The venturi meter, flow nozzles, and orifice meters are the best for this kind of application. The detailed design and performance data of flow meters are summarized in Ref. [Miller, 1983; Chermissionoff, 1979; ASME, 1971]. In this study, the venturi meter was used. In case of venturi meter, there is an appreciable distance between the pressure taps, and a persistent decrease in diameter exerts a significant impact on the differential developed along the venturi meter [Miner, 1956; Hooper, 1950]. The venturi meter is more accurate (accuracy is $\pm 0.75\%$ of actual flow for the installed model 2300), and self-cleaning device. It allows the smooth flow and efficient pressure recovery. Finally, the pressure loss is very low compared with that of other flow meters; the investigated pressure loss for different flow meters is shown in Figure 4.3 [Fox and McDonald, 1998]. The empirical equations for pressure loss calculation are summarized in Ref. [Miller, 1983] for different flow meters.

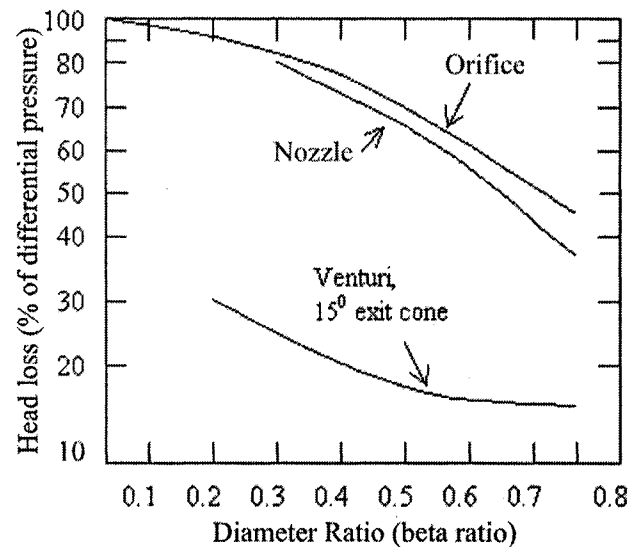


Figure 4.3 Comparison of the pressure loss in a venturi meter with respect to other head devices [after Fox and McDonald, 1998].

The schematic of the venturi meter of model 2300 shown in Figure 4.4, where L_{ven} is the total length, L_{venti} is the upstream length to high pressure tap, L_{veno} is the downstream length after the pressure tap, T_c is the width of the pressure tap, F is the thickness of the venturi meter, d is the throat diameter and D_{Ci} is the inlet diameter.

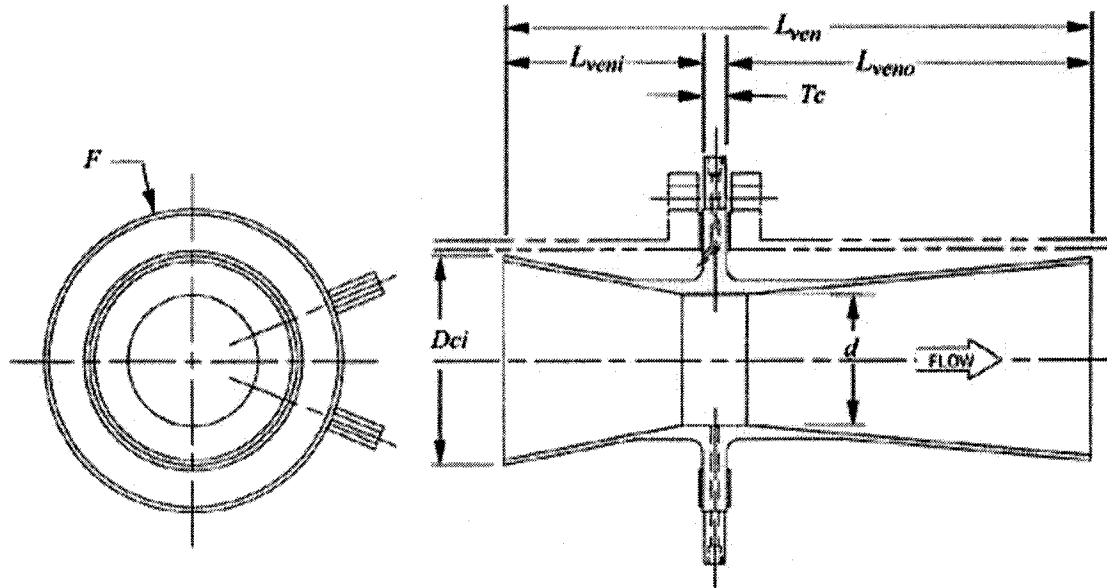


Figure 4.4 Schematic of a venturi meter of model 2300 [Lambda, 2004].

4.1.2 Volumetric airflow rate measurement using the Venturi meter

The volumetric airflow rate through a duct was determined using venturi meter. The underlying principle of the venturi meter is Bernoulli's streamline energy equation. Accordingly, when a flow is contracted, kinetic energy increases at the expense of available potential energy (static pressure). Assume an incompressible fluid, no friction, and a uniform velocity distribution at the inlet and at the throat. By neglecting the small elevation difference, the pressure difference between the taps located at the full circular section and in vicinity of the contraction (Figures 4.4) is related as [White, 1999]

$$\Delta p = \frac{1}{2} \rho_0 (U_{throat}^2 - U_{upst}^2). \quad (4.1)$$

The velocity profiles are assumed to be uniform along the upstream and throat of the venturi meter. Hence, the continuity equation can be deduced as

$$A_{throat} U_{throat} = A_{upst} U_{upst}, \quad (4.2)$$

where A_{throat} is the venturi meter throat area, A_{upst} is the area of the full circular section at the upstream of the venturi meter.

In practical situation, small amount of energy converted into heat within viscous boundary layers tends to lower the actual velocity of real fluids to some extent. Hence, a factor, discharge coefficient (C_D) was introduced to account for the viscosity of fluids. The flow rate can be calculated from Equations (4.1) and (4.2) as

$$Q_{ven} = C_D \frac{A_{throat}}{\sqrt{1-\beta^4}} \sqrt{\frac{2\Delta p}{\rho}}, \quad (4.3)$$

where Δp is the pressure difference between the inlet and throat sections and β (beta ratio) is defined as a ratio of throat diameter to inlet diameter, which is 0.7 for the installed model 2300. It is specified that the discharge coefficient (C_D) is 0.995 for the model 2300 [Lambda, 2005]. The dependent parameters, pressure difference (Δp) can be converted in Pa by applying the following

$$\Delta p = \Delta h \times \rho_{liquid} \times g, \quad (4.4)$$

where Δh is the pressure differential across the venturi meter in inch of water, ρ_{liquid} is the density of the liquid (i.e., water) and g is the gravitational acceleration, which was calculated as

$$g = 9.78 \left(1 + 0.0053 \sin^2 \varphi - 0.0000069 \sin^2 2\varphi \right) - 0.003086H, \quad (4.5)$$

where φ is the latitude in degrees and H is the altitude above sea level in km [Harris, 2005]. For Windsor $\varphi = 42.3$ and $H = 0.19$ km was estimated [Weather underground, 2005]. Since the atmospheric conditions of the test room could be changed every day, the effects of temperature and moisture need to be considered in flow measurement. To account the variations of atmospheric conditions, the density of the atmospheric air (ρ) was calculated as (ANSI/ASHRAE, 1999)

$$\rho = \frac{(p_b - 0.378 \times p_{par})}{R(T_{dry} + 273.15)}, \quad (4.6)$$

where R is the gas constant taken as 287.1 J/kgK [ANSI/ASHRAE, 1999], T_{dry} is the dry bulb temperature and the partial vapor pressure, p_{par} , was deduced as

$$p_{par} = p_{sat} - p_b \left(\frac{T_{dry} - T_{wet}}{1500} \right), \quad (4.7)$$

where T_{wet} is the wet bulb temperature and p_{sat} is the saturated vapor pressure at wet bulb temperature was deduced as [ANSI/ASHRAE, 1999]

$$p_{sat} = 3.25T_{wet}^2 + 18.6T_{wet} + 692. \quad (4.8)$$

4.2 The measuring instrument for point velocity

The point velocities were measured using a velocity meter of TSI Model 8345 (range = 0 to 30 m/s, accuracy = 3% of reading or ± 0.015 m/s whichever is greater, response time = 200 ms, operable temperature range = -17.8°C to 93.9°C); see Ref. [TSI, 2002] for details. The estimated uncertainty of the velocity meter is $\pm 3.3\%$ to 3.5% of the reading; see Appendix A. The velocity meter consists of a heated-element sensor, which operates on the hot-wire anemometry principle [King, 1914]. A heated element, placed in a flowing air stream, will be cooled. The rate of cooling is proportional to the velocity of air movement. King [1914] showed that the heat loss in a moving fluid from electrically heated sensor/element could be expressed as

$$h = KT + (2\pi KS\rho d_{wire} U)^{0.5} T, \quad (4.9)$$

where, h is the rate of heat loss per unit length of wire, d_{wire} is the diameter of wire, T is the temperature of air above ambient temperature, K is the thermal conductivity of fluid (air), S is the specific heat at constant volume of fluid (air), ρ is the density of fluid (air), U is the velocity of fluid (air). Bradshaw [1971] provided a simplified relation between h and U for a given wire operating at a constant temperature in a same fluid (air, for example) as

$$h = A_1 + B_1 U^{0.45}, \quad (4.10)$$

where A_1 and B_1 are constant for a given instrument; see Ower and Pankhurst [1977] for details. The heated element is maintained at a constant temperature. The reason to choose the constant temperature mode is the constant operational temperature and thereby constant heated wire resistance to maintain the overheat ratio; so the thermal inertia of the sensor

element is automatically adjusted during the variation of the flow conditions [Ossofsky, 1948; Weske, 1943]. As air flows over the heated sensor, heat is lost from the element. To compensate the heat loss from the sensor/element, additional current is required. The current is monitored as a measure of air velocity. This kind of sensor has a notable performance at low velocities [Burgess et al., 2004]. The schematic of the velocity meter is shown in Figure 4.5.

A secondary check for the measured mean velocity was realized via the use of a 2.38 mm Pitot-static tube, where the flow dynamic pressure was recorded using the Meriam Instrument supplied digital manometer. The estimated uncertainty of the digital manometer meter is $\pm 7.5\%$ to 12.4% of the reading; see Appendix A. The pitot static tube connected with digital manometer is shown in Figure 4.6. The schematic of the Pitot-static tube is also shown in Figure 4.7. The velocity head was measured using manometer as [SMACNA, 1983]

$$p_v = p_{total} - p_{static}, \quad (4.11)$$

where p_{total} is the total pressure, p_{static} is the static pressure and p_v is the dynamic pressure which was recorded using the manometer.



Figure 4.5 Schematic of velocity meter connected in duct during measurement.

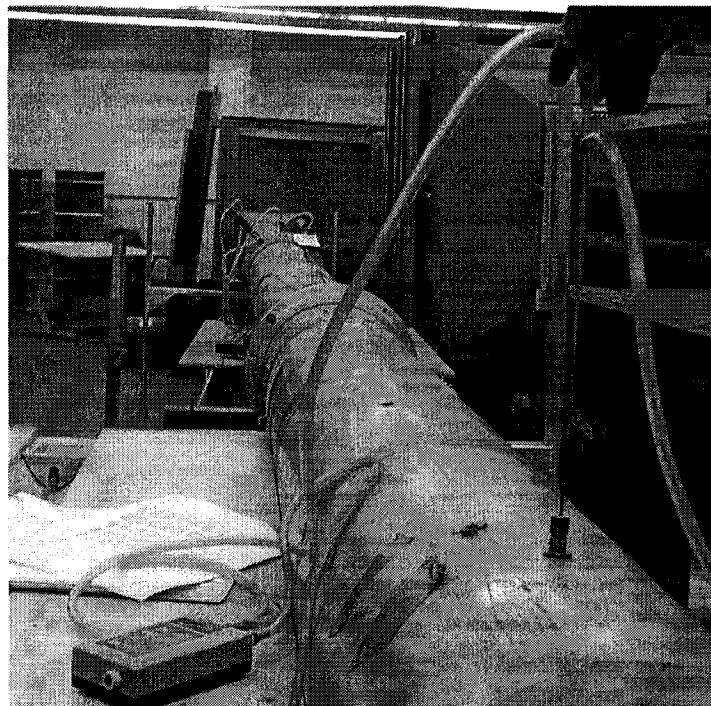


Figure 4.6 Schematic of the manometer connected with Pitot-static tube.

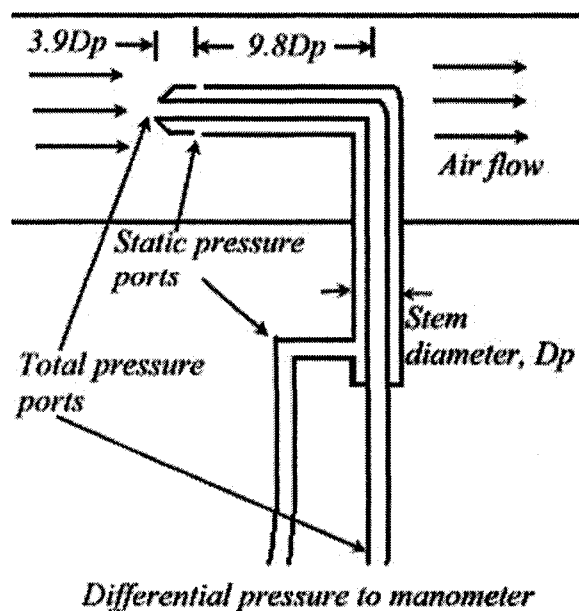


Figure 4.7 Pitot static tube with stem diameter $D_p = 2.38$ mm (drawing not in scale).

The instantaneous velocities at different locations were quantified using a TSI IFA 300 constant temperature, hot-wire anemometer system; see TSI instructions manual [TSI, 2000] for details. The locations were selected randomly at $1.34D$ upstream of the venturi meter and at $4D$ upstream of the exit of the circular duct. In this investigation, a single sensor hot-wire probe consists of a short length of a fine diameter ($3.8 \mu\text{m}$ diameter) wire (made by tungsten) attached to two prongs made of stainless steel, was used for velocity measurement. The good frequency response is obtained using the hot wire probe due to its small size and well-defined characteristics [Brunn, 1995]. An automatic calibrator controlled by a computer and a nozzle facility were employed for the calibration of hot-wire probe; see Appendix B for calibration details. The traversing for extracting velocities at specified position has been performed by the positioning table/traversing mechanism (60×60 cm traversing in each axis, resolution $10 \mu\text{m}$, accuracy $\pm 1.64 \mu\text{m/cm}$, traversing speed 10 mm/s).

4.3 Specifying the velocity measurement points

The volumetric flow rate was estimated via mean velocity, which was deduced from the point velocity measured using the Equal Area and Log-Tchebycheff techniques. The locations of the measurement points specified for the Equal Area method differ somewhat from those for the Log-Tchebycheff method. A measuring instrument for the Equal Area method, i.e., Pitot-static tube or hot wire probe was placed at the center points of equal areas over the cross section of the duct [Alnor, 2004; ISO 1988; SMACNA, 1983], whereas those for the Log-Tchebycheff method are intended to divide each equal-area element into two sub-elements of equal volume flow rate [Alnor, 2004; Gladstone, 1996; ISO 1988; ASHRAE, 1988]. For the conditions (size of the circular duct, D , Re , etc) considered here, six and eight measurement points per diameter was used [Alnor, 2004; Flow Kinetics, 2002; ASHRAE, 1988; ISO, 1988]; see Table 4.1. The traversing section for the straight duct was at 490 cm ($19D$) from the venturi meter and 105 cm ($4.0D$) from the exit. According to the specification, the traversing for measurements are to be taken a minimum of 8.5 duct diameters downstream from the last fitting, which could be 5 diameters with a straightener and 2.5 duct diameters upstream from any disturbances in case of HVAC system field measurement [AABC, 2002; Howell and Sauer, 1990; ASHRAE, 1988]. The duct was traversed along four equally spaced diameters (every 45° across the specified traversing plane). Hence, 24 measurement points for six-point traversing and 32 measurement points for eight-point traversing were taken for both Equal Area and Log-Tchebycheff techniques; see Figure 4.2.

Table 4.1 Locations of measurement points for the Equal Area and Log-Tchebycheff methods for circular duct flow

Traversing-method	Number of points	Dimensionless radii of measuring positions (r/D)			
		Position 1	Position 2	Position 3	Position 4
Equal Area	6-point	0.204	0.353	0.457	-
	8-point	0.177	0.306	0.395	0.468
Log-Tchebycheff	6-point	0.188	0.362	0.468	-
	8-point	0.166	0.306	0.4	0.476

Figure 4.8 depicts the different locations for the Equal Area and Log-Tchebycheff traversing techniques, in which six-point traversing per diameter is shown, where the small circles signify the locations for the Equal Area method and the pluses correspond to those for the Log-Tchebycheff method. Note that while the two points around the duct center are farther away from the duct wall, the other four points corresponding to the Log-Tchebycheff method are closer to the duct wall, as compared to those points associated with the Equal Area method; see Table 4.1. This indicates the fact that the Log-Tchebycheff method aims at accounting for the near wall velocity gradient.

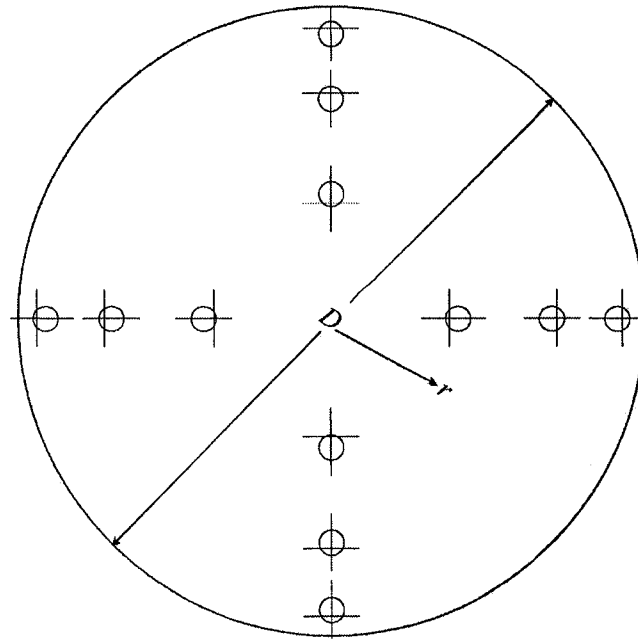


Figure 4.8 Sample measurement points (six points per diameter) for circular duct flow. Circles (O) for the Equal Area method and pluses (+) for the Log-Tchebycheff method.

4.4 Experimental methods and procedures

In the experiments, air was blown through a circular duct. The gate damper was fixed for the experiment to get a specified amount of air supply. Prior to the experiment, the hot wire sensor was calibrated and installed precisely on hot wire probe support. The manometer for the pressure differential across the venturi meter was set and initialized to zero. A traversing table was prepared according to the Table 4.1 for each of the traversing hole as shown in Figure 4.2.

The data was collected after a certain period of time (approximately 30 minutes) subsequent to the blower startup to allow the flow to be steady and uniform. The barometric pressure and the dry and wet bulb temperatures were recorded every 15-20 minutes during the experiment to observe the effect of atmospheric condition. The velocity

in a single point using hot wire sensor was measured approximately at $1.34D$ upstream and $19D$ downstream of the venturi meter. Further, the instantaneous velocity was measured at $1.34D$ upstream of the venturi meter for checking the uniformity and steadiness of the airflow approaching venturi meter. The data was collected by means of a TSI supplied velocity meter of model 8345 according to the Equal Area traversing technique along the horizontal and vertical planes; see Figure 4.9. The pressure difference along the venturi meter was recorded using a digital manometer. At the same time, the point velocity was measured using a manometer via Pitot-static tube and/or velocity meter at $4D$ upstream from the exit; see Figure 4.2. The origin i.e., the coordinate of the position of the measuring instrument for traversing was fixed. Then the point velocities were measured using the pre-defined traversing table. All the data were collected for a same flow rate that controlled by a continuous control damper.

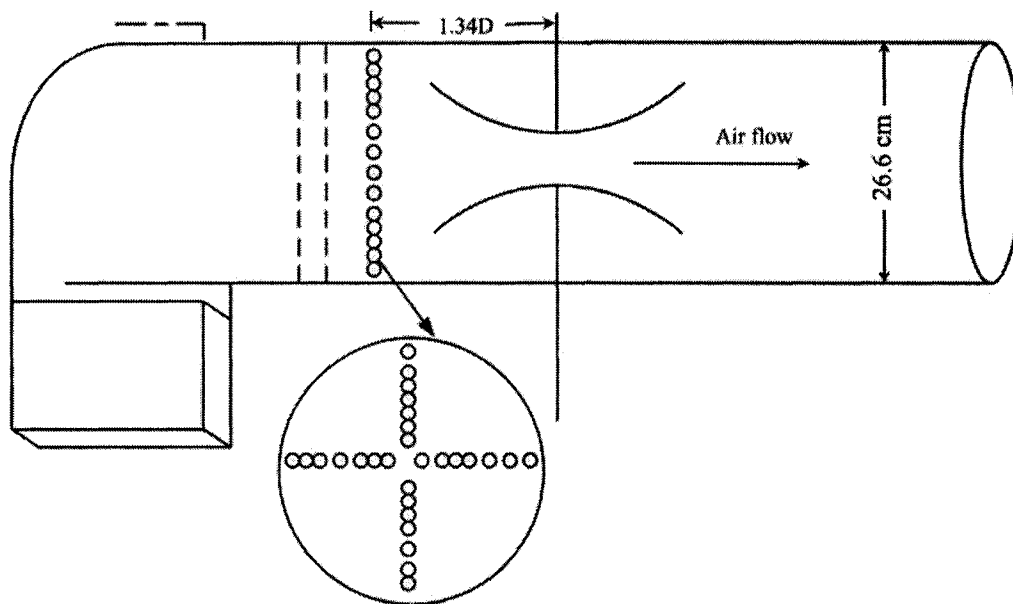


Figure 4.9 Schematic of the duct with 14 x 14 measuring grid at upstream of venturi meter
(drawing not in scale).

4.5 Measurement and data collection

In experiment, every effort was given to ensure that the system was stabilized before starting the data collection, even though during the experiment and data collection process some fluctuations were observed. To take these variations into account, during each experiment, three to four data samples for each of the parameters were collected. Then, the mean of the samples was taken as follows

$$F = \frac{1}{n} \sum_{i=1}^n F_i, \quad (4.12)$$

where F is considered any measured parameters, i is the counter of any repeated measurements and n is the total number of data readings.

4.5.1 Measurement of approach air velocity upstream of the venturi meter

The approach air velocity was measured at $1.34D$ upstream of the venturi meter using velocity meter as shown in Figure 4.9. The velocity meter has an uncertainty of $\pm 3.4\%$ of the reading; see Appendix A. The velocity was measured at 28 locations (horizontally and vertically evenly spaced 14×14 grid points) over the cross sections and the mean velocity was recorded following Equation (4.12). To have an airflow measurement at standard environment, the dry-bulb temperature and barometric pressure were recorded and the velocity was corrected as [TSI, 2002]

$$U_{corr} = U_{vm} \left[\frac{273.15 + T_{dry}}{273.15 + 21.1} \right] \frac{101.4}{p_b}, \quad (4.13)$$

where p_b is the barometric pressure, U_{vm} is the point velocity measured by velocity meter. Further, a correction factor of 5-percent, suggested by Laufer [1954] due to non-linear behavior of the velocity meter sensor, was introduced with Equation (4.13). Nevertheless, the observed intensity was (4.5-6.5) % using hot-wire system at different locations.

4.5.2 Reference flow rate deduced using the venturi meter

The volumetric flow rate was determined using Equations (4.3). In this respect, the independent parameters, pressure head (Δh) was measured using manometer across the venturi meter, wet bulb (T_{wet}) and dry bulb (T_{dry}) temperatures were measured using thermometer and barometric pressure (p_b) was measured using barometer. The required thermo-physical properties i.e, water density (ρ_{water}) was estimated from the average temperature of the room during the experiment. The measurements of independent parameters are discussed in the following subsections.

Measurement of pressure head (Δh)

The pressure difference (Δh) across the venturi meter was recorded using a digital manometer. The manometer has an uncertainty of $\pm 2.96\%$ to 8.95% of the reading. The manometer reads the pressure difference between the upstream and throat regions of the venturi meter, which is shown in Figure 4.4. At beginning of each experiment, the manometer was set to zero and the data was recorded after a nominal amount of time. Following Equation (4.12), the mean pressure head (Δh) for each experiment was deduced.

Measurements of wet bulb (T_{wet}) and dry bulb (T_{dry}) temperatures

The dry bulb and wet bulb temperatures were recorded using a standard mercury-in-glass thermometer (accuracy of ± 0.5 °C) from experimental room in °C. The thermometer has an uncertainty of $\pm 3.05\%$ of the reading. The dry-bulb temperature of air was measured by a thermometer, which was freely exposed to the air but shielded from radiation and moisture. As suggested by Bureau of Metrology [2005], wet-bulb temperature was measured with same kind of thermometer whose bulb was wrapped by a muslin sleeve that was moistened by pure water. The temperatures were recorded during the experiment every 15-20 minutes and mean temperature was calculated.

Measurements of barometric pressure

The barometric pressure was measured using mercury meter (accuracy 0.5% of the reading, resolution 0.1 mm of Hg). The barometer has an uncertainty of 1.88% of the reading. The pressure also recorded every 15-20 minutes during the experiment and was averaged using Equation (4.12).

4.5.3 Flow rate estimation using Equal Area and Log-Tchebycheff methods

The mean velocity of approach air at the traversing section was used to estimate the volumetric flow rate through a circular duct. At each location, three to four measurements of air velocity were obtained consecutively and then averaged to establish a mean velocity for that location. The mean air velocity was estimated for the Pitot-static tube as [SMACNA, 1983]

$$U = C' \sqrt{\frac{2p_v}{\rho}}, \quad (4.14)$$

where C' is the design correction depends on the spacing of the static pressure holes, which was taken as 1.003 suggested by Flow kinetics [2002] for this kind of configuration; see Figure 4.7. Assuming the air as an ideal gas i.e., compressibility factor is unity and by implying the ideal gas constant, the density was calculated using Equation (4.6).

It is observed that the boundary has an effect on point velocity measured using Pitot-static tube. An extensive amount of research [Knudsen et al., 1958; Das et al., 1969; MacMillan, 1956; Livsey, 1956; Laufer, 1954; Khan, 2004] already observed regarding the correction for the wall bounded flow. Laufer [1954] suggested that the velocity is corrected for the flow through circular duct/pipe as

$$U_{Corr} = U \sqrt{1 - \frac{\bar{u}^2}{U^2}}, \quad (4.15)$$

which was the order of 5% or less. In Equation (4.15), \bar{u} is the velocity fluctuations close to the wall and in this study the point velocity was corrected using Equation (4.15). For the case of the velocity meter, the mean velocity was calculated using Equation (4.13). Finally, the volumetric flow rate was calculated according to Equation (2.1) as multiplying the corrected mean velocity with cross section area of the duct.

CHAPTER 5

RESULTS AND DISCUSSIONS

The focus of the current study was on the estimation of volumetric flow rate via discrete velocity measurements at finite points across a duct section. The accuracy of the two volumetric flow estimation techniques, Equal Area and Log-Tchebycheff, was studied both numerically and experimentally for airflow in a circular duct. This chapter focuses on the numerical results, experimental results and comparison between them.

5.1 Numerical results

The laminar and turbulent flow fields for circular duct flow over a range of Reynolds numbers from 200 to 54000 were investigated using commercial CFD code FLUENT. The laminar model was employed for the laminar cases ($Re = 200$ to 2300), while the κ - ϵ model was invoked for the turbulent cases ($Re = 2300$ to 54000). Both laminar and turbulent models were utilized for the $Re = 2300$ case. On the accuracies of Equal Area and Log-Tchebycheff methods, the six-point and eight-point traversing was utilized at different planes ($L/D = 20, 40$ and 60) from the uniform velocity at entrance.

5.1.1 Flow development

The development of the flow was visualized from the duct centerline, streamwise (axial) velocity, U_c variation along the duct. For Re ranging from 200 to 20000, U_c/U_{max} , where U_{max} is the centerline velocity at the outlet of the duct ($x = 60D$), is plotted as a

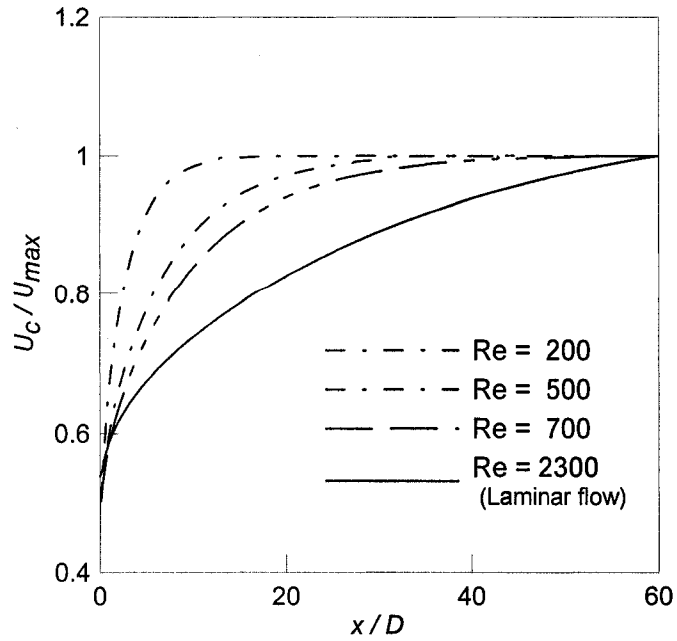
function of the normalized axial distance, x/D , as shown in Figure 5.1. The entrance length (L_e) for fully developed flow can be estimated as [White, 1999]

$$\frac{L_e}{D} \approx 0.06 \text{ Re}, \text{ for laminar flow} \quad (5.1)$$

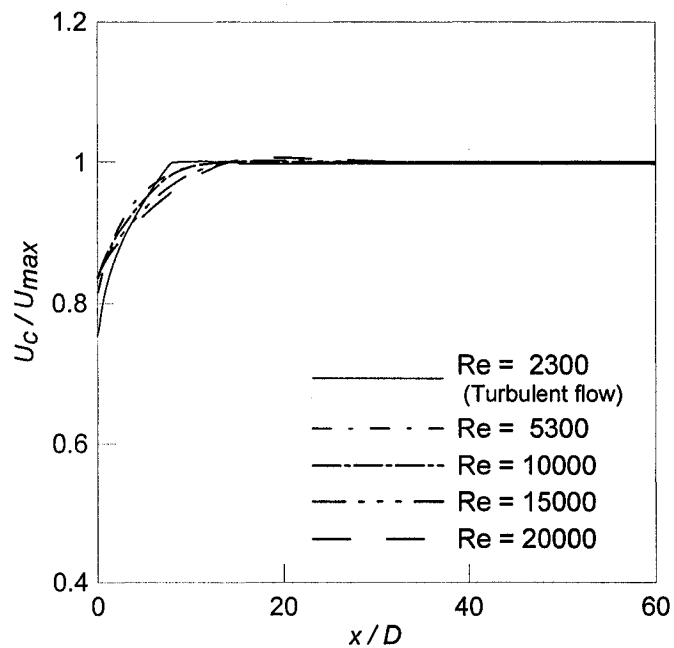
and

$$\frac{L_e}{D} \approx 4.4 \text{ Re}^{1/6}, \text{ for turbulent flow.} \quad (5.2)$$

In other words, the dependence of the entrance length, L_e , on the Reynolds number is different depending on whether the flow is laminar or turbulent. The simulated U_c/U_{max} versus x/D results give values of L_e/D as 12.0, 31.2, 43, 18.5, 20.6, 22 and 23.5 for $\text{Re} = 200, 500, 700, 5300, 10000, 15000$ and 20000 respectively. These simulated entrance lengths for fully developed flow agree well with those predicted by Equations (5.1) and (5.2), which are 12, 30, 42, 18.37, 20.42, 21.85 and 22.92; see White [1999], Miller [1983] and/or Benedict [1980] for details. Note that the model duct length, $L/D = 60$, considered in the simulations is less than the entrance length ($L_e/D = 138$) for $\text{Re} = 2300$ case if the flow is laminar. Thus, the axial, centerline velocity for the $\text{Re} = 2300$ case simulated using the Laminar model as illustrated in Figure 5.1(a) is still developing, i.e., U_c has not leveled off. On the other hand, the same flow at $\text{Re} = 2300$, calculated based on the Turbulent model is fully developed; as shown in Figure 5.1(b). We also see from Figure 5.1(a) and Equation (5.1) that in the laminar flow regime the axial velocity along the duct centerline approaches and levels off at U_{max} progressively later with increasing Re . There is a sudden and significant decrease in entrance length when the flow changes from laminar to turbulent (the $\text{Re} = 2300$ cases). In the turbulent flow regime, the increase in entrance length with increasing Re is smaller; compare Equation (5.2) with Equation (5.1).



(a) Laminar flow.



(b) Turbulent flow

Figure 5.1 The effect of Re on the axial, centerline velocity development along the duct

(a) Laminar flow (b) Turbulent flow.

5.1.2 U_{max}/U_{mean} at fully developed zone

The empirical relations between U_{mean} and U_{max} were verified from the present numerical simulation at the fully developed zone for different Reynolds number. In case of laminar flow, the theory based on the conservation of mass for an incompressible and isentropic flow with no slip boundary condition at the wall states that the maximum axial velocity, which occurs at the duct centerline, is twofold the average velocity [Fox and McDonald, 1998]. The simulated relations (U_{max}/U_{mean}) show a good agreement with the theory in the laminar flow ($Re = 200$ to 700) case; see Table 5.1.

Table 5.1 The fully developed axial velocity along the duct centerline with respect to the mean velocity.

Re	U_{max} (m/s)	U_{mean} (m/s)	* U_{max}/U_{mean}
200	0.032	0.016	2.00
500	0.078	0.039	1.99
700	0.108	0.054	1.99

*The theoretical value is 2.

In case of turbulent flow ($Re = 2300$ to 20000), the relation between mean velocity (U_{mean}) and maximum velocity (U_{max}) at fully developed zone was determined as [White, 1999]

$$U_{mean} = U_{max} \left(1 + 1.33\sqrt{f_t}\right)^{-1}, \quad (5.3)$$

where f_t is the friction factor for the turbulent region, which can be computed explicitly as [Colebrook, 1939]

$$f_t = \left(1.8 \log \frac{Re}{6.9} \right)^{-2} . \quad (5.4)$$

The simulated U_{mean}/U_{max} were compared with those calculated using Equations (5.3) and (5.4) over a range of $Re = 2300$ to 20000 . Figure 5.2 shows that the curves obtained in the current investigation are in good agreement with that of theoretical estimations. It is also observed that U_{mean}/U_{max} increases with Re .

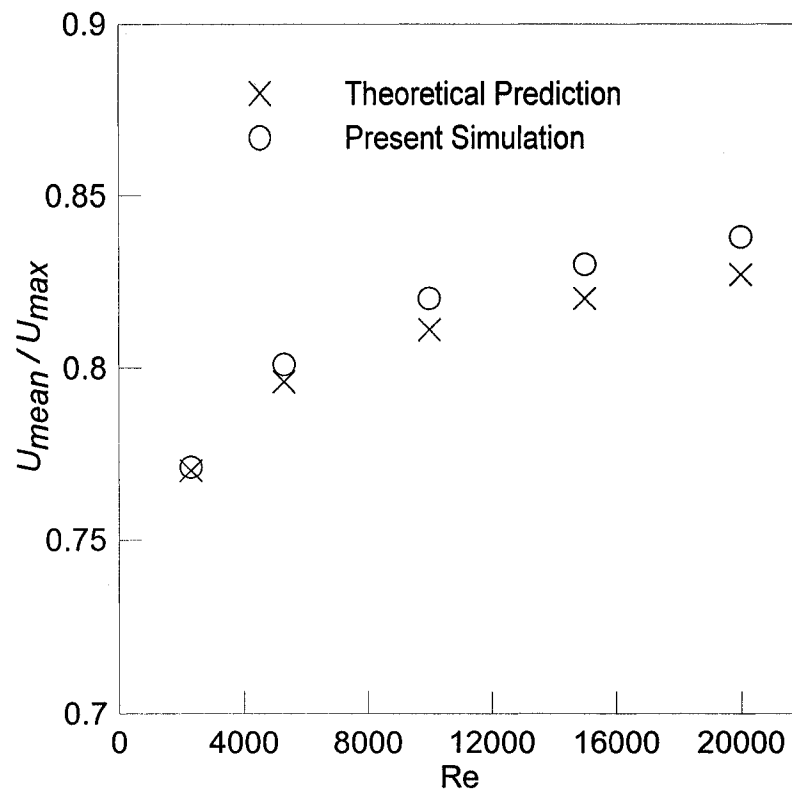


Figure 5.2. The comparison of simulated U_{mean}/U_{max} with theoretical prediction for turbulent flow ($Re = 2300$ to 20000).

5.1.3 Axial velocity distribution at outlet

One of the most important parameters for the flow field is the streamwise (axial) velocity distribution along the radial direction. The velocity profiles at fully developed zone for the laminar and turbulent flows can be shown as [Fox and McDonald, 1998]

$$U = U_{max} \left(1 - \frac{4r^2}{D^2} \right), \text{ for laminar flow,} \quad (5.5)$$

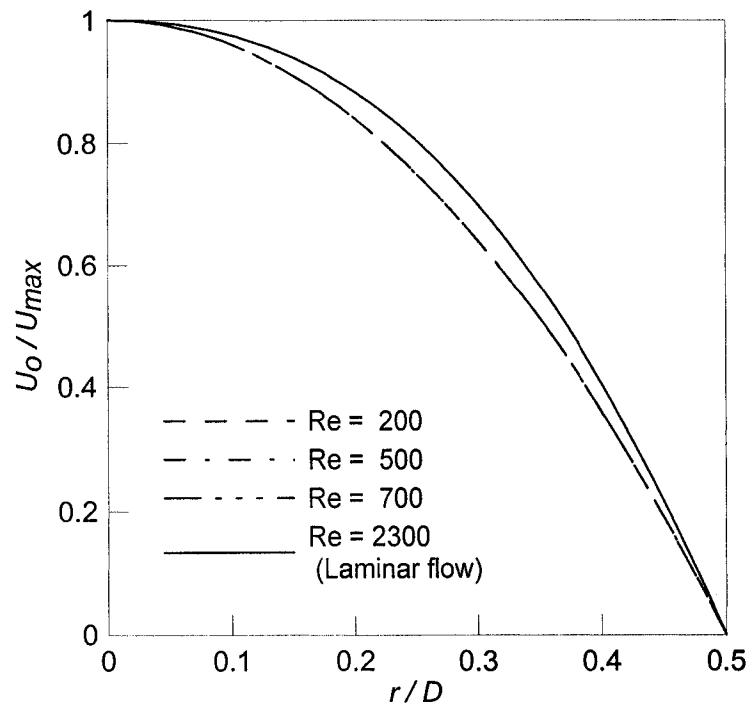
and

$$U = U_{max} \left(1 - \frac{2r}{D} \right)^{1/m}, \text{ for turbulent flow,} \quad (5.6)$$

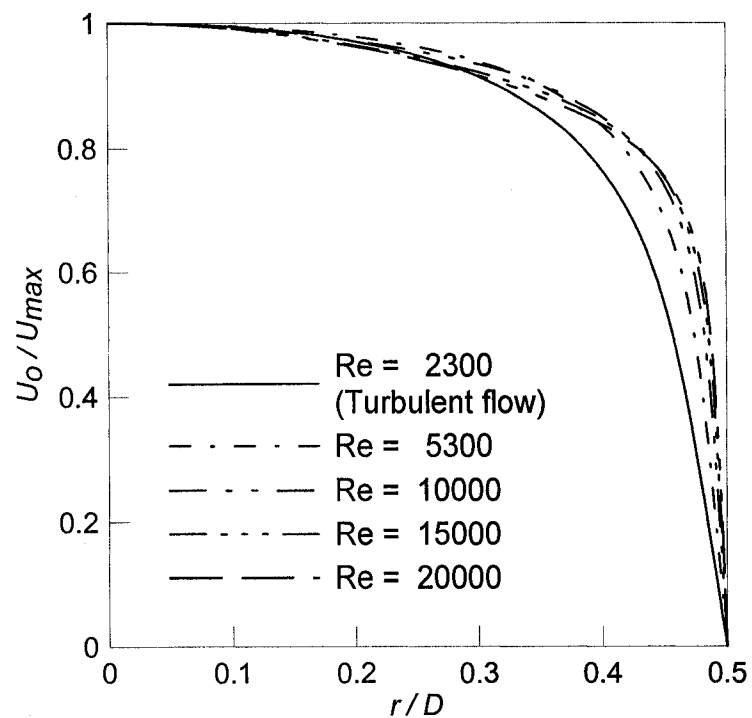
where index, m is defined as:

$$m = 1.66 \log \text{Re.} \quad (5.7)$$

The fully developed axial velocity (the streamwise velocity at the duct outlet) along the radial direction, U_o , normalized by U_{max} (the duct centerline velocity at $x = 60D$) is plotted against the normalized radial distance, r/D , in Figure 5.3. Figure 5.3(a) portrays a parabolic behavior at fully developed zone, which indicates a good agreement with Equation (5.5). Note that the ‘laminar’ $\text{Re} = 2300$ case is slightly different as the duct length considered is not long enough for this flow to become fully developed, when the calculations invoke the Laminar model; on the other hand, the ‘turbulent’ $\text{Re} = 2300$ case is fully developed. As expected from Equation (5.6), unlike the fully developed laminar flow profile, which is independent of Re , the turbulent flow profile becomes progressively flatter with increasing Re ; see Figure 5.3(b).



(a) Laminar flow



(b) Turbulent flow.

Figure 5.3 The effect of Re on the axial velocity profile at $x = 60D$

(a) Laminar flow (b) Turbulent flow.

The mean velocity profile across the duct (\bar{U}) normalized by maximum mean velocity (the centerline velocity at the developed zone), \bar{U}_{max} , is compared with available data as depicted in Figure 5.4. It is seen that the agreement between numerical result and available experimental published data [Browne and Dinkelacker, 1995; Benedict, 1980] is within satisfactory range.

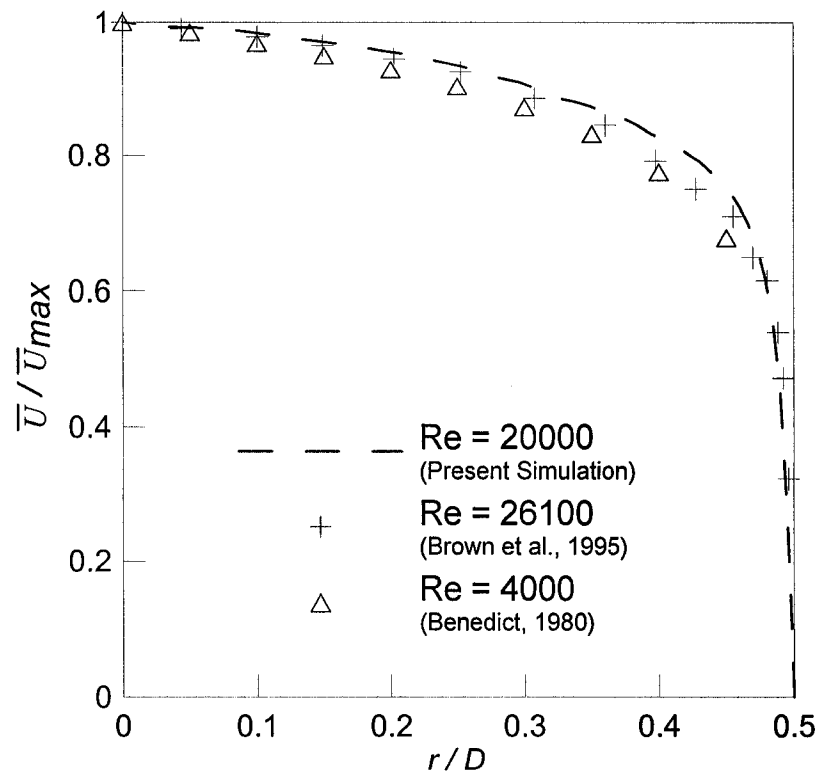


Figure 5.4 Comparison of mean velocity profiles with available published data

The mean flow properties obtained from available previous findings [Eggels et al., 1994; Westerweel, 1993; Weiss, 1993; Unger and Friedrich, 1991 and Kim et al., 1987] were compared with the present simulated flow properties as summarized in Table 5.2. Note that Re_C is the Reynolds number based on centerline velocity (U_C) at fully developed

zone, Re is the Reynolds number based on mean velocity (U_{mean}), Re_{τ} is the Reynolds number based on wall shear velocity, U_{τ} , which is defined as

$$U_{\tau} = \sqrt{\frac{\tau_w}{\rho}} \quad (5.8)$$

where τ_w is the wall shear stress.

Table 5.2 Comparison of the mean flow properties obtained from present numerical simulation with some past findings.

	DNS (E)	DNS (U)	PIV	LDA	HWA	KMM	Present_study
Re_C	6950	6950	7100	7200	7350	6600	6716
Re	5300	5300	5450	5450	5600	5600	5300
Re_{τ}	360	360	366	371	379	360	358
U_C/U_{mean}	1.31	1.31	1.30	1.32	1.31	1.16	1.26
U_C/U_{τ}	19.31	19.29	19.38	19.39	19.4	18.2	18.61
U_{mean}/U_{τ}	14.73	14.74	14.88	14.68	14.76	15.63	14.96

DNS (E) is direct numerical simulation by Eggels et al. [1994], DNS (U) is direct numerical simulation by Unger and Friedrich [1991], LDA is laser doppler anemometry and PIV is particle image velocimetry by Westerweel [1993], HWA is hot-wire anemometry by Weiss [1993] and KMM is DNS data by Kim et al. [1987].

It is shown that the ratio of U_C/U_{mean} from the present investigation is 3.8% less than that of the direct numerical simulation of DNS (E). Hence, the U_C/U_{mean} with uncertainty of the present study could be estimated as $1.26 \pm 3.8\%$ [Zhu et al., 2002].

5.1.4 Friction Coefficient

The wall friction contributes directly to the head loss in a duct flow and hence, the required power to move the fluid. Consequently, a reliable numerical model should produce the correct friction coefficient (C_f), which is defined as [Fox and McDonald, 1998; Ward-Smith, 1980]

$$C_f = \frac{2\tau_w}{\rho U_{mean}^2}, \quad (5.9)$$

where the wall shear stress (τ_w) for laminar flow in a smooth duct can be calculated as [Fox and McDonald, 1998]

$$\tau_w = \frac{D\Delta p}{4L} \quad (5.10)$$

and the pressure gradient (Δp) is

$$\Delta p = \frac{32LU_{mean}\mu}{D^2}. \quad (5.11)$$

Equations (5.9), (5.10) and (5.11) illustrate that the coefficient of friction is inversely proportional to the Reynolds number for laminar flows i.e., $C_f Re = 16$; see Table 5.3.

For turbulent flow in a smooth duct, the wall shear stress can be calculated as [Fox and McDonald, 1998]

$$\tau_w = 0.0332\rho U_{mean}^2 \left[\frac{2\mu}{\rho D U_{mean}} \right]^{0.25}. \quad (5.12)$$

Substituting Equation (5.12) into Equation (5.9) gives

$$C_f = 0.0791 Re^{-0.25}, \quad (5.13)$$

which is the Blasius [1913] correlation for turbulent flow in a smooth duct as mentioned by Rohsenow et al. [1998]. Hence, the friction coefficient for turbulent flow also decreases with increasing Reynolds number; but in a slower rate compared to laminar flow. Table 5.3 shows the sample simulated friction coefficient which corresponds to the turbulent flow with $Re = 5300$ compares well with those in the literature [Moyekens and Muralikrishnan, 2003; Eggels et al., 1994].

Table 5.3 Comparison of simulated friction factors with those in the open literature.

Re	$C_{f,num}$	$C_{f,theoretical}$	C_{f}^* , numerical	C_{f}^{**} , experimental
200	0.08	0.08	0.08	-
500	0.03	0.03	0.03	-
700	0.02	0.02	0.02	-
5300	0.01	0.01	0.01	0.01

* Moyekens, S., and Muralikrishnan, R., Developing flow in a pipe, lowlab.fluent.com/exercise/pdfs/developing_flow_in_pipe01.pdf, 2003.

** Eggels, J. G. M., Unger, F., Weiss, M. H., Westerweel, J., Adrian, R. J., Frienrich, R. and Nieuwstadt, F. T. M., Fully developed turbulent pipe flow: a comparison between direct numerical simulation and experiment, *J. Fluid Mech.*, v268, p175-209, 1994.

5.1.5 Effect of location on accuracies of Equal Area and Log-Tchebycheff methods

The numerically simulated axial velocity across the duct radius at $x/D = 20, 40$ and 60 are portrayed in Figure 5.5. The measurement locations utilized in the Equal Area and Log-Tchebycheff methods are shown as circles and pluses, respectively, on the velocity

lines. Figure 5.5(a) corresponds to the $Re = 500$ laminar case and Figure 5.5(b) represents the $Re = 10000$ turbulent case.

As expected, the velocity profile of the turbulent case varies negligibly with axial distance (x) for the fully developed flow is reached at x/D of 20. On the other hand, Figure 5.5(a) shows that the laminar velocity profile becomes progressively more pointed at the duct centerline as the flow develops from a uniform velocity inlet. Due to the specific locations of the measurement points, the average velocity based on the Equal Area method is reduced slightly while that deduced via the Log-Tchebycheff method is increased slightly, with increasing axial distance (x) along the centerline in the laminar flow development regime; see Table 5.4, the laminar $Re = 2300$ case, in particular.

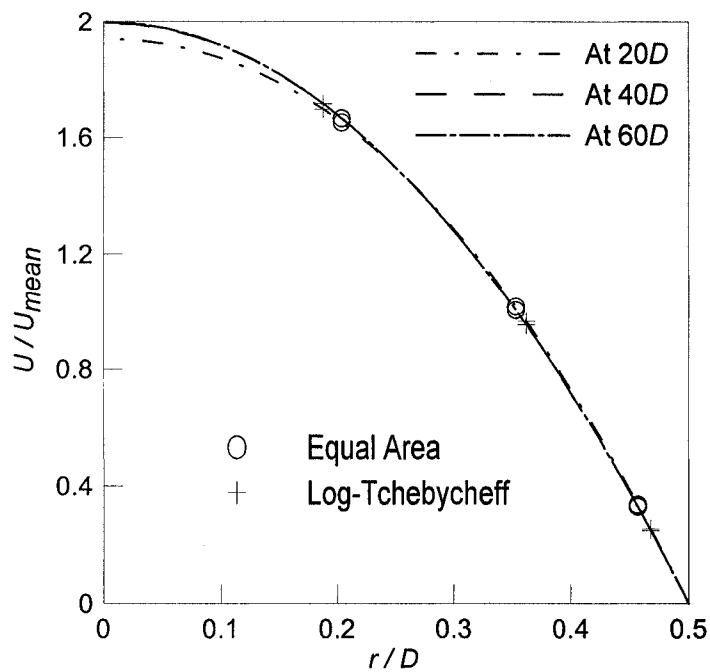
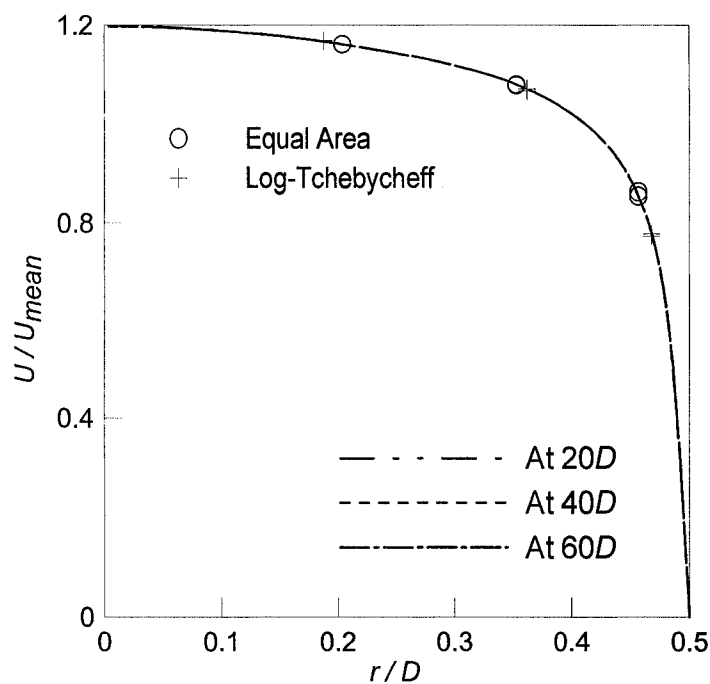
(a) $Re = 500$ (b) $Re = 10000$.

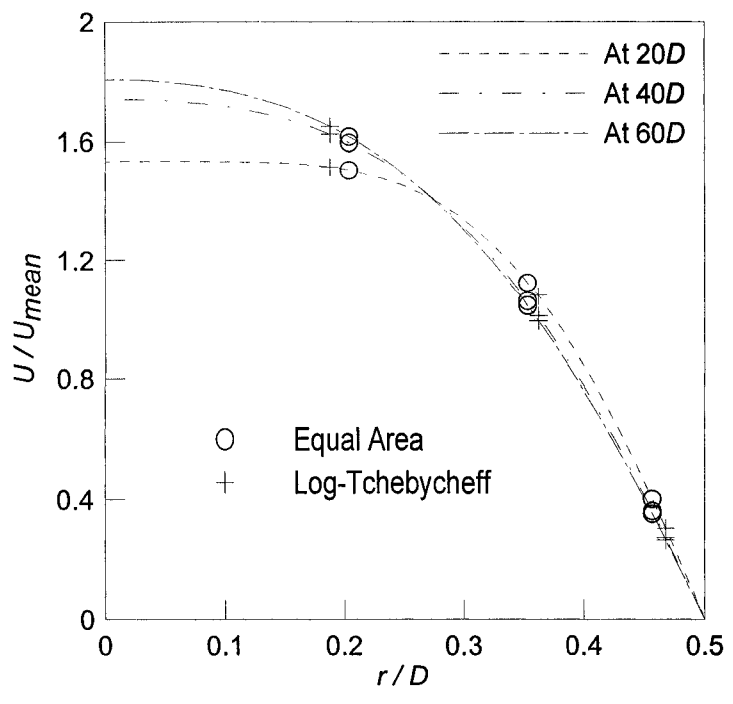
Figure 5.5 The effect of location ($x/D = 20, 40$ and 60) on the velocity profile and accuracies of mean velocities via the Equal Area and Log-Tchebycheff methods for

(a) $Re = 500$ (b) $Re = 10000$.

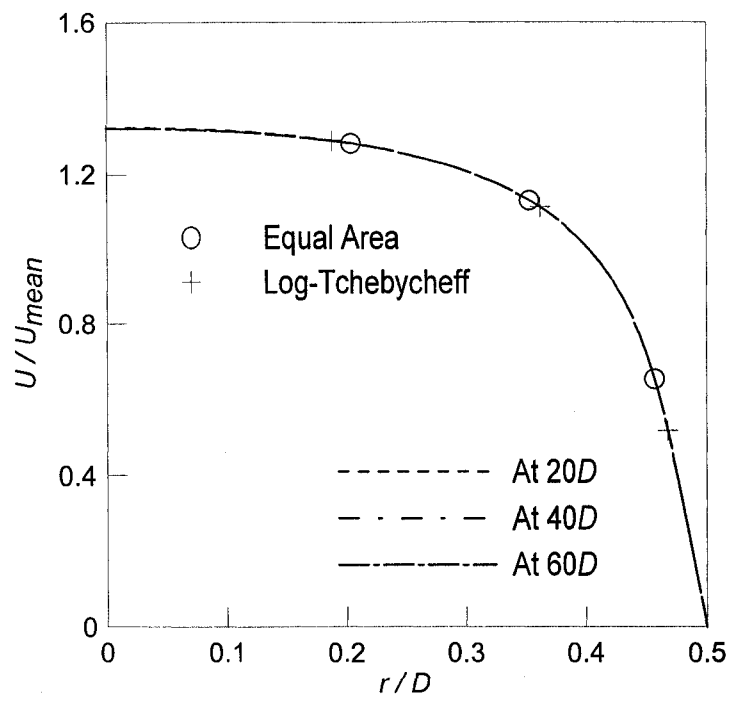
Table 5.4 The accuracies of the Equal Area and Log-Tchebycheff methods in deducing the mean velocity at $x/D = 20, 40$ and 60 (six points per diameter).

Re	U_{mean} [m/s]	U_{EA} [m/s]			U_{LT} [m/s]		
		20D	40D	60D	20D	40D	60D
200	0.0156	0.0156	0.0156	0.0156	0.0151	0.0151	0.0151
500	0.0390	0.0390	0.0390	0.0390	0.0379	0.0379	0.0379
700	0.0540	0.0541	0.0540	0.0540	0.0525	0.0525	0.0525
2300 (Laminar model)	0.1774	0.1792	0.1790	0.1786	0.1713	0.1720	0.1725
2300 (Turbulent model)	0.1774	0.1792	0.1791	0.1791	0.1726	0.1726	0.1726
5300	0.4100	0.4236	0.4236	0.4236	0.4083	0.4083	0.4083
10000	0.7710	0.7955	0.7955	0.7955	0.7750	0.7750	0.7750
15000	1.1560	1.1894	1.1900	1.190	1.1649	1.1649	1.1649
20000	1.5420	1.5841	1.5843	1.5843	1.5540	1.5540	1.5540
54000	4.1540	4.2392	4.2400	4.2400	4.1798	4.1799	4.1799

The special case at $Re = 2300$ is plotted in Figure 5.6, where the velocity profile can be seen to vary significantly with axial distance (x) along the centerline of the circular duct when the flow is laminar, i.e., when the laminar model is invoked. In practice, however, there are many inherent disturbances such as vibrations and surface roughness and hence, the flow is most likely turbulent when Re approaches 2300. This turns out to be good thing as the entrance length and consequently, the average velocity variation with duct length are reduced significantly; see Figure 5.6(b) and Table 5.4.



(a) $Re = 2300$, Laminar flow.



(b) $Re = 2300$, Turbulent flow

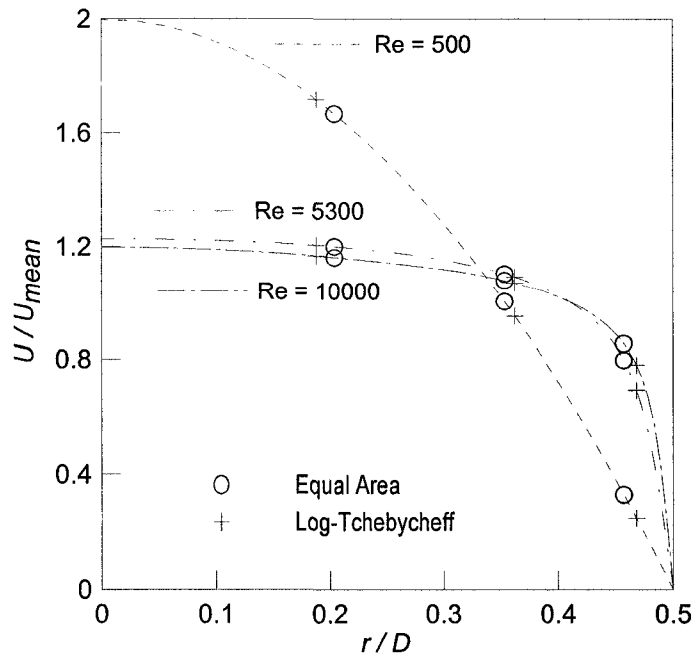
Figure 5.6 The influence of flow regime on the velocity profile and the mean velocities estimated via the Equal Area and Log-Tchebycheff methods for $Re = 2300$

(a) Laminar flow (b) Turbulent flow.

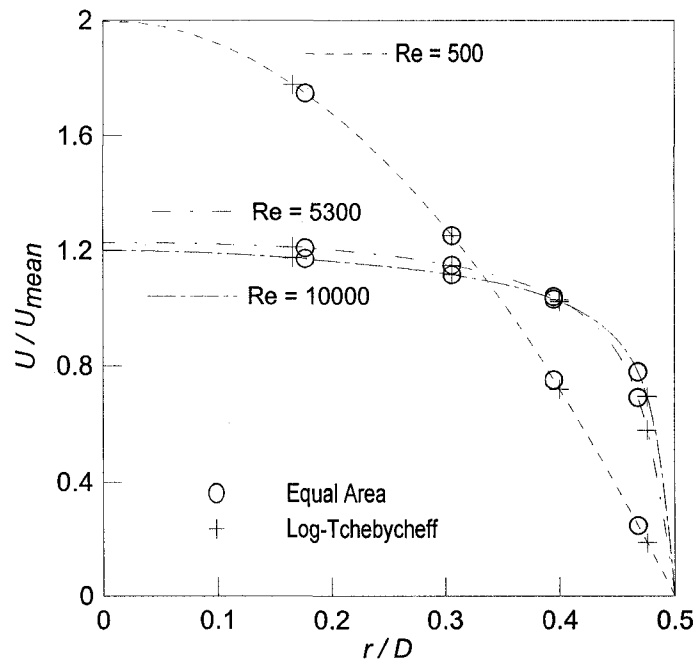
5.1.6 Effect of number of measurement points

With a fully developed flow, one still has the question of whether increasing the number of measurement points would really make a difference. Figure 5.7 shows the effects of the number of measurement points on the accuracies of the two methods in deducing the average velocity followed by the volumetric flow rate. The six and eight points per diameter traverses are depicted in Figures 5.7 (a) and (b), respectively.

The corresponding volumetric flow rates estimated are tabulated in Table 5.5. Increasing the number of measurement points from six to eight points per diameter do not affect the accuracy of the Equal Area method over the range of Re from 200 to 700; see Table 5.5 and Figure 5.8. For the range of Re 200 to 700, the volume flow rates estimated by the Equal Area method coincide with the true value (0% error). Beyond Re of 700, the Equal Area method starts to progressively over-predict the volume flow rate (average velocity), and increasing the number of measurement points decreases the over-prediction to some extent. On the other hand, the Log-Tchebycheff method under-estimates the average velocity for Re up to about 5300; see Figure 5.8 and Table 5.5. Increasing the number of measurement points decreases the under-estimations, rather significantly in the low Re range (200 to 700) and only marginally for Re from 2300 to 5300. Note that the average velocity under-estimation is less than 1% at Re of 5300. The Log-Tchebycheff estimation changes from negligible under-estimation (-0.4%) to very slight over-estimation (0.78% in case of six points per diameter traversing and 0.59% in case of eight points per diameter traversing) when Re increases from 5300 to 54000.



(a) Six points per diameter



(b) Eight points per diameter.

Figure 5.7 The effects of number of measurement points and Re on the accuracies of Equal Area and Log-Tchebycheff methods in deducing the mean velocity at $x/D = 60$

(a) Six points per diameter (b) Eight points per diameter.

Table 5.5 The accuracies of the Equal Area and Log-Tchebycheff methods in estimating the volumetric airflow rate at $x/D = 60$.

Re	Actual flow rate [m ³ /hr]	Equal Area				Log-Tchebycheff			
		Six points		Eight points		Six points		Eight points	
		Flow	Error	Flow	Error	Flow	Error	Flow	Error
		Rate [m ³ /hr]	(%)	Rate [m ³ /hr]	(%)	Rate [m ³ /hr]	(%)	Rate [m ³ /hr]	(%)
200	1.68	1.68	0	1.68	0	1.63	-2.98	1.66	-1.19
500	4.21	4.21	0	4.21	0	4.09	-2.85	4.15	-1.43
700	5.83	5.83	0	5.83	0	5.67	-2.74	5.72	-1.89
2300 (Laminar)	19.16	19.29	0.67	19.28	0.63	18.63	-2.76	18.64	-2.71
2300 (Turbulent)	19.16	19.33	0.88	19.32	0.84	18.64	-2.71	18.65	-2.66
5300	44.28	45.75	3.32	45.21	2.10	44.10	-0.40	44.10	-0.40
10000	83.26	85.91	3.18	85.19	2.32	83.70	0.53	83.32	0.07
15000	124.85	128.81	3.17	127.68	2.27	125.81	0.77	125.36	0.41
20000	166.53	171.10	2.74	169.97	2.10	167.83	0.78	167.42	0.53
54000	448.63	457.92	2.10	456.84	1.83	451.45	0.63	451.29	0.59

Relative error = (estimated flow rate - actual flow rate) × 100% / actual flow rate.

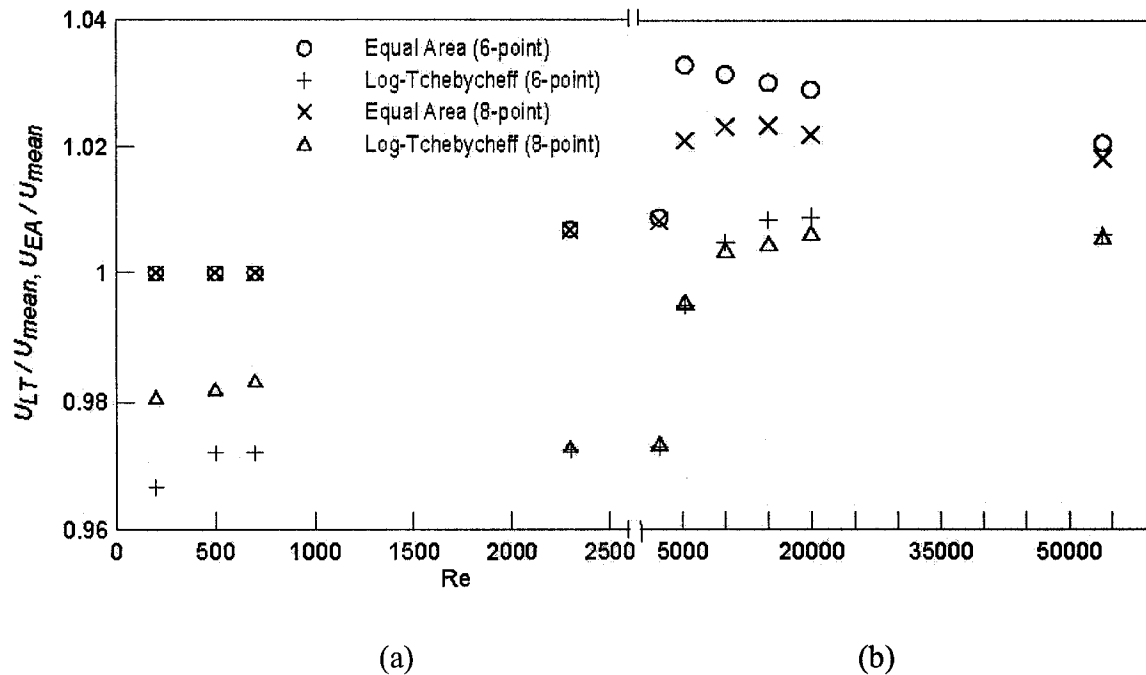


Figure 5.8 The effects of flow model, number of measurement points and Re on the deviations of U_{EA} and U_{LT} from U_{mean} at $x/D = 60$. (a) Laminar flow; (b) Turbulent flow.

5.2 Experimental results

The experiments were performed for different setups depending on the available facilities and the existing limitations. It was assumed that the airflow was steady, no air leaked through the duct wall and there was negligible temperature difference between the inside and outside of the duct. The Equal Area and Log-Tchebycheff methods were utilized for different number of measurement locations (six and eight points per diameter). In the experiment, the air was blown through a straight circular duct at a constant speed and the volumetric airflow rate was estimated using Equal Area and Log-Tchebycheff methods at $4D$ upstream from the exit (approximately $31D$ downstream from the blower). The accuracy of the traversing methods was confirmed by comparing the calculated flow rate

with the reference flow rate determined by the venturi meter. The following sections deal with experimental results.

5.2.1 Flow profile

The flow profile entering the venturi meter was quantified using hotwire, velocity meter and Pitot-static tube. The instantaneous velocity was measured using hotwire anemometer at a single point at $1.34D$ upstream of the venturi meter. The point was selected randomly at $0.45D$ distance from the inner side of the duct. The velocity was collected at a sample rate of 10 kHz with a sampling time of 25.6 sec. The instantaneous velocity variation with time is depicted in Figure 5.9 in which the steadiness of the velocity profiles can be inferred. The steady flow was also verified by time averaging the velocity data of the above-mentioned sampling using three different time durations, $t_1 = 0$ to 10 sec, $t_2 = 0$ to 20 sec and $t_3 = 0$ to 25.6 sec respectively. The obtained time-averaged velocity of the aforementioned time duration is 2.854 m/s, 2.851 m/s and 2.855 m/s, which is nearly identical; see Figure 5.9.

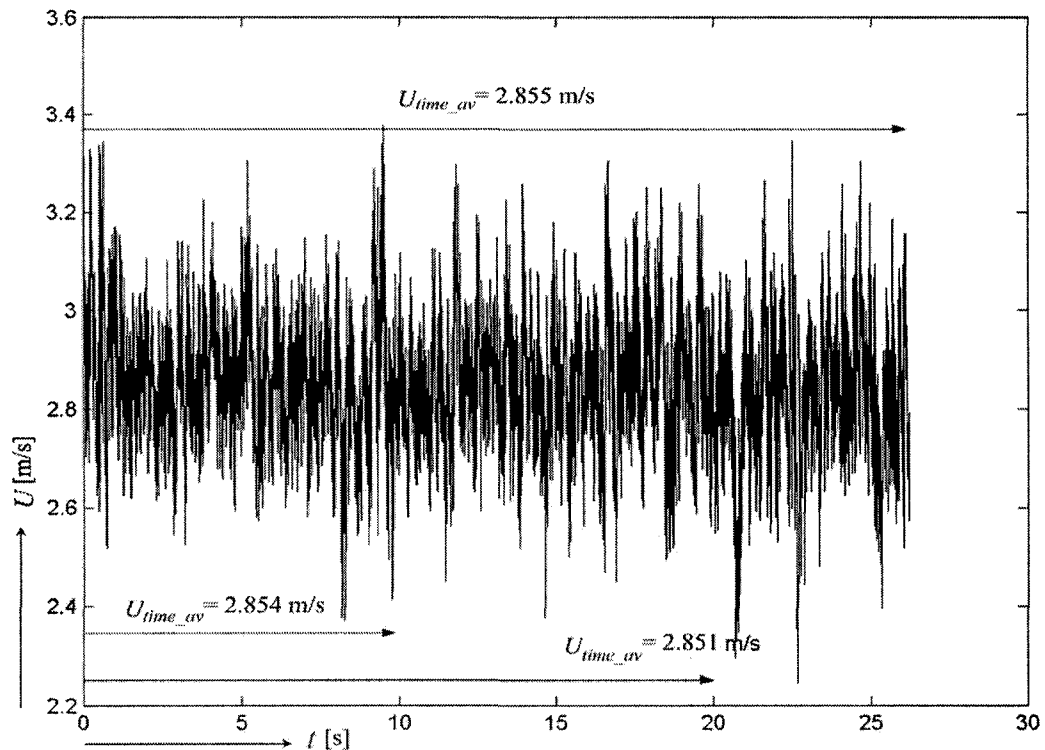


Figure 5.9 Instantaneous velocity at $1.34D$ upstream of the venturi meter.

The point velocities were measured for Re of 54800 and 99400 at $1.34D$ upstream of the venturi meter using velocity meter and Pitot-static tube with manometer. The estimated uncertainties for the averaged point velocity were $\pm 5.15\%$ to $\pm 6.15\%$ in case of velocity meter and $\pm 8.5\%$ to $\pm 13.5\%$ in case of the Pitot-static tube with digital manometer; see Appendix A. The velocity profiles obtained via the velocity meter are depicted in Figure 5.10. For proper plotting of the velocity profiles along the cross section, the measurements were extended beyond the defined (14×14) measurement grid points in Section 4.3 to cover the distance up to the duct wall. Figure 5.10 depicts the mean velocity profiles normalized by the centerline velocity (\bar{U}/\bar{U}_{max}) as a function of the normalized radial distance, y_{tr}/D with typical error bar, where y_{tr} is the distance from one side of the duct to the other. In both cases, the velocity profiles were observed to be reasonably flat for

the entire cross section outside the boundary layer. The boundary layer edge was roughly identified as the point where nominal velocity starts decreasing significantly. It was found that a single point measurement at the upstream of the venturi meter could fairly represent the steady flow.

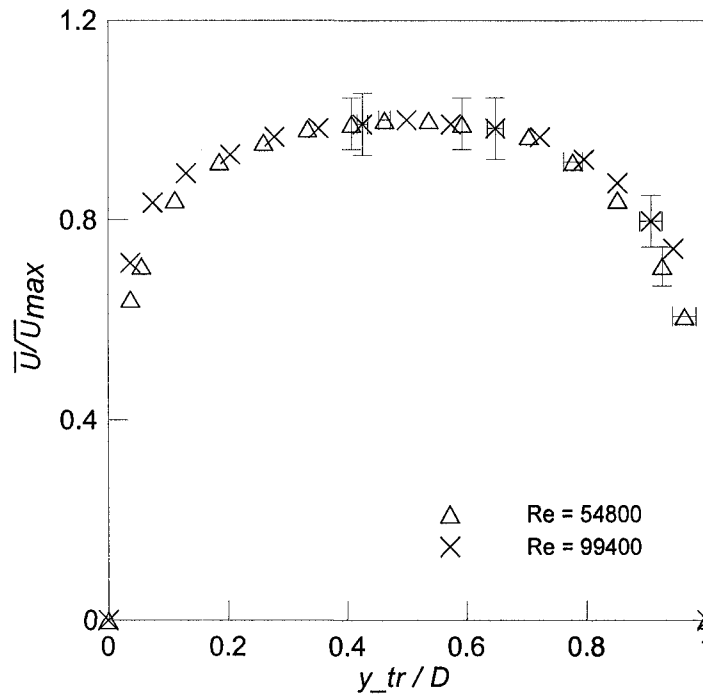


Figure 5.10 Axial mean velocity normalized by the centerline velocity as a function of the distance from one side of the circular duct.

The flow profile also checked at $4D$ upstream from the exit. The instantaneous velocity measured using hot wire anemometer system at a single point, which was selected randomly at $0.75D$ distance from the inner side of the duct. The sample was collected at a rate of 10 kHz with a period of 6.5 sec. The velocity variation with time is shown in Figure 5.11. A time averaging of the instantaneous velocity is also quantified by dividing the velocity data into three different time durations, $t_1 = 0$ to 2 sec, $t_2 = 0$ to 4 sec and $t_3 = 0$ to 6.5 sec. The obtained time average velocity is 1.501 m/s, 1.502 m/s and 1.501 m/s

respectively. It is observed that the point velocity measured using velocity meter at this point was 1.51 m/s, which is approximately 5.3% higher than that of the hot-wire.

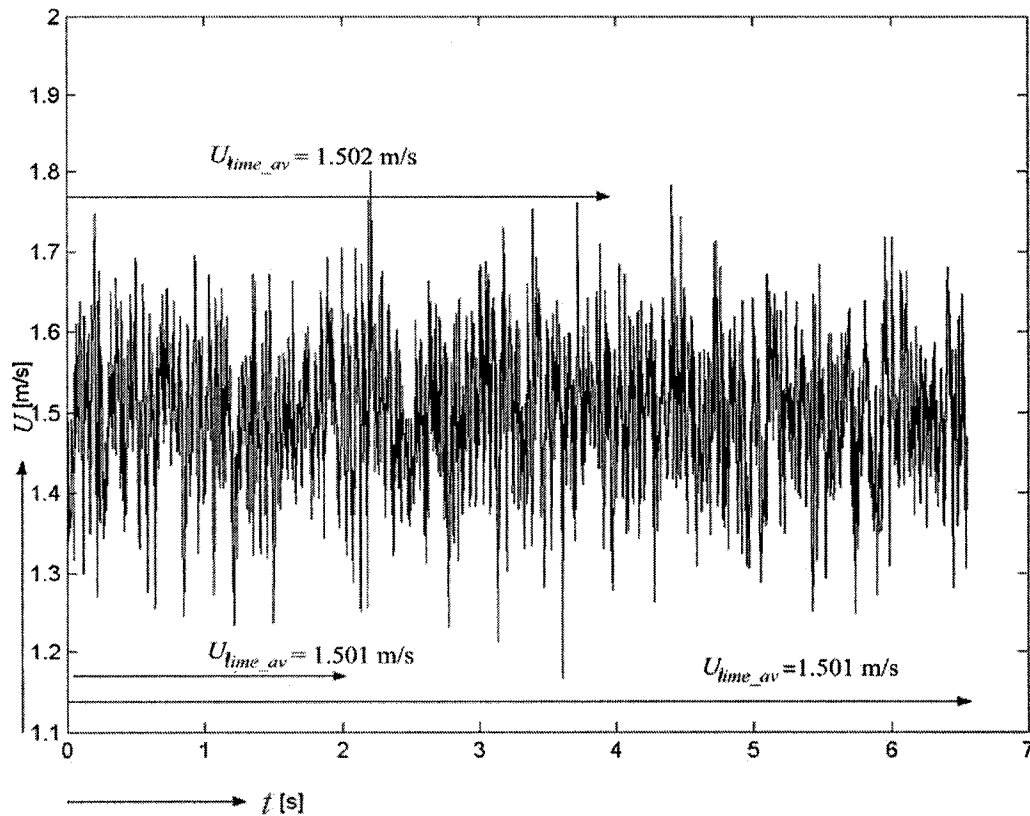
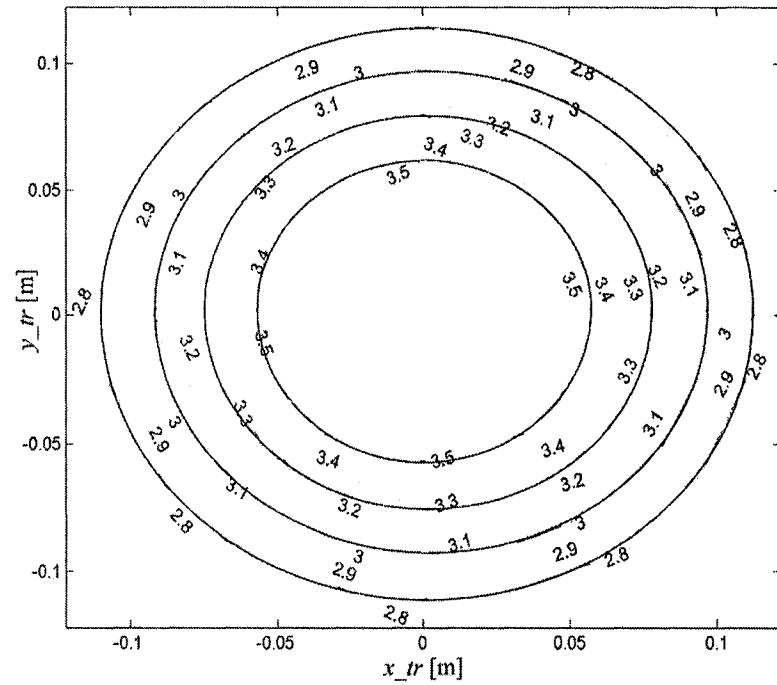


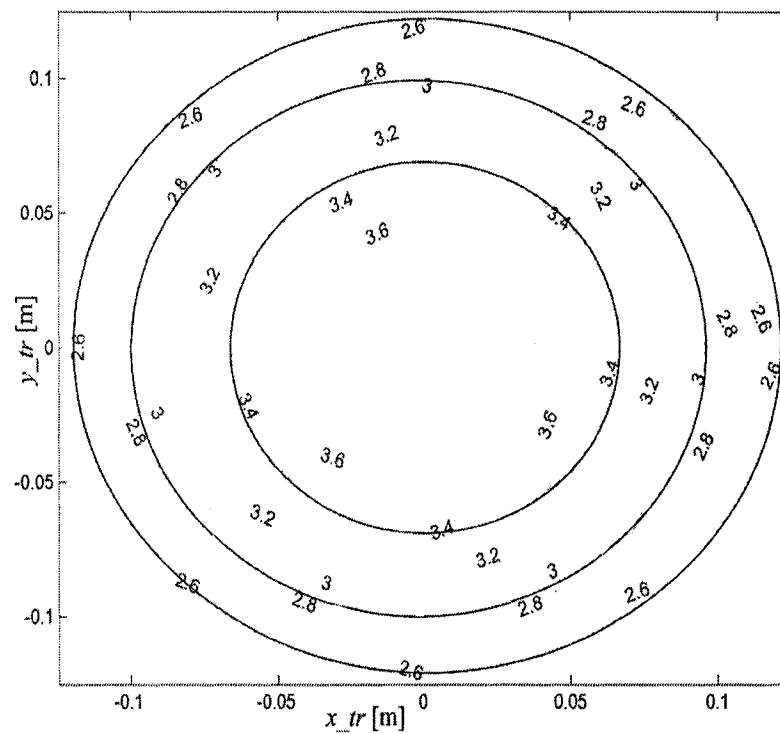
Figure 5.11 Instantaneous velocity at $4D$ upstream from the exit.

5.2.2 Accuracy of Equal Area and Log-Tchebycheff on mean velocity deduction

The experimental data for $Re = 54800$ obtained using six-point Equal Area and Log-Tchebycheff methods are depicted in Figure 5.12. Figure 5.12(a) presents the velocity distribution using the Equal Area method, whereas Figure 5.12(b) corresponds to the Log-Tchebycheff method. The velocity contours obtained through these two methods are similar, but the extent of deviation is more for the Equal Area method. The estimated uncertainty for point velocity varied from 5.15% to 6.15% in all cases; see Appendix A.



(a) Equal Area.



(b) Log-Tchebycheff.

Figure 5.12 Air velocity contour for $Re = 54800$ using six-point traversing at $4D$ upstream from the exit (a) Equal Area (b) Log-Tchebycheff.

Figure 5.13 depicts the effect of number of measurement points on the Equal area and Log-Tchebycheff techniques at $Re = 54800$. To get the profiles for the entire cross section, the measurements were extended beyond the measuring grids defined by both the Equal Area and Log-Tchebycheff methods to cover the distance up to the duct wall. As the circular duct is small ($D = 26.6$ cm), the difference between the measurement points specified in Equal Area method and those specified in the Log-Tchebycheff method is small. In case of six points traversing, the distance of the first three points from the duct wall are 11.5 mm, 39.1 mm and 78.7 mm for the Equal Area method, whereas those are 8.5 mm, 36.7 mm and 83.0 mm for the Log-Tchebycheff method.

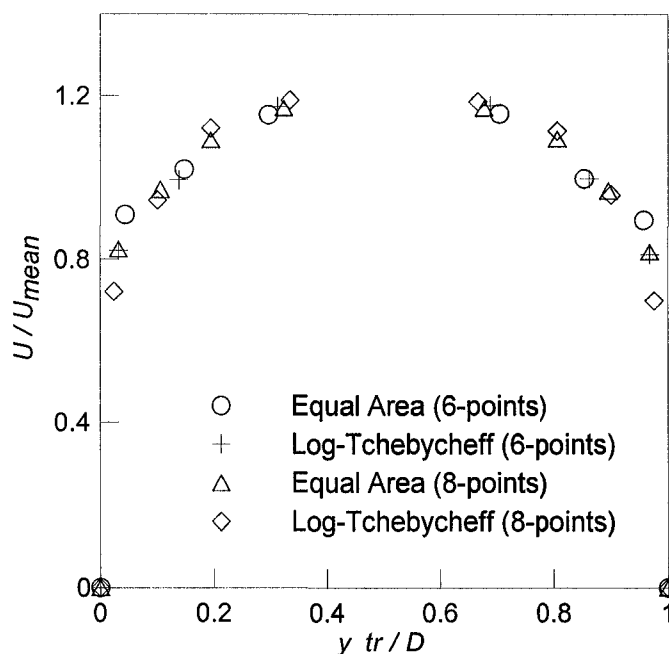


Figure 5.13 The effect of measurement points on the accuracies of Equal Area and Log-Tchebycheff methods ($Re = 54800$).

Figure 5.14 depicts the velocity profiles (3-dimensional plot) for the case of $Re = 99400$. Figure 5.14(a) presents the velocity profile for the six-point Equal Area traversing, whereas Figure 5.14(b) depicts the six-point Log-Tchebycheff traversing.

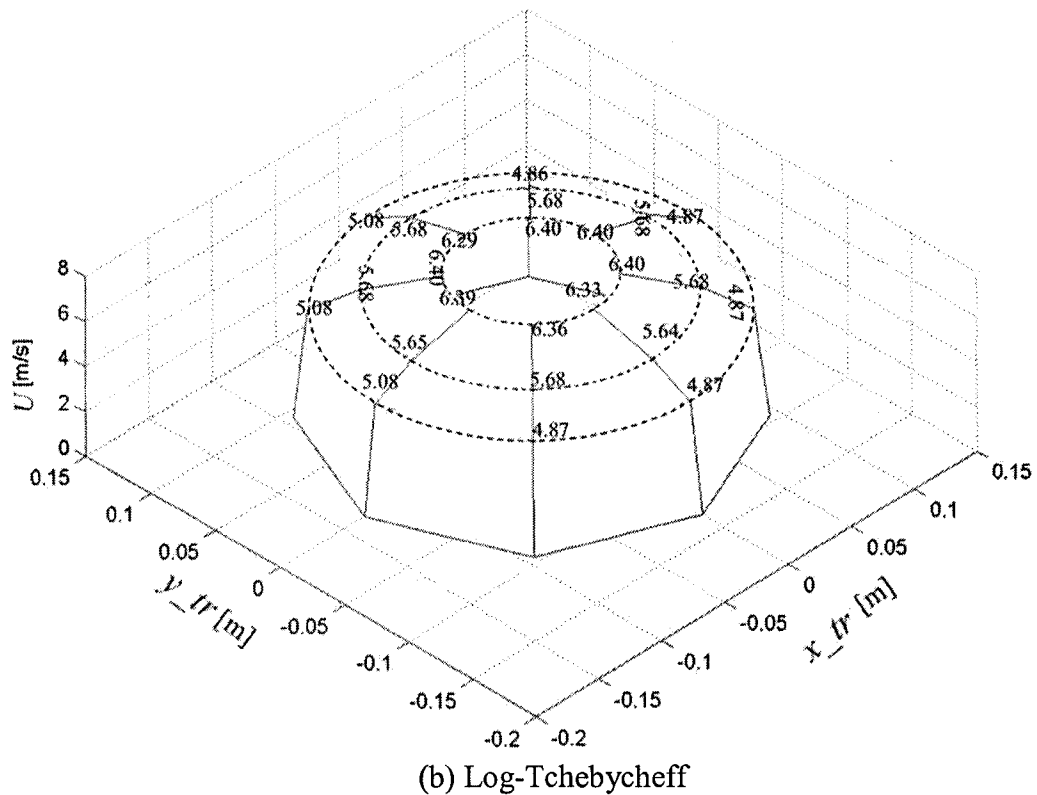
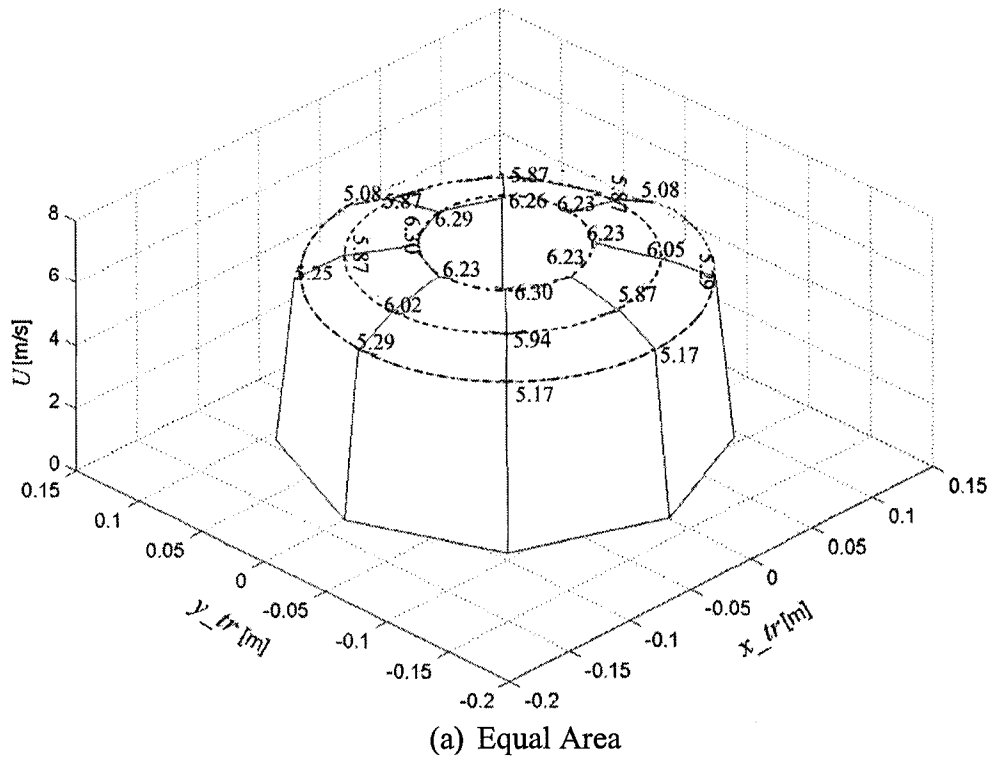


Figure 5.14 Air velocity contour for $Re = 99400$ case using six-point traversing at $4D$ upstream from the exit (a) Equal Area (b) Log-Tchebycheff.

The velocity profiles shown in Figure 5.15 by the error bars considering 95% reliability intervals for $Re = 24400$ and 54800 . Figure 5.15(a) presents the profiles for $Re = 24400$ case, the mean velocity deduced using Equal Area methods differs than that of Log-Tchebycheff method by 2.0% for six-point traversing, whereas 1.5% for eight-point traversing. It is also observed that the mean velocity over predict slightly with reference velocity of 1.397 m/s in both cases; 3.06% in case of Equal Area method, whereas 1.02% in case of Log-Tchebycheff method. Figure 5.15(b) depicts the profiles for $Re = 54800$ case. The mean velocity calculated using Equal Area technique differs about 2.20% to 2.67% from the reference velocity of 3.08 m/s, whereas -0.41% to -0.69% in case of Log-Tchebycheff technique. The profiles obtained using six points traversing for Equal Area and Log-Tchebycheff methods, are similar in both cases; see Figure 5.15.

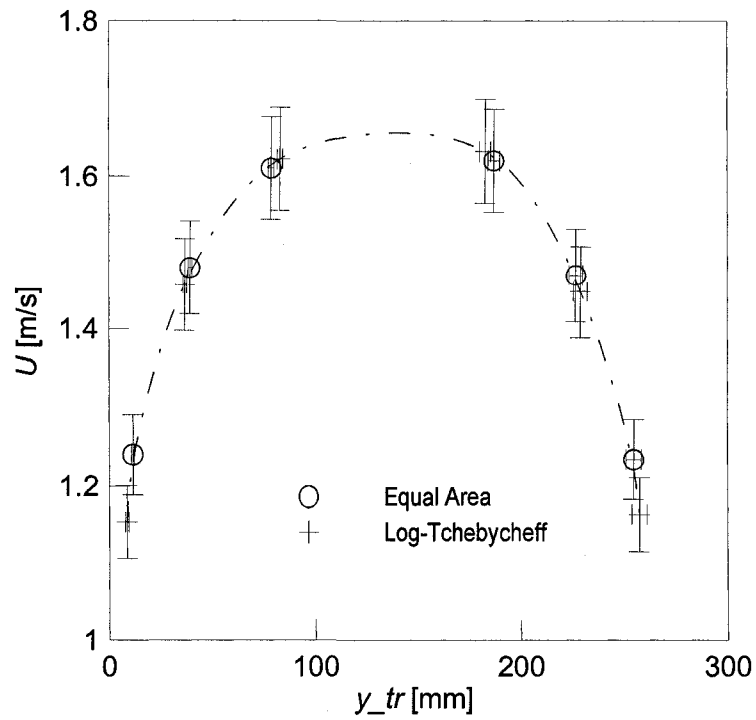
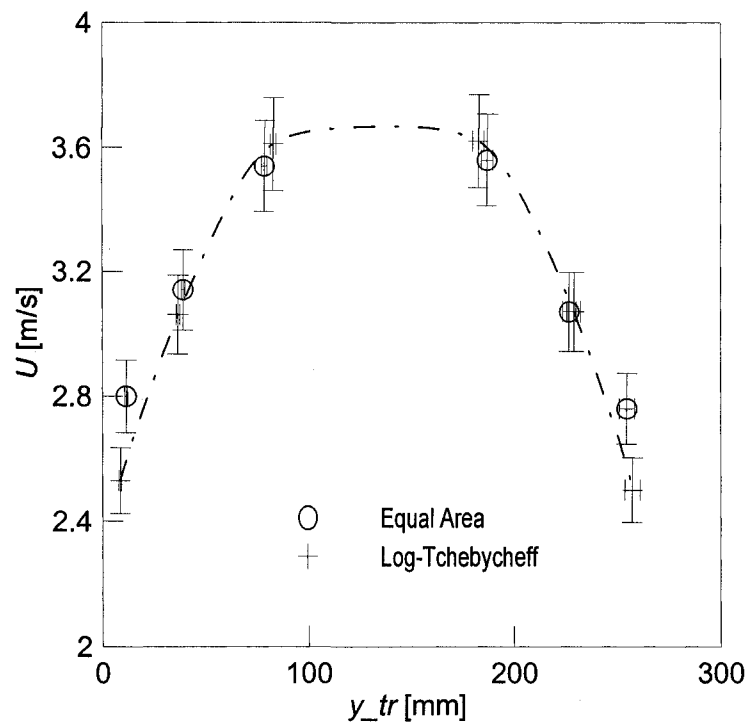
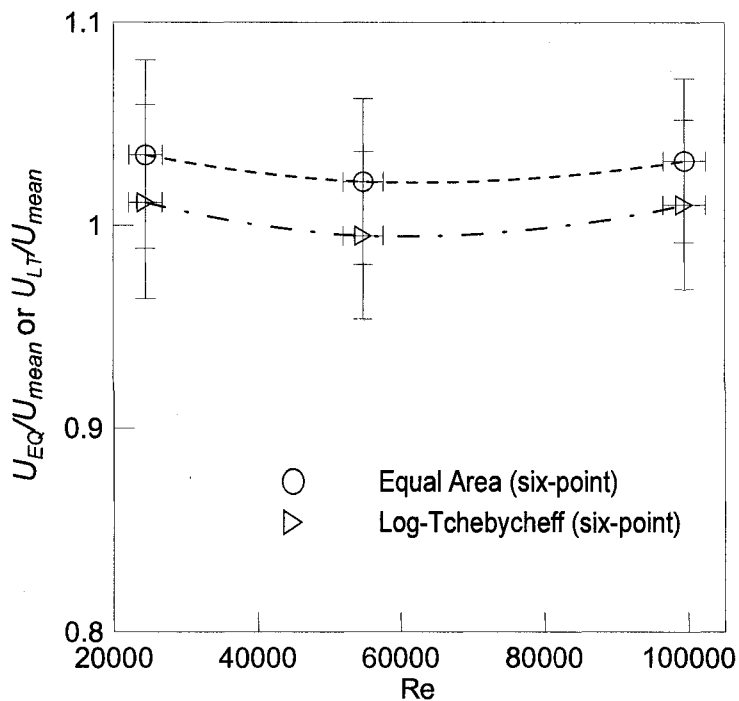
(a) $Re = 24400$.(b) $Re = 54800$.

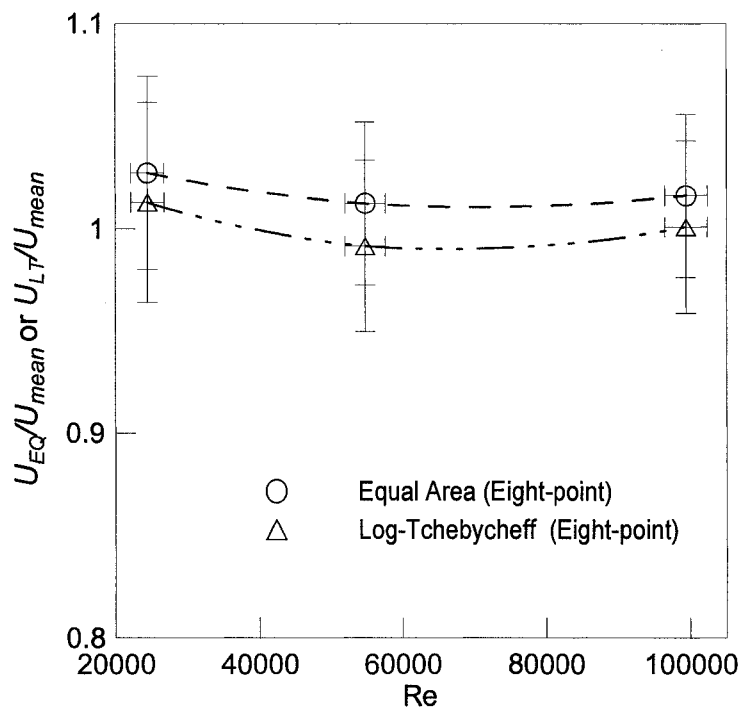
Figure 5.15 Velocity profile using Equal Area and Log-Tchebycheff six-point traversing

(a) $Re = 24400$ (b) $Re = 54800$.

The effect of the number of measurement points on the accuracies of Equal Area and Log-Tchebycheff methods were also observed experimentally. The six and eight points per diameter traversing for different Re depicted in Figures 5.16 and 5.17 respectively. In all cases ($Re = 24000$ to 100000), the mean velocities using Equal Area method are about 2 to 4% higher than the reference velocities, whereas the mean velocities obtained by the Log-Tchebycheff method are varied from -0.7% to $+1.02\%$ with the reference values. It is observed that the increase the number of measurement points per diameter does not affect the accuracy of the Log-Tchebycheff methods over the Re of 24000 to 100000; see Figure 5.17. On the other hand, increasing the number of measurement points in Equal Area method, decreases the over prediction slightly.



(a) Six points per diameter.



(b) Eight points per diameter.

Figure 5.16 Effects of number of measurement points and Re on the accuracies of Equal Area and Log-Tchebycheff methods (a) Six-point (b) Eight-point.

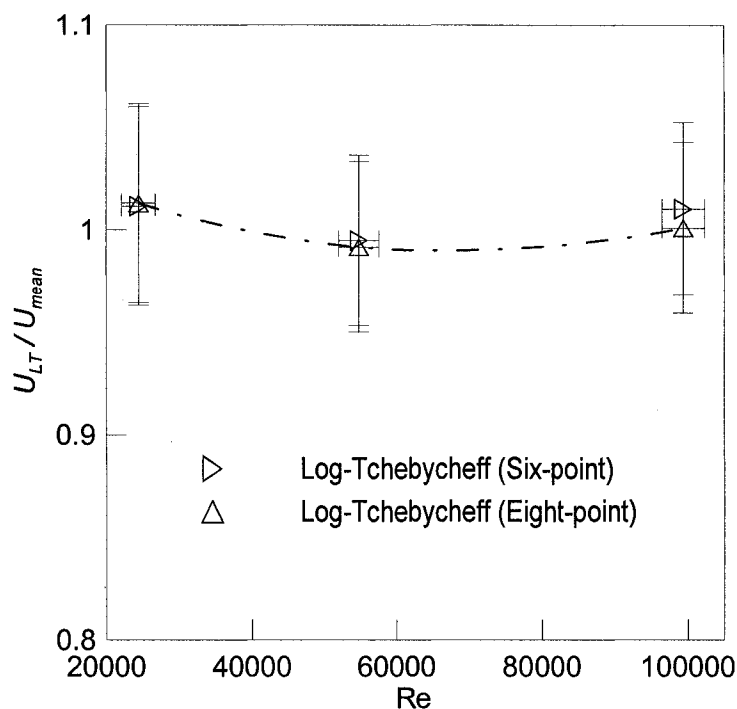


Figure 5.17 Effects of measurement points and Re on the accuracies of Log-Tchebycheff methods.

5.2.3 Accuracy of Equal Area and Log-Tchebycheff on airflow rate calculation

The volumetric airflow rate using the mean velocity deduced from the Equal Area and Log-Tchebycheff methods are shown in Table 5.6. Table 5.6 depicts the airflow rates calculated using the Equal Area method is overestimated by 2 to 4%, whereas the flow rates obtained using the Log-Tchebycheff method are varied from a negative value of -0.69% to a positive value of 1.02% with the reference flow rates. The above all uncertainty was estimated as 5.5 to 12%; see Appendix A. Further, in the case of $Re = 54800$, the air flow rate obtained using the Equal Area method over predicts 2.67% for six-point traversing and 2.20% for eight-point traversing, whereas the Log-Tchebycheff method under predicts the flow rate with 0.41% and 0.69% for six and eight points

traversing respectively. Again, in case of $Re = 24400$ and 99400 , the flow rates are higher than reference values corresponds to the respective Re by both methods. Nevertheless, the flow rates obtained with the Log-Tchebycheff method are more consistent and within $\pm 1\%$ error with reference flow rates; see Table 5.6. The error was calculated as

$$\text{Error} = \frac{Q - Q_{ref}}{Q_{ref}} \times 100\%, \quad (6.1)$$

where, $Q \approx Q_{EQ}$ or Q_{LT} ; Q_{EQ} is the flow rate deduced using Equal Area, Q_{LT} is the flow rate deduced using Log-Tchebycheff method and Q_{ref} is the reference flow rate calculated using venturi meter.

Table 5.6 Accuracies of the Equal Area and Log-Tchebycheff methods in estimating the volumetric airflow rate.

		Equal Area				Log-Tchebycheff			
		Six-point		Eight-point		Six-point		Eight-point	
Re	Q_{ref} [m ³ /s]	Q_{EQ} [m ³ /s]	Error [%]	Q_{EQ} [m ³ /s]	Error [%]	Q_{LT} [m ³ /s]	Error [%]	Q_{LT} [m ³ /s]	Error [%]
24400	0.0782	0.0806	3.06	0.0802	2.56	0.0790	1.02	0.0790	1.02
54800	0.1724	0.1771	2.67	0.1762	2.20	0.1717	-0.41	0.1712	-0.69
99400	0.3141	0.3240	3.15	0.3192	1.62	0.3173	1.02	0.3144	0.10

5.3 Comparison of numerical results with experimental results

The experimental velocity profiles were compared with the simulated profiles over a range of Re from 20000 to 55000. The profile obtained from the experiment ($Re = 24400$) is verified with the numerical result ($Re = 20000$) and some available literature [Benedict, 1980]; see Figure 5.18. The results show a good agreement.

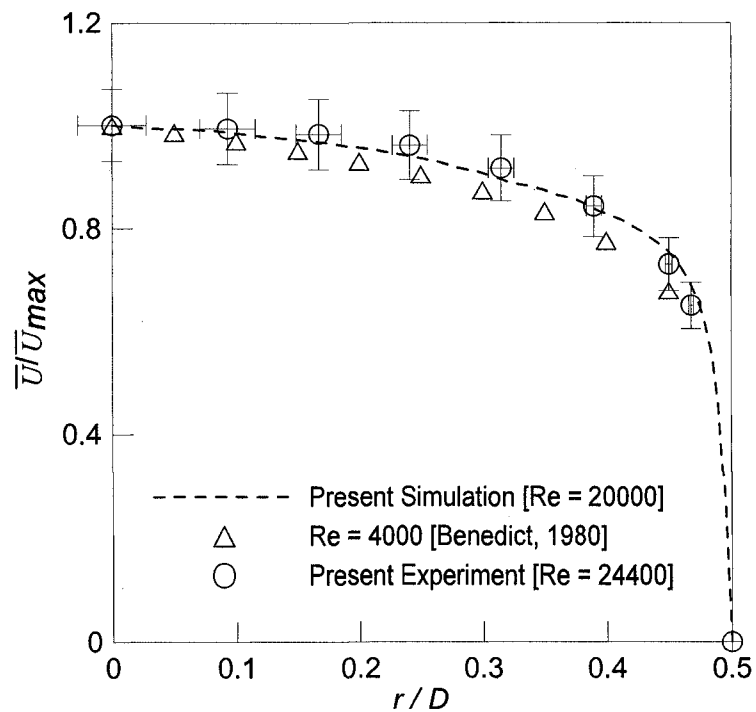
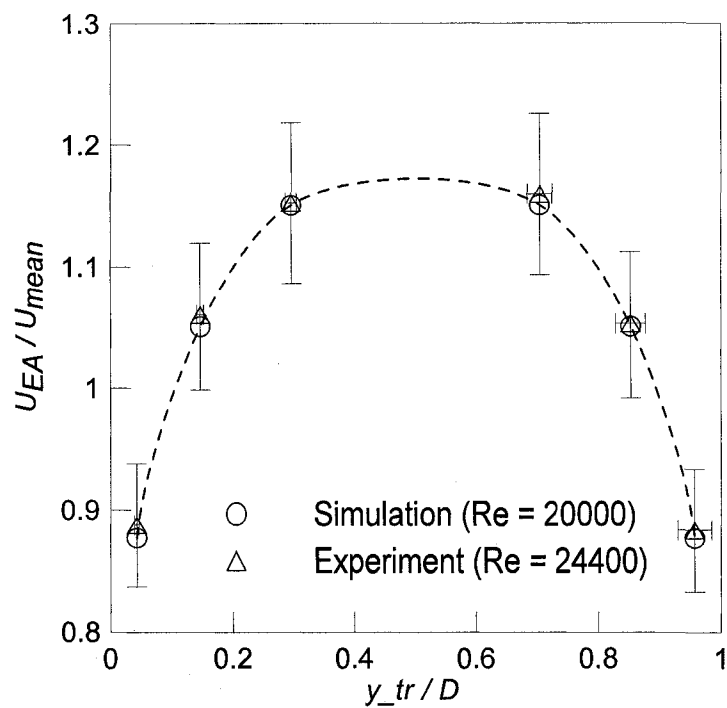
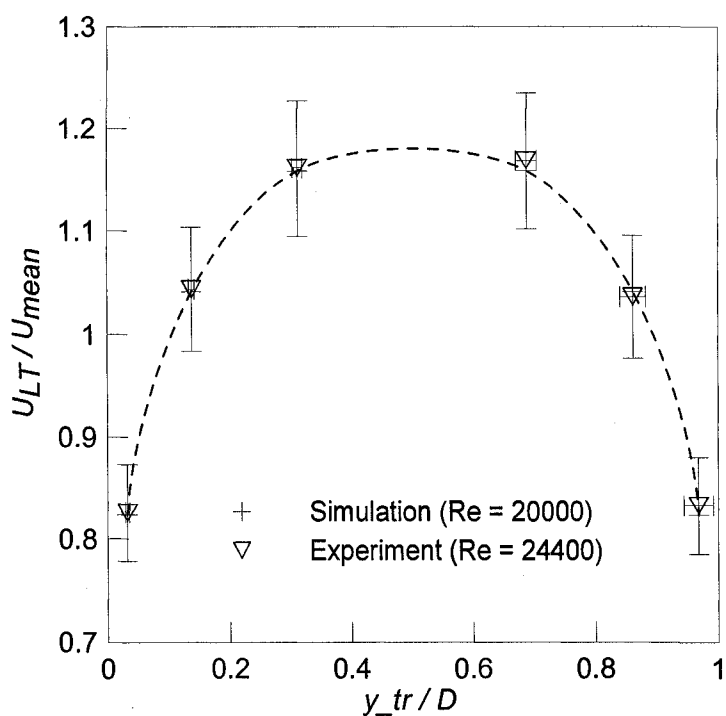


Figure 5.18 Comparison of normalized axial mean velocity as a function of the distance from the center of the duct

Figures 5.19 and 5.20 represent the point velocities normalized by the reference/mean velocity from experimental investigations and numerical simulations. The experimental data was collected at $29D$ from the air straightener, which was the distance from entrance of the duct in simulation. Figures 5.19(a) and 5.20(a) represent the profiles for the Equal Area method, whereas Figures 5.19(b) and 5.20(b) represent the profiles for the Log-Tchebycheff method. The difference between the numerical and experimental results seems to come within the range of experimental uncertainty for all y_{tr}/D , where y_{tr} is the distance from one side of the duct to another side. Eventually, it is referred that the velocity profiles obtained using both the Equal Area and Log-Tchebycheff methods, whether experiment or numerical simulation, are similar.

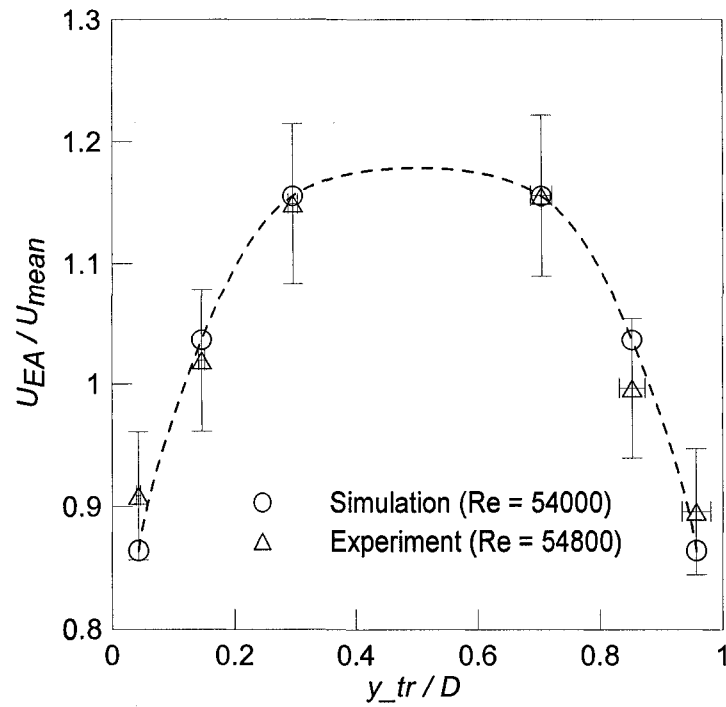


(a) Equal Area

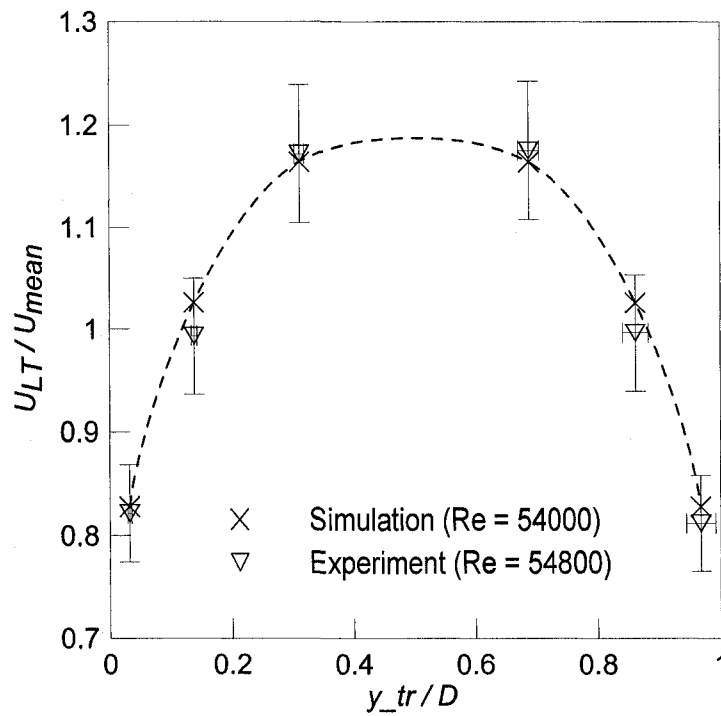


(b) Log-Tchebycheff

Figure 5.19 Comparison of numerical simulation at $Re = 20000$ and experimental investigation at $Re = 24400$ (a) Equal Area (b) Log-Tchebycheff.



(a) Equal Area method



(b) Log-Tchebycheff method.

Figure 5.20 Comparison of numerical simulation at $Re = 54000$ and experimental investigation at $Re = 54800$ (a) Equal Area method (b) Log-Tchebycheff method.

Figure 5.21 represents the accuracies of the Equal Area and Log-Tchebycheff methods on the estimation of the volumetric flow rate through a circular duct. The volumetric flow rate normalized with the reference flow rate (Q_{EQ}/Q_{ref} or Q_{LT}/Q_{ref}) from the experimental investigations and numerical simulations for the range of $Re = 20000$ to 55000 depicts in Figure 5.21. It is observed that all the cases except experimental Log-Tchebycheff technique (six points or eight points per diameter) for $Re = 54400$, over estimate the flow rate; see Table 5.5 and Table 5.6. The uncertainty bars shown in Figure 5.21 only for experimental results, which indicate the variations of experimental result, are within range of simulated results. Above all, the excellent agreement between the numerical predictions and the experimental results over the entire range of Re indicates that the Log-Tchebycheff method provides a better accuracy in volumetric flow rate estimation through a circular duct.

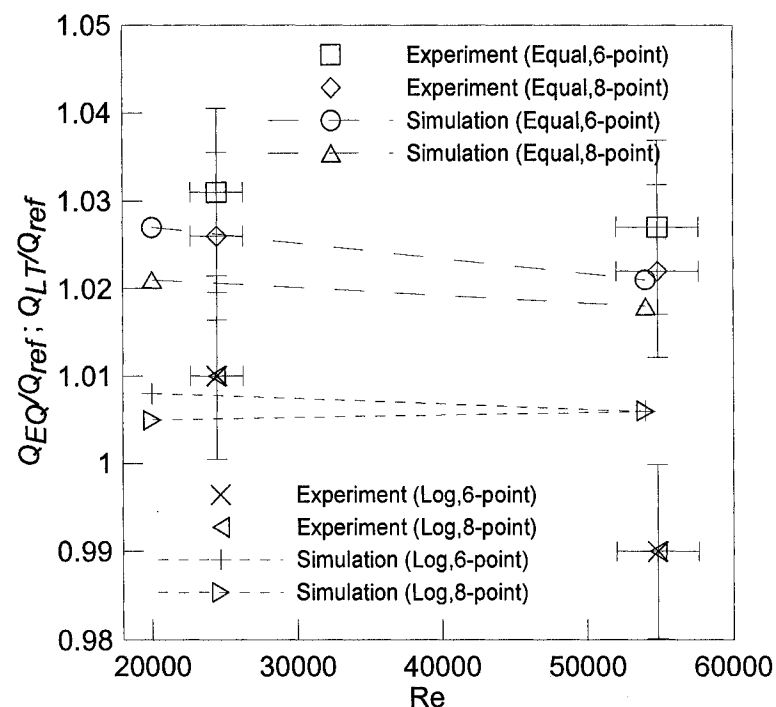


Figure 5.21 Effect of measurement points on the accuracies of Equal Area and Log-Tchebycheff methods for different Re .

CHAPTER 6

CONCLUSIONS AND RECOMMENDATIONS

The volumetric airflow rate estimations using Equal Area and Log-Tchebycheff methods through a circular duct were studied numerically and experimentally over a range of Reynolds numbers. The numerical simulations were performed for Re of 200 to 54000 using FLUENT 6.1, whereas the experimental investigations were conducted for Re from approximately 20000 to 100000. The numerical simulations were conducted 2-dimensionally with a uniform entrance velocity into a straight circular duct of $60D$ length by invoking the laminar model for $Re = 200$ to 2300 , and the “standard κ - ϵ ” model for the range of Re from 2300 to 54000 . The accuracies of the Equal Area and Log-Tchebycheff methods in estimating the volumetric flow rate were evaluated at $20D$, $40D$ and $60D$ downstream of the duct entrance with the simulated velocity profiles. On the other hand, the experimental investigations were conducted by blowing air through a straight circular duct of $35D$ ($D = 0.266$ m) length for Re of 24400 , 54800 and 99400 . The flow rate deduced using Lambda Square (model 2300) venturi meter was utilized as the reference for assessing the accuracies of the Equal Area and Log-Tchebycheff techniques. The estimated flow rates from the experiments were also compared with those of simulations. The following conclusions and recommendations are summarized from the numerical simulations and experimental observations.

6.1 Conclusions

The following conclusions can be drawn from the 2-dimensional numerical simulations.

- The fully developed entrance length, the ratio U_{mean}/U_{max} and the mean velocity profile at fully developed zone agreed well with analytical results and available published data. The mean flow properties (i.e., U_C/U_{mean} , U_{mean}/U_τ , U_C/U_τ etc) were also verified with some previous findings.
- The simulated friction coefficients for different Re agreed well with some theoretical and available results.
- In the laminar regime (Re = 200 to 2300), the Equal Area method was found to estimate the volumetric flow rate more accurately, in which the percentage error varied from 0 to 0.67%. On the other hand, the Log-Tchebycheff method tends to under-predict flow rate slightly, - 1.19 to -2.98%.
- In the turbulent regime (Re = 5300 to 54000), the Equal Area method over-predicts the flow rate by 1.83% to 3.32%, while the Log-Tchebycheff method predicts the actual flow rate relatively well; the error varies from -0.40 to 0.78%.
- Increasing the number of measurement points helps in reducing the volumetric flow rate under- or over-estimations, especially when these errors are significant. In other words, increasing the number of traverse points from six to eight reduces the under-estimation of the Log-Tchebycheff method in the low

Re regime i.e., -2.98% to -1.19% for Re = 200 case and the over-estimation of the Equal Area method in the high Re range i.e., 3.32% to 2.10% for Re = 5300 case respectively.

The followings are the main conclusions drawn from the experiments.

- The volumetric airflow rates deduced using Equal Area method over-predicts with respect to the reference value obtained from the venturi meter. The over-predictions are 3.06%, 2.67% and 3.15% using six points traversing and 2.56%, 2.20% and 1.62% using eight points traversing for Re of 24400, 54800 and 99400 respectively.
- In case of the Log-Tchebycheff method, the estimated airflow rates are within $\pm 1\%$ with respect to the reference flow rates. The deviations are 1.02%, -0.41% and 1.02% using six points traversing and 1.02%, -0.69% and 0.10% using eight points traversing for Re of 24400, 54800 and 99400 respectively.
- The overall uncertainty was estimated to be 5 to 12%. Thus, while Log-Tchebycheff method shows a better accuracy than the Equal Area method, the differences between those two methods and the corresponding difference from the reference (venturi meter) flow rate are smaller than this overall uncertainty. This is probably one reason behind the continuous Log-Tchebycheff versus Equal Area disputes.

6.2 Recommendations

The followings are possible undertakings for future work on volumetric airflow rate estimation.

- Expand the study over a wider range of Reynolds number.
- Extend this study to include the square or rectangular ducts.
- Study the effect of bend on the accuracies of Equal Area and Log-Tchebycheff methods.
- Investigate the effect of damper for different duct geometry, i.e., circular, square and rectangular ducts.

REFERENCES

- AABC, National standards for total system balance, Associated Air Balance Council, Washington, D.C., 2002.
- Abernethy, R.B., Benedict, R.P., and Dowdell, R.B., ASME measurement uncertainty. J. Fluids Engg., Trans. ASME., v.107, p.161-164, 1985.
- Aichlen W. The geometric place of the mean velocity for the turbulent flow in smooth and rough pipes, Z.F. Naturforschung, v.2, p.108-110, 1947.
- Akashi, K., Watanabe, H. and Koga, K., Flow Rate Measurement in Pipe Line with Many Bends, Technical Review, Mitsubishi Heavy Industries, Ltd., 1978.
- Alnor, A practical guide to performance measurements in mechanical, Heating, Ventilating and Air Conditioning systems, www.alnor.com/downloads/handbooks/2980237A_Alnor_HVAC_Handbook_2004.pdf, 2004.
- ANSI/ASME 19.1-1985, Measurement Uncertainty-part 1, American National standard, New York, 1990.
- ANSI/ASHRAE 51-1999, Laboratory Methods of Testing Fans for Aerodynamic Performance Rating, An American National Standard, 1999.
- ASHRAE Standard 111-1988, Practices for Measurement, Testing, Adjusting, and Balancing of Building Heating, Ventilation, Air-Conditioning, and Refrigeration Systems, American Society of Heating, Refrigeration and Air Conditioning Engineers, Atlanta, Ga., 1988.
- ASME, Measurement uncertainty for fluid flow in closed conduits, American Society of Mechanical Engineers, New York, 1983.

- ASME, Fluid Meters: Their theory and Application, American Society of Mechanical Engineers, New York, 1971.
- ASME, Hydraulic Prime Movers, Power Test Codes P.T.C. 18-1949, American Society of Mechanical Engineers, New York, p102-142, 1949.
- Austin, S.B., Chilled water system optimization, ASHRAE Transactions 35, 7, 50-56, 1993.
- Benedict, R.P., Fundamentals of Pipe Flow, John Wiley & Sons, Toronto, 1980.
- Blasius H., Das Ähnlichkeitsgesetz bei Reibungsvorgängen in Flüssigkeiten. Forsch. Arb. Ing.-Wes., Berlin, 131-137, 1913.
- Boussinesq, J. Theory of the turbulent flow, Mem.Pre.par.div.Sav, 23, Paris, France, 1877.
- B.S.I. 1042, Methods for the measurement of fluid flow in pipes, British Standards Institution, London, 1973.
- Bradshaw, P., An Introduction to turbulence and its measurement, Pergamon Press Oxford, 1971.
- Browne, L.W.B. and Dinkelacker, A., Turbulent pipe flow: pressures and velocities, Fluid Dynamics Research, v.15, p.177-204, 1995.
- Bruun H.H., Hot-Wire Anemometry, Oxford University press. New York, 1995.
- Bureau of Metrology, <http://www.bom.gov.au/climate/glossary/wetbulb.shtml>, Climate Glossary, Australian Government, 2005.

- Burgess, W.A., Ellenbecker, M.J. and Treitman, R.D., Airflow measurement techniques in ventilation for control of the work environment, John Wiley & Sons, Inc., 2nd Edition, p.43-89, 2004.
- Chen, Q., Indoor Airflow, Air Quality and Energy Consumption of Buildings, thesis, Delft University of Technology, Delft, The Netherlands, 1988.
- Chen, Q., Comparison of different k- ϵ models for indoor airflow computations, Num. Heat Transfer, v.28 part B, p.353-369, 1995.
- Cheremisinoff, N.P., Practical fluid dynamics for Engineers and Scientists, Technomic Publishing Company, 1990.
- Cheremisinoff, N.P., Applied Fluid Flow Measurement-Fundamentals and Technology, Marcel Dekker Inc., New York and Basel, 1979.
- Chow, T.T., Zhang, Q.G., Lin, Z., and Song, C.L., Global optimization of absorption chiller system by generic algorithm and neural network, Energy and Buildings, v.34, p.103-109, 2002.
- Coffin J., Mesures des débits en grandes sections. Partie 1: Methode d'integration entièrement numérique des courbes de séparation des vitesses, ICMG report No. 20, 1966.
- Colebrook, C.F., Turbulent Flow in Pipes, with particular reference to the transition between the smooth and rough pipe laws, J. Inst. Civ. Lond., v.11, p.133-156, 1939.
- Coleman, H.W. and Steele, W.G., Experimentation and uncertainty analysis for engineers, John Wiley & Sons, New York, 1989.

Dally, J.W., Riley, W.F. and McConnel, K.G., Instrumentation for Engineering measurements, John Wiley & Sons, New York, 1984.

Das, H.K. and Quarmby, A., Displacement effects on pitot tube at low speeds, J. Roy. Aero. Soc., v58, p.837-851, 1969.

Editorial, Journal of Heat Transfer: Policy on Reporting Uncertainties in Experimental Measurements and Results, Journal of Heat Transfer, Trans. ASME, v.115, p.5-6, 1993.

Editorial, Journal of Fluids Engineering: Policy on reporting uncertainties in experimental measurements and results, Journal of Fluids Engineering, Trans. ASME, v.113, p.313-314, 1991.

Eggels, J. G. M., Unger, F., Weiss, M. H., Westerweel, J., Adrian, R. J., Frienrich, R. and Nieuwstadt, F. T. M., Fully developed turbulent pipe flow: a comparison between direct numerical simulation and experiment, J. Fluid Mech., v268, p175-209, 1994.

Environmental Protection Agency (EPA) of United States and the United States Consumer Product Safety Commission (CPSC) Office of Radiation and Indoor Air, The inside story: A guide to indoor air quality (6604J), EPA Document #402-k-93-007, <http://www.epa.gov/iaq/pubs/insidest.html>, April 1995.

Figliola, R.S. and Beasley, D.E., Theory and design for mechanical measurements, 3rd edition, John Wiley & Sons, Inc., New York, 2000.

Fisk, W. and Rosenfeld A., Estimates of improved productivity and health from better indoor environments, International Journal of Indoor Air Quality and Climate, v.7, p.158-172, 1997.

Flow Kinetics LLC., Using a Pitot-static tube for velocity and flow rate measurement, www.flowmeterdirectory.com/flowmeter_artc/flowmeter_artc_02111201.html, 2002.

Fluent Inc, FLUENT 6.1 User Guide, 2003.

Fox, R.W., McDonald, A.T., Introduction to fluid mechanics. Toronto: John Wiley & Sons; 1998.

Gladstone, G. and Bevirt, W.D., HVAC testing, adjusting, and balancing manual, 3rd Edition, New York, McGraw-Hill, 1996.

Harris, R.D., Technical Note 001, Water level accuracy and correcting for errors due to gravitational acceleration and liquid density, In-Situ Inc, 2005.

Health Canada, Publications on health and air quality; Dampness, mold and indoor air, Air health effects div, http://www.hc-sc.gc.ca/english/iyh/environment/indoor_air.html, 2004.

Hooper, L.J., Calibrations of Six Beth-Flow Meters at Alden Hydraulic Laboratory, Worcester Polytechnic Institute, Transactions of the ASME, p.1099-1110, 1950.

Howell, R.H. and Sauer Jr., H.J., Field measurement of air velocity: Pitot traverse or vane anemometer?, ASHRAE Journal, p.46-52, 1990.

ISO 3354, Measurement of fluid flow in closed conduits, International Organizations for standardization, 1988.

ISO 5168, Measurement of fluid flow - Estimation of uncertainty of a flow - Rate measurement, International Organizations for standardization, 1978.

ISO 5167, Measurement of fluid flow by means of pressure differential devices, Part 1: Orifice plates, nozzles and venturi tubes inserted in circular cross-section conduits running full, Reference number: ISO 5167-1, 2003.

- Jaakkola, J.J.K., Heinonen, O.P. and Seppänen O., Sick building syndrome, sensation of dryness and thermal comfort in relation to room temperature in an office building: need for individual control of air temperature, *Environment International*, v15, p.163-168, 1989.
- Joseph, E. B., III, P.E., To Use Log-Tchebycheff or Not to Use Log-Tchebycheff, Is That the Question? *TAB journal*, p.2-5, summer 2001.
- Khan, M.G., Study of cross flow cooling and heating of air via an in-line elliptical tube array heat exchanger, A MASc. thesis, University of Windsor, Ontario, Canada, 2004.
- Kim, J., Moin, P. and Moser, R., Turbulent statistics in fully developed channel flow at low Reynolds number, *J. Fluid Mech.*, v.177, p.133-166, 1987.
- King, L.V., On the convection of Heat from small Cylinders in a Stream of Fluid, *Phil. Trans. Soc.*, A214, p.373-384, 1914.
- Kinghorn, F.C., Mchugh, A., and Duncan, W., An experimental comparison of two velocity area numerical integration techniques, *water power*, v.25, p.330-335, 1973.
- Kirkup, L., Calculating and Expressing Uncertainty in Measurement, Department of Applied Physics, Faculty of Science, University of Technology, Sydney, Australia, 2002.
- Klaassen, C.J. and House, J.M., Equal Area vs. Log-Tchebycheff, *HPAC Heating, Piping, Air Conditioning Engineering*, v.73, p.31-35, 2001.
- Kline, S.J. and McClintock, F.A., Describing uncertainties in single-sample experiments, *Mechanical Engineering*, v.75, p.3-8, 1953.
- Kline, S.J., The purpose of uncertainty analysis, *Journal of Fluids Engineering, Transaction of ASME*, v.107, p.153-160, 1985.

- Knudsen J.C. and Katz, D.L., Fluid dynamics and heat transfer, McGraw Hill, 1958.
- Kosonen, R. and Tan, F., The effect of perceived indoor air quality on productivity loss, Energy and Buildings, v.36, p.981-986, 2004.
- Lambda Square Inc., Model 2300 insert fiberglass venturi-Typical specification, Lambda Square Inc., New York, www.lambdasquare.com, 2005.
- Laufer, J., The structure of turbulence in fully developed flow, NACA Rep. 1174, 1954.
- Lauder, B.E., and Spalding, D.B., The numerical computation of turbulent flows, Comput. methods appl. Mech. Eng., v.3, p.269-289, 1974.
- Lee, S-C., Lee, J-H., and Oh, M-D., Measurement and predictions for the flow distribution of a complex duct system with loop for energy saving, Int. J. of Energy Research, v.25, p.263-273, 2001.
- Livsey, J.A., The behavior of transverse cylindrical and forward-facing total head probes in transverse total-pressure gradients, J. Aero. Sci., v.23, p.949-958, 1972.
- Lu, L., Cai, W., Xie, L., Li, S. and Soh, Y.C., HVAC system optimization-in-building section, Energy and Buildings, v.37, p.11-22, 2005.
- MacFerran, E. L., Equal Area vs. Log-Tchebycheff, Penton Publishing Co., p.26-31, Dec 1999.
- Macmillan, F.A., Experiments on Pitot tubes in shear flow, R. & M., 3028, 1956.
- Miller, R., Flow Measurement Engineering Handbook, McGraw-Hill, New York, 1983.

- Miner, I.O., Providence, R.I., The Dall Flow Tube, Transactions of the ASME, p.475-479, 1956.
- Moffat, R.J., Using uncertainty analysis in the planning of experiment, J. Fluids Engineering, Transaction ASME, v.107, p.173-178, 1985.
- Moyekens, S., and Muralikrishnan, R., Developing flow in a pipe, flowlab.fluent.com/exercise/pdfs/developing_flow_in_pipe01.pdf, 2003.
- Nieuwstadt, F.T.M., Turbulentie, Utrecht: epsilon uitgaven, The Netherlands, 1992.
- Nikuradse, J., The laws of turbulent flow in smooth pipes, Forschungsh. Ver. Dtsch. Ing. Ausgabe B, v.3, p.356-367, 1932.
- Osofsky, E., Constant temperature operation of the hot-wire anemometer at high frequency. Rev. Sci. Instr., v.123, p.393-413, 1948.
- Ower, E. and Pankhurst, R.C., The measurement of airflow, 5th edition, Pergamon Press, 1977.
- Patankar, S.V., Numerical heat transfer and fluid flow, Hemisphere, Washington, D.C., 1980.
- Perry, R.H. and Green, D.W., Perry's chemical engineering handbook, 7th edition, McGraw-Hill, New York, p.8-10, 1997.
- Richardson, G., Traversing for accuracy in a rectangular duct, TAB journal, p.20-27, summer 2001.
- Rohsenow, W.M, Hartnett, J.P and Cho, Y.I., Handbook of heat transfer, New York, McGraw-Hill, 1998.

Salami, L.A., Errors in the velocity area method of measuring asymmetric flows in circular pipes, Modern developments in flow measurement, ed. C. G. Clayton. Proc Int Conf., Harewell, p.381-400, 1971.

Schlichting, H., Boundary layer theory, 4th edition, McGraw-Hill, 1960.

Schwenk, D. M., Air flow measurement accuracy, US Army Corps of Engineers, Construction Engineering Research laboratories, p.1-27, 1997.

SEI, Swiss rules for Hydraulic Turbines, Swiss Electronic Committee publication, N0. 178e, p.36-40, 1947.

Sheet Metal and Air Conditioning Contractors National Association (SMACNA) Inc. HVAC Systems Testing, Adjusting and balancing, 1st edition, Virginia, USA, 1983.

Srinivasan, K., Measurement of air leakage in air-handling units and air conditioning ducts, Energy and Buildings, v.37, p.273-277, 2005.

Taylor, B.N. and Kuyatt, C.E., Guidelines for Evaluating and Expressing the Uncertainty of NIST Measurement Results, NIST Technical Note 1297, 1994.

Tennekes, H. and Lumley, J.L., A first course in turbulence, MIT Press, Cambridge, Massachusetts, USA, 1972.

Tsal, R.J. and Behls, H.F., Using the T-method for the duct system design, ASHRAE Journal, v32, no.3, p.30-45, 1990.

TSI Incorporated. Model 1129 Automated Air Velocity Calibrator, Fluid Mechanics Instrument Division. MN, USA, 2003.

- TSI Incorporated, Velocicalc portable air velocity meter, model-8345, MN, USA, 2002.
- TSI Incorporated, IFA 300 Constant Temperature Anemometer Systems, Fluid Mechanics Instrument Division, MN, USA, 2000.
- Unger, F. and Friedrich, R., Large eddy simulation of fully-developed turbulent pipe flow, Flow simulation of High Performance Computers I, NNFM, v.38, p.201-216, 1993.
- Versteeg, H.K. and Malalasekera, An introduction to computational fluid dynamics: The finite volume method, Prentice Hall, 1995.
- Ward-Smith A.J., Internal fluid flow, Oxford, Clarendon Press, 1980.
- Weather Underground, <http://www.wunderground.com/global/statins/71538>, the Weather Underground Inc., 2005.
- Weiss, M.H., Drag reduction with riblets in pipe flow, PhD thesis, University of Calgary, Canada, 1993.
- Weske, J.R., A hot-wire circuit with very small time lag, NACA Technical Note No. 881., 1943.
- Westerwell, J., Digital particle image velocimetry: theory and application, PhD thesis, Delft University of Technology, the Netherlands, 1993.
- Wheeler, A.J. and Ganji, A.R., Introduction to Engineering Experimentation, Prentice Hall, 1996.
- White, F. M, Viscous fluid flow, 4th edition, New York, McGraw-Hill, 1999.
- Wilcox, D.C., Turbulence modeling for CFD. California: DCW Inc; 1994.

Winternitz, F.A.L. and Fischl, C.F., A simplified integration technique for pipe-flow measurement, *Water Power*, v.9, p.225-234, 1957.

Wyon, D.P. Healthy Buildings and their impact on productivity, *Proc. Indoor Air'93*, v6, p.3-13, Helsinki, Finland, 1993.

Yavuzkurt, S., A guide to uncertainty analysis of hot-wire data, *Journal of Fluids Engg.*, v.106, p.181-186, 1984.

Zhu, J.Z. and He, G., Error estimation and uncertainty propagation in computational fluid mechanics, ICASE Interim Report No. 41, NASA/CR-2002-211744, 2002.

APPENDIX A

UNCERTAINTY ANALYSIS AND ERROR ESTIMATION

It is well-known fact in engineering that all measurements have errors, which originate from various sources. These errors are the differences between the measured value and the true value. Furthermore, the errors in experiment have two components: a fixed (bias) error and a random (precision) error [Wheeler and Ganji, 1996; Abernethy et al., 1985]. Depending on the experimental situations, the above-mentioned error limits have been identified based on some assumptions and considerations. The question is how to combine bias and precision errors raged over many committees in several societies i.e., ASME, SAE, ISA, ISO etc. The committee approval for combining is either addition or root-sum-square methods, which will be decided by the analyst and thereafter, a handful of studies [Khan, 2004; Coleman and Steele, 1989; Abernethy et al., 1985; Kline, 1985; Moffat, 1985; Yavuzkurt, 1984; Kline and McClintock, 1953] have been conducted on these issues. The guidelines have also been prescribed in some editorial [Kirkup, 2002; Taylor and Kuyatt, 1994; ASME journal of Heat Transfer Editorial, 1993; the ASME Journal of Fluids Engineering Editorial, 1991; ISO, 1978].

A.1 Evaluating Uncertainty

An experimental analysis may involve various sources in which errors may arise. One of the useful classifications of errors is accidental error, fixed error and mistake [Kline and McClintock, 1953], which are arbitrarily calibration errors, data acquisition

errors, data reduction errors and conceptual errors. Each of these sources exhibits the bias and precision components. The bias (B) and precision (P) errors were calculated by using root-sum-square (RSS) method as follows:

$$B = \pm\sqrt{B_1^2 + B_2^2 + B_3^2 + \dots + B_z^2} \quad (\text{A.1})$$

and

$$P = \pm\sqrt{P_1^2 + P_2^2 + P_3^2 + \dots + P_z^2} , \quad (\text{A.2})$$

where z is the total number of error sources. The RSS method, for combining, was used as [Coleman and Steele, 1989]

$$E = \pm\sqrt{B^2 + P^2} . \quad (\text{A.3})$$

In current study the errors incurred due to independent parameters that were measured directly using instruments for the experimental purpose and dependent parameters that were obtained from the independent parameters or thermo physical properties. The independent parameters are generally the basic dimensions of the duct (D) and the basic experimental variables U , T and P . The dependent parameters that are functions of the independent parameters are dimension of the duct (A) and the experimental parameters (Q_{ven} or Q_{ref} , U_{EA} , U_{LT} etc.).

In error determination for the independent parameters, the precision error is random in individual measurements and its estimation depends on the sample size, whereas the bias error is independent of sample size. The bias errors (B) were taken same as single measurement and the precision errors (P) were calculated from the statistical method using the standard deviation of the measurement. It is noted that the instruments'

resolution and accuracy were considered as the bias error [Coleman and Steele, 1989; Moffat, 1985].

In case of dependent variables, some measurand, F , depends on N quantities written as F_1 through to F_N , such that,

$$F = f(F_1, F_2, F_3 \dots \dots \dots F_N), \quad (\text{A.4})$$

where the quantities F_1, F_2, \dots, F_N , are measurands and may depend on other quantities. Note that sometimes the symbols F_1, F_2, \dots, F_N are used to represent quantities. At other times the same symbols are used to represent the true value of the quantities. The confidence level of the uncertainty for F should be same as confidence level of the uncertainty in the F_i 's.

The absolute uncertainty can be estimated as

$$E_F = \left[\sum_{i=1}^N \left(E_{F_i} \frac{\partial F}{\partial F_i} \right)^2 \right]^{1/2}, \quad (\text{A.5a})$$

where the partial derivatives $\sum_{i=1}^N \frac{\partial F}{\partial F_i}$ are derived from the functional relationship as deduced in Equation (A.4) and the uncertainties, E_{F_i} , are the uncertainties in the measured variables F_i , if independent calculated from Equation (A.3). The relative uncertainty is generally defined as:

$$\frac{E_F^2}{F^2} = \left(\frac{F_1}{F} \frac{\partial F}{\partial F_1} \right)^2 \left(\frac{E_{F_1}}{F_1} \right)^2 + \left(\frac{F_2}{F} \frac{\partial F}{\partial F_2} \right)^2 \left(\frac{E_{F_2}}{F_2} \right)^2 + \dots + \left(\frac{F_N}{F} \frac{\partial F}{\partial F_N} \right)^2 \left(\frac{E_{F_N}}{F_N} \right)^2, \quad (\text{A.5b})$$

where E_F/F is the relative uncertainty of the result and the factors, E_{F_i}/F_i are the relative uncertainties for each variables.

In current study, the measurement parameters were related to dimension of the duct and locations of the measuring point-velocity. For each test, the uncertainty was

carried out explicitly and independently. The sample calculations for the uncertainty are presented separately in the subsection.

A.2 Instrumental and Measurements' Uncertainty of Independent Parameters

The instruments used in the study have errors associated with them. The value of the interest variable measured repeatedly for accidental errors study and the data was recorded as:

$$F_j = \frac{1}{n} \sum_{i=1}^n F_i, \quad (\text{A.6})$$

where n = number of repeated measurements and $j = 1 \dots N$ (N = sample size). The sample mean (\bar{F}) and the sample standard deviation S_F of the interest parameters have been calculated as,

$$\bar{F} = \frac{1}{N} \sum_{j=1}^N F_j, \quad (\text{A.7})$$

and

$$S_F = \sqrt{\frac{1}{N-1} \sum_{j=1}^N (F_j - \bar{F})^2}. \quad (\text{A.8})$$

The standard deviation of the mean ($S_{\bar{F}}$) for the sample was deduced using the following relation,

$$S_{\bar{F}} = \frac{S_F}{\sqrt{N}}. \quad (\text{A.9})$$

The precision limit, P_{F_i} for a single measurement F_i was estimated as

$$P_{\bar{F}} = P_{dimension} = t_d \cdot S_{\bar{F}}, \quad (\text{A.10})$$

where t_d is a function of the 95% confidence level [Wheeler and Ganji, 1996]. In determining the t_d function, the degrees of freedom for individual parameters can be estimated as $(N-1)$. Besides, the degrees of freedom (w) can be estimated for combined precision index using Welch-Satterthwaite formula as [ANSI/ASME, 1990; ASME, 1983]

$$w = \frac{\left[\left(\frac{\partial F}{\partial F_1} \times S_{F_1} \right)^2 + \dots + \left(\frac{\partial F}{\partial F_N} \times S_{F_N} \right)^2 \right]^2}{\frac{\left(\frac{\partial F}{\partial F_1} \times S_{F_1} \right)^4}{\sqrt{w_{F_1}}} + \dots + \frac{\left(\frac{\partial F}{\partial F_N} \times S_{F_N} \right)^4}{\sqrt{w_{F_N}}}}, \quad (\text{A.11})$$

where, $S_{F_1} \dots S_{F_N}$ are the precision index for individual parameters and $w_{F_1} \dots w_{F_N}$ are the degrees of freedom for individual parameters. The following sections describe the error calculation of the independent parameters.

A.2.1 Uncertainties of diameter of the duct ($F = D$)

The diameter of the duct was measured for 31 populations using an ELECTRONIC digital caliper. The caliper has an instrumental error (i.e. the accuracy) of $B_{accuracy} = 0.00004$ m and an instrumental bias limit (i.e. the resolution) of $B_{resolution} = 0.00001$ m. According to Equation (A.1), the total bias error, which is fixed for any dimensional measurements related to this experiment, was estimated as:

$$B_{\bar{F}} = B_{\bar{D}} = \pm 4.12 \times 10^{-5} \text{ m}. \quad (\text{A.12})$$

The duct dimension has been measured for 31 sides at the end; three to four repeated measurements were taken for each data. Hence, the sample mean from Equation (A.7) can be calculated as:

$$\bar{D} = \frac{1}{31} \sum_{j=1}^{31} D_j = 0.266 \text{ m}. \quad (\text{A.13})$$

The standard deviation of the sample from Equation (A.8)

$$S_D = \sqrt{\frac{1}{N-1} \sum_{j=1}^N (D_j - \bar{D})^2} = \sqrt{\frac{1}{30} \sum_{j=1}^{31} (D_j - \bar{D})^2} = \pm 0.00406 \text{ m.} \quad (\text{A.14})$$

The standard deviation of the sample mean from Equation (A.9)

$$S_{\bar{D}} = \frac{S_D}{\sqrt{N}} = \pm 7.3 \times 10^{-4} \text{ m.} \quad (\text{A.15})$$

For $(N-1) = (31-1) = 30$ degrees of freedom, the t-distribution value at 95% confidence level is 2.086 [Coleman and Steele, 1998]. Thus the mean precision limit from Equation (A.10) is

$$P_{\bar{F}} = P_{\bar{D}} = t_d \cdot S_{\bar{D}} = \pm 1.5 \times 10^{-3} \text{ m.} \quad (\text{A.16})$$

Thus the overall uncertainties in diameter measurements of the circular duct were calculated using Equation (A.5).

The absolute uncertainty as

$$E_{\bar{F}} = E_{\bar{D}} = \pm \sqrt{(B_{\bar{F}})^2 + (P_{\bar{F}})^2} = \pm 1.5 \times 10^{-3} \text{ m} \quad (\text{A.17})$$

and relative uncertainty as

$$\frac{E_{\bar{F}}}{\bar{F}} = \frac{E_{\bar{D}}}{\bar{D}} = \pm \sqrt{\left(\frac{B_{\bar{F}}}{\bar{D}}\right)^2 + \left(\frac{P_{\bar{F}}}{\bar{D}}\right)^2} = \pm 5.6 \times 10^{-3} \quad (\text{A.18})$$

i.e., in percentile form = 0.56%.

A.2.2 Uncertainty of barometric pressure ($F = p_b$)

The Barometric pressure was measured using mercury barometer. It has an instrumental error (i.e. the accuracy) of $B_{accuracy} = 0.5\%$ of the reading and an instrumental bias limit (i.e. the resolution) of $B_{resolution} = 0.1$ mm of Hg. The zeroth order uncertainty

for manometer can be estimated by assuming a probability of 95% as [Figliola and Beasley, 2000]

$B_0 = 0.5$ of the resolution. According to Equation (A.1), the total bias error was estimated as

$$B_{\bar{F}} = B_{\text{barometer}} = \sqrt{0.01 + 2.5 \times 10^{-5} p_b^2} \text{ mm of Hg.} \quad (\text{A.19})$$

Based on the configuration of the barometer, to adjust the manometer accurately an error $P_{\text{adjust}} = \pm 0.1$ mm of Hg was introduced as a precision error. In addition to this, a readability error of $P_{\text{read}} = \pm 0.1$ mm of Hg was considered as a precision error. Thus the total precision errors were estimated as

$$P_{\bar{F}} = P_{\text{barometer}} = \pm \sqrt{P_{\text{adjust}}^2 + P_{\text{read}}^2} = \pm 0.14 \text{ mm of Hg} \quad (\text{A.20})$$

The overall uncertainty was estimated as

$$E_{\bar{F}} = E_{\text{barometer}} = \pm \sqrt{B_{\bar{F}}^2 + P_{\bar{F}}^2} = \pm \sqrt{0.03 + 2.5 \times 10^{-5} p_b^2} \text{ mm of Hg} \quad (\text{A.21})$$

For the barometric pressure of 750 mm of Hg, the absolute uncertainty was estimated as

$$E_{\bar{F}} = E_{\text{barometer}} = \pm \sqrt{(0.03) + 2.5 \times 10^{-5} (750)^2} = \pm 14.09 \text{ mm of Hg} \quad (\text{A.22})$$

and relative uncertainty as

$$\frac{E_{\bar{F}}}{F} = \frac{E_{\text{barometer}}}{p_b} = \pm \sqrt{\left(\frac{B_{\bar{F}}}{F}\right)^2 + \left(\frac{P_{\bar{F}}}{F}\right)^2} = \pm 1.88 \quad (\text{A.23})$$

i.e., in percentile form = 1.88%.

A.2.3 Uncertainties of atmospheric temperature ($F = T$)

The dry bulb and wet bulb temperatures were measured. The total bias error estimated for temperature is fixed for both cases. It has an instrumental error (i.e. the

accuracy) of $B_{accuracy} = \pm 0.5$ °C and in absence of resolution, the total bias error was estimated following Equation (A.1) as

$$B_{\bar{F}} = B_T = \pm 0.5 \text{ } ^\circ\text{C}. \quad (\text{A.24})$$

Based on the responses to the last digit of the thermometer, a digital error of $P_{digit} = \pm 0.25$ °C was introduced as a precision error. In addition to this, a readability error of $P_{read} = \pm 0.25$ °C was considered as a precision error. Thus the total precision errors were estimated as

$$P_{\bar{F}} = P_T = \pm \sqrt{P_{digit}^2 + P_{read}^2} = \pm 0.35 \text{ } ^\circ\text{C}. \quad (\text{A.25})$$

The overall uncertainty was estimated as

$$E_{\bar{F}} = E_T = \pm \sqrt{B_{\bar{F}}^2 + P_{\bar{F}}^2} = \pm 0.61 \text{ } ^\circ\text{C}. \quad (\text{A.26})$$

For the temperature reading of $T = 20$ °C, the relative uncertainty was estimated as

$$\frac{E_{\bar{F}}}{\bar{F}} = \frac{E_T}{T} = \frac{0.61}{20} = 0.0305 \approx 3.05\%. \quad (\text{A.27})$$

A.2.4 Uncertainty of pressure difference along the venturi meter ($F = \Delta h$)

The pressure difference along the venturi meter was recorded using a digital manometer in terms of inch of H₂O. The accuracy of the manometer is $\pm 0.25\%$ of the reading and the resolution is 0.01 inch of H₂O. For better estimation, the zeroth order uncertainty for manometer can be estimated by assuming a probability of 95% as [Figliola and Beasley, 2000]

$B_0 = 0.5$ of the resolution. Hence the instrument bias error could be considered as

$$B_0' = \pm \sqrt{(0.0025\Delta h)^2 + (0.005)^2} \text{ inch of H}_2\text{O}. \quad (\text{A.28})$$

The venturi meter has to be concentric with the circular duct. Practically, there could be some misalignment. The error associated with this misalignment can be accounted as bias error of $\pm 1\%$ of the measured Δh was introduced as [Coleman and Steele, 1989]

$$B_1 = \pm 0.01 \Delta h \text{ inch of H}_2\text{O} . \quad (\text{A.29})$$

Hence the bias error associated with manometer can be estimated as

$$B_{mano} = \pm \sqrt{B_0'^2 + B_1^2} = \pm \sqrt{(2.5 \times 10^{-5} + 1.06 \times 10^{-4} \Delta h^2)} \text{ inch of H}_2\text{O} . \quad (\text{A.30})$$

Accuracy of the venturi meter, i.e., $\pm 0.75\%$ of actual flow was considered as bias error.

Hence the total bias error was estimated as

$$B_{\bar{F}} = B_{ven} = \pm \sqrt{(2.5 \times 10^{-5} + 1.06 \times 10^{-4} \Delta h^2 + 5.625 \times 10^{-5} \Delta h^2)} \text{ inch of H}_2\text{O} . \quad (\text{A.31})$$

Based on the manometer, on the responses of the last digit, a digital error of $P_{digit} = 0.005$ inch of H_2O was introduced as a precision error. Thus the total precision errors were estimated as

$$P_{\bar{F}} = P_{mano} = \pm \sqrt{P_{digit}^2} = \pm 0.005 \text{ inch of H}_2\text{O} . \quad (\text{A.32})$$

The overall uncertainty was estimated as

$$E_{\bar{F}} = E_{mano} = \pm \sqrt{B_{\bar{F}}^2 + P_{\bar{F}}^2} = \pm \sqrt{(1.6225 \times 10^{-4} \Delta h^2 + 5 \times 10^{-5})} \text{ inch of H}_2\text{O} . \quad (\text{A.33})$$

Sample calculation –for venturi meter pressure differential

For the pressure differential of $\Delta h = 0.265$ inch of H_2O , the absolute uncertainty was estimated as

$$E_{\bar{F}} = E_{\Delta h} = \pm \sqrt{B_{\bar{F}}^2 + P_{\bar{F}}^2} = \pm \sqrt{(1.6225 \times 10^{-4} \times (0.07) + 5 \times 10^{-5})} = 0.0078 \text{ inch of H}_2\text{O} . \quad (\text{A.34})$$

And the relative uncertainty is deduced as

$$\frac{E_{\bar{F}}}{\bar{F}} = \frac{E_{\Delta h}}{\Delta h} = \frac{0.0078}{0.265} = 0.0296 \approx 2.96\%. \quad (\text{A.35})$$

The uncertainty is varied from 2.96% to 8.95% for different Δh .

A.2.5 Uncertainty of point velocity using velocity meter

The point velocity was recorded using velocity meter of TSI Model 8345, which measures the velocity in terms of m/s. The accuracy of the velocity meter is $\pm 3\%$ of the reading or 0.015 m/s whichever is greater. In absence of the resolution, the instrumental error could be considered as bias error

$$B_{vel_meter} = \pm \sqrt{(9 \times 10^{-4} U_{vm}^2 + 0)} \text{ m/s} = 0.03 U_{vm} \text{ m/s}. \quad (\text{A.36})$$

The velocity meter has to be right aligned for accurate measurements. Practically, this will not be the case always. Hence a misalignment error should be considered as a bias error, which is $\pm 1\%$ of the reading [Coleman and Steele, 1989], i.e.,

$$B_{vel_install} = \pm 0.01 U_{vm} \text{ m/s}. \quad (\text{A.37})$$

Hence, the total bias errors for this measurement were estimated as

$$B_{\bar{F}} = B_{vel} = \pm \sqrt{(1 \times 10^{-3} U_{vm}^2)} = 0.0316 U_{vm} \text{ m/s}. \quad (\text{A.38})$$

Based on the responses of the last digit of the velocity meter, a digital error of $P_{digit} = \pm 0.05$ m/s was introduced as a precision error. In addition to this, a readability error of $P_{read} = \pm 0.05$ m/s was considered as a precision error. Thus the total precision errors were estimated as

$$P_{\bar{F}} = P_{vel} = \pm \sqrt{P_{digit}^2 + P_{read}^2} = \pm 0.071 \text{ m/s}. \quad (\text{A.39})$$

The overall uncertainty was estimated as

$$E_{\bar{F}} = E_{vel} = \pm\sqrt{B_{\bar{F}}^2 + P_{\bar{F}}^2} = \pm\sqrt{(1 \times 10^{-3} \times U_{vm})^2 + 5 \times 10^{-3}} \text{ m/s} . \quad (\text{A.40})$$

Sample Calculation

For the velocity reading of $U_{vm} = 5 \text{ m/s}$; the absolute uncertainty was estimated as

$$E_{\bar{F}} = E_{vel} = \pm\sqrt{B_{\bar{F}}^2 + P_{\bar{F}}^2} = \pm\sqrt{(1 \times 10^{-3} \times (5))^2 + 5 \times 10^{-3}} = \pm 0.17 \text{ m/s} . \quad (\text{A.41})$$

And the relative uncertainty is deduced as

$$\frac{E_{\bar{F}}}{\bar{F}} = \frac{E_{vel}}{U_{vm}} = \frac{0.17}{5} = 0.034 \approx 3.40\% . \quad (\text{A.42})$$

A.3 Uncertainties of the thermo-physical property of fluid ($F = \rho_{water}$)

The thermo-physical properties, if taken from any table, can be accounted as bias error limit, though they may have some precision error. According to the Editorial of ASME Journal of Heat Transfer [1993] and Coleman and Steele [1989], the uncertainty for respective thermo-physical property may be 0.25 to 0.5 times the absolute value or even higher. Generally, the evaluations of the thermo-physical properties were based on average temperature calculated from the individual measurement. As mentioned by Equation (4.3) in Section 4.4, for a given operating condition, the temperatures were measured to give different population. From these populations, the mean, maximum, and minimum value could be obtained as required. The uncertainties in thermo physical properties of can be estimated as

$$E_{property} = \frac{1}{2} \left(\left| Property@T_{room, max} - Property@T_{room, min} \right| \right), \quad (\text{A.43})$$

For evaluating the fluid properties, room temperatures and pressures were calculated using Equations (4.15), (4.16) and (4.17) described in section 4. The uncertainties of these variables also estimated; see section A.2.2 and A.2.3. Over the experimental duration, the atmospheric conditions inside the duct could be varied. Considering the experimental conditions, the variation was observed very little e.g., ± 0.5 kPa, which was within uncertainty limit. Nevertheless, the duct was open to atmosphere. So, the effect of variation of the atmospheric conditions was neglected.

Density of water ($F = \rho_{water}$)

As prescribed earlier, the temperature was recorded for every test. One of the mean temperature, $T_{mean} = 18$ °C and pressure, $P_{mean} = 750$ mm of Hg was recorded. Hence the temperatures are in range of 18 ± 0.61 °C and pressure are in range of 750 ± 4.09 mm of Hg (mercury). The obtained density was 998.6 kg/m³ from the mean atmospheric conditions.

$$\text{Absolute: } E_{\rho_{water}} = \frac{1}{2} \left(\rho_{water@T_{room,max}} - \rho_{water@T_{room,min}} \right) = 0.11 \frac{\text{kg}}{\text{m}^3}, \quad (\text{A.44})$$

$$\text{Relative: } \frac{E_{\rho_{water}}}{\rho_{water}} = \frac{0.11}{998.6} \approx 0.11\%. \quad (\text{A.45})$$

A.4 Propagation of uncertainty from independent to dependent parameters

The uncertainties of the dependent parameter are calculated according to the relationship with the independent parameters. The uncertainties associated with these dependent parameters are discussed and estimated in the following subsections.

A.4.1 Uncertainty in the area of the duct ($F = A$)

The area of the duct is calculated as

$$A = \frac{\pi}{4} D^2 \quad (\text{A.46})$$

The area of the duct was calculated from the mean diameter of the duct. So the calculated mean area of the duct was

$$\bar{A} = \frac{\pi}{4} \bar{D}^2 = \frac{\pi}{4} \times (0.264 \text{ m})^2 = 0.056 \text{ m}^2. \quad (\text{A.47})$$

The associated uncertainty was estimated as,

$$E_{\bar{F}} = E_{\bar{A}} = \left[\left(\frac{\partial \bar{A}}{\partial \bar{D}} E_{\bar{D}} \right)^2 \right]^{1/2} = \frac{\partial \bar{A}}{\partial \bar{D}} E_{\bar{D}}, \quad (\text{A.48})$$

where, from Equation (A.46), $\frac{\partial \bar{A}}{\partial \bar{D}} = \frac{\pi}{4} \times 2\bar{D} = 0.418$ and from Equation (A.17)

$$E_{\bar{D}} = \pm 1.49 \times 10^{-3} \text{ m}.$$

Now the absolute uncertainty is,

$$E_{\bar{F}} = E_{\bar{A}} = \left[\left(\frac{\partial \bar{A}}{\partial \bar{D}} E_{\bar{D}} \right)^2 \right]^{1/2} = \frac{\partial \bar{A}}{\partial \bar{D}} E_{\bar{D}} = 0.418 \times (1.49 \times 10^{-3}) = 6.23 \times 10^{-4} \text{ m}^2 \quad (\text{A.49})$$

and the relative uncertainty is

$$\frac{E_{\bar{F}}}{\bar{F}} = \frac{E_{\bar{A}}}{\bar{A}} = \frac{6.23 \times 10^{-4}}{0.056} = 0.0111, \quad (\text{A.50})$$

which giving, $(0.011) \times 100 = 1.11\%$.

A.4.2 Uncertainty associated with gravitational acceleration ($F = g$)

The uncertainty of a constant parameter is zero. As mentioned earlier, the gravitational acceleration (g) is a function of latitude (ϕ) and altitude (H); see Equation (4.10). So the uncertainty can be assumed as

$$E_{\bar{F}} = E_g = \left[\left(E_{\phi} \frac{\partial g}{\partial \phi} \right)^2 + \left(E_H \frac{\partial g}{\partial H} \right)^2 \right]^{1/2}, \quad (\text{A.51})$$

where E_{ϕ} and E_H are the uncertainty components for latitude (ϕ) and altitude (H). The partial derivatives were calculated from Equation (4.10). Since ϕ and H are constant a specific area, so E_{ϕ} and E_H can be estimated as zero. So uncertainty of g also zeros.

A.4.3 Uncertainty of Δp

The absolute uncertainty of Δp was estimated based on Equation (4.9) as

$$E_{\bar{F}} = E_{\Delta p} = \left[\left(E_{\Delta h} \frac{\partial \Delta p}{\partial \Delta h} \right)^2 + \left(E_{\rho_{water}} \frac{\partial \Delta p}{\partial \rho_{water}} \right)^2 + \left(E_g \frac{\partial \Delta p}{\partial g} \right)^2 \right]^{1/2}, \quad (\text{A.52})$$

where $E_{\Delta h}$, $E_{\rho_{water}}$ and E_g are the uncertainty components for differential pressure (Δh), water density (ρ_{water}) and gravitational acceleration (g). The partial derivatives were calculated from Equation (4.9). For 0.265 inch of H_2O (0.0067 m of H_2O), the uncertainty of the pressure difference along the venturi meter can be calculated from Equation (A.52) as

$$E_{\Delta p} = \left[(0.0296 \times 0.0067 \times 998.6 \times 9.803)^2 + (0.011 \times 998.6 \times 0.0067 \times 9.803)^2 + 0 \right]^{1/2} \\ = 2.07 \text{ Pa}, \quad (\text{A.53})$$

$$\text{Relative: } \frac{E_{\Delta p}}{\Delta p} = \frac{1.94}{0.0067 \times 998.6 \times 9.803} \approx 3.16\%. \quad (\text{A.54})$$

The uncertainty is varied from 3.16% to 9% for different reading.

A.4.4 Uncertainty of p_{sat}

The absolute uncertainty of the saturated vapor pressure at wet bulb temperature was estimated as according to Equation (4.13)

$$E_{\bar{F}} = E_{p_{sat}} = \left[\left(E_{T_{wet}} \frac{\partial p_{sat}}{\partial T_{wet}} \right)^2 \right]^{1/2}, \quad (A.55)$$

where $U_{T_{wet}}$ is the uncertainty component for wet bulb temperature, which already described in section A.2.3 (i.e., $E_{T_{wet}} = 0.61$ °C). The partial derivative was calculated from Equation 4.13 as

$$\frac{\partial p_{sat}}{\partial T_{wet}} = 6.5T_{wet} + 18.6. \quad (A.56)$$

Now from Equation (A.55), the uncertainty for $T_{wet} = 15$ °C could be estimated

$$\text{Absolute: } E_{P_{sat}} = \left[\left(0.61 \times 116.1 \right)^2 \right]^{1/2} = 70.82 \text{ Pa}, \quad (A.57)$$

$$\text{Relative: } \frac{E_{P_{sat}}}{p_{sat}} = \frac{70.82}{3.25 \times 15^2 + 18.6 \times 15 + 692} \approx 4.77\%. \quad (A.58)$$

A.4.5 Uncertainty of the p_{par}

The absolute uncertainty of the partial vapor pressure (P_{par}) can be estimated as

$$E_{\bar{F}} = E_{p_{par}} = \left[\left(E_{p_{sat}} \frac{\partial p_{par}}{\partial p_{sat}} \right)^2 + \left(E_{p_b} \frac{\partial p_{par}}{\partial p_b} \right)^2 + \left(E_{T_{dry}} \frac{\partial p_{par}}{\partial T_{dry}} \right)^2 + \left(E_{T_{wet}} \frac{\partial p_{par}}{\partial T_{wet}} \right)^2 \right]^{1/2}, \quad (A.59)$$

where $E_{T_{wet}}$, $E_{T_{dry}}$, E_{p_b} , $E_{p_{sat}}$ is the uncertainty component for wet bulb temperature, dry bulb temperature, vapor pressure and saturated vapor pressure respectively. The partial

derivative was calculated from Equation 4.12. For the data reading, $T_{dry} = 18^{\circ}\text{C}$, $T_{wet} = 15^{\circ}\text{C}$, and $p_b = 750$ mm of Hg, the uncertainty estimated from Equation (A.59) is

Absolute:

$$E_{P_{par}} = \left[(70.82 \times 1)^2 + \left(0.0188 \times 100658.4 \times \frac{-3}{1500} \right)^2 + \left(0.61 \times \frac{100658.4}{1500} \right)^2 + \left(0.61 \times \frac{100658.4}{1500} \right)^2 \right]^{1/2} \quad (\text{A.60})$$

$$= 91.3 \text{ Pa}$$

$$\text{Relative: } \frac{E_{\bar{F}}}{F} = \frac{E_{P_{par}}}{P_{par}} = \frac{91.3}{1502} = 0.0607 \approx 6.07\%$$

A.4.6 Uncertainty of the air density ($F = \rho$)

Assuming zero uncertainty of the gas constant, the absolute uncertainty of the air density (ρ) can be estimated from Equation (4.11) as:

$$E_{\bar{F}} = E_{\rho} = \left[\left(E_{P_{par}} \frac{\partial \rho}{\partial P_{par}} \right)^2 + \left(E_{P_b} \frac{\partial \rho}{\partial P_b} \right)^2 + \left(E_{T_{dry}} \frac{\partial \rho}{\partial T_{dry}} \right)^2 \right]^{1/2}, \quad (\text{A.61})$$

where $E_{T_{dry}}$, E_{P_b} , $E_{P_{par}}$ is the uncertainty component for dry bulb temperature, vapor pressure and partial vapor pressure respectively. The partial derivative was calculated using Equation 4.11. For the data reading, $T_{dry} = 18^{\circ}\text{C}$, and $p_b = 100658.4$ Pa, $p_{par} = 1502$ Pa (calculated from Equations (4.12) and (4.13)) the uncertainty estimated from Equation (A.61) is

Absolute:

$$E_{\rho} = \left[\left(91.3 \times \frac{-0.378}{287.1 \times 291.15} \right)^2 + \left(1892.4 \times \frac{1}{287.1 \times 291.15} \right)^2 + \left(0.61 \times \frac{100658.4}{287.1} \times \left(\frac{-1}{291.15} \right)^2 \right)^2 \right]^{1/2} \quad (\text{A.62})$$

$$= 0.0228 \text{ kg/m}^3$$

$$\text{Relative: } \frac{E_{\bar{\rho}}}{\rho} = \frac{0.0228}{1.19} \approx 1.91\% \quad (\text{A.63})$$

A.4.7 Uncertainty in the volumetric flow rate using the venturi meter ($F = Q_{ven}$)

The volumetric flow rate using venturi meter is calculated as

$$Q_{ven} = C_D \frac{A_{throat}}{\sqrt{1-\beta^4}} \sqrt{\frac{2\Delta p}{\rho}}, \quad (\text{A.64})$$

where the Δp was calculated from the differential pressure across the venturi meter using digital manometer as

$$\Delta p = \Delta h \rho_{\text{water}} g, \quad (\text{A.65})$$

for $\Delta h = 0.08$ inch of H_2O , water density (ρ_{water}) = 998.6 kg/m^3 and $g = 9.803 \text{ m/s}^2$; the pressure difference can be calculated as 19.87 Pa with 2.96% uncertainty. The density of the air calculated from Equation 4.10 as 1.19 with 1.91% uncertainty.

The throat area (A_{throat}) and beta ratio (β) is constant, though coefficient of discharge ($C_D = 0.995$) has a bias error mentioned as [ANSI/ASME, 1990]

$$\frac{B_{C_D}}{C_D} = 0.00122, \quad (\text{A.66})$$

There is no precision error considered; hence the total error calculated for the C_D can be estimated as:

$$\frac{E_F}{F} = \frac{E_{C_D}}{C_D} = \left[\left(\frac{B_{C_D}}{C_D} \right)^2 \right]^{1/2} = 0.00122 \approx 0.122\%. \quad (\text{A.67})$$

Hence, the absolute uncertainty of the flow rate (Q_{ven}) can be estimated from Equation (A.64) as

$$E_{\bar{F}} = E_{Q_{ven}} = \left[\left(E_{C_D} \frac{\partial Q_{ven}}{\partial C_D} \right)^2 + \left(E_{\Delta p} \frac{\partial Q_{ven}}{\partial \Delta p} \right)^2 + \left(E_{\rho} \frac{\partial Q_{ven}}{\partial \rho} \right)^2 \right]^{1/2}, \quad (\text{A.68})$$

where $E_{C_D}, E_{\Delta p}, E_{\rho}$ is the uncertainty component for discharge coefficient (C_D), pressure differential (Δp) across the venturi meter and air density (ρ) respectively. The partial derivative was calculated using Equation 4.8 of section 4. Now the absolute uncertainty is,

$$E_{Q_{ven}} = \left[(0.0012 \times 0.1734)^2 + (1.7884 \times 4.34 \times 10^{-3})^2 + (0.0191 \times 1.19 \times 0.07)^2 \right]^{1/2} = 0.0079 \text{ m}^3 \quad (\text{A.69})$$

and the relative uncertainty is

$$\frac{E_{\bar{F}}}{F} = \frac{E_{Q_{ven}}}{Q_{ven}} = \frac{0.0079}{0.17} = 0.0458, \quad (\text{A.70})$$

which giving, $E_{Q_{ven}} (\%) = (0.0458) \times 100 = 4.58\%$.

The uncertainty for flow rate is found 1.84% to 5.5%.

A.4.8 Uncertainty of Reynolds number ($F = \text{Re}$)

The Reynolds number is calculated as

$$\text{Re} = \frac{\rho U_{mean} D}{\mu}, \quad (\text{A.71})$$

where U_{mean} and μ in Equation (A.71) can be calculated as [ANSI/ASME, 1990]

$$U_{mean} = \frac{Q_{ven}}{A} \quad (\text{A.72})$$

and

$$\mu = (17.23 + 0.048T_{dry}) \times 10^{-6}. \quad (\text{A.73})$$

Hence, the uncertainty of the of Re is depends on uncertainty of mean velocity (U_{mean}), defined in Equation (A.72), and uncertainty of the μ , defined in Equation (A.73). The uncertainty of the mean velocity and μ is discussed in following subsections:

A.4.9 Uncertainty of mean velocity ($F = U_{mean}$)

The absolute uncertainty of the mean velocity can be estimated as

$$U_{\bar{F}} = U_{U_{mean}} = \left[\left(U_{Q_{ven}} \frac{\partial U_{mean}}{\partial Q_{ven}} \right)^2 + \left(U_A \frac{\partial U_{mean}}{\partial A} \right)^2 \right]^{1/2}, \quad (A.74)$$

where $E_{Q_{ven}}$, E_A are the uncertainty component for flow rate along venturi meter and cross sectional area of the duct respectively. The partial derivative was calculated using Equation (A.72). For the volumetric flow rate ($Q_{ven} = 0.17 \text{ m}^3/\text{s}$), the uncertainty can be estimated as

Absolute:

$$E_{\bar{F}} = E_{U_{mean}} = \left[\left(0.0079 \times \frac{1}{0.056} \right)^2 + \left(6.19 \times 10^{-4} \times \frac{0.17}{0.056 \times 0.056} \right)^2 \right]^{1/2} = 0.145 \frac{\text{m}}{\text{s}}, \quad (A.75)$$

$$\text{Relative: } \frac{E_{\bar{F}}}{\bar{F}} = \frac{E_{U_{mean}}}{U_{mean}} = \frac{0.145}{3.08} = 4.71\%. \quad (A.76)$$

A.4.10 Uncertainty of ($F = \mu$)

The absolute uncertainty of μ can be estimated using Equation (A.73) as

$$E_{\bar{F}} = E_{\mu} = \left[\left(E_{T_{dry}} \frac{\partial \mu}{\partial T_{dry}} \right)^2 \right]^{1/2} = \left[0.61 \times 0.048 \times 10^{-6} \right] = 2.93 \times 10^{-8} \frac{\text{N-s}}{\text{m}^2}. \quad (A.77)$$

So the uncertainty of the Reynolds number can be estimated as

$$E_{Re} = \left[\left(E_{\rho} \frac{\partial Re}{\partial \rho} \right)^2 + \left(E_{U_{mean}} \frac{\partial Re}{\partial U_{mean}} \right)^2 + \left(E_D \frac{\partial Re}{\partial D} \right)^2 + \left(E_{\mu} \frac{\partial Re}{\partial \mu} \right)^2 \right]^{1/2} \quad (A.78)$$

$$= 2810,$$

where E_{ρ} , E_D , $E_{U_{mean}}$ and E_{μ} are the uncertainty component for air density, duct diameter, mean flow and dynamic viscosity respectively. The partial derivative was calculated using Equation (A.71). For the flow rate ($Q_{ven} = 0.17 \text{ m}^3/\text{s}$), the uncertainty can be estimated as

Absolute:

$$E_{Re} = \left[\left(0.0228 \times 4551556 \right)^2 + \left(0.1458 \times 17733.33 \right)^2 + \left(1.49 \times 10^{-3} \times 20533333 \right)^2 + \left(2.93 \times 10^{-8} \times 3 \times 10^9 \right)^2 \right]^{1/2} \quad (A.79)$$

$$= 2810$$

$$\text{Relative: } \frac{E_{\bar{F}}}{F} = \frac{E_{Re}}{Re} = \frac{2810}{54820} = 5.12 \% . \quad (A.80)$$

A.4.11 Uncertainty of measurement locations

The uncertainty of the locations is related with the length-measuring instrument. Mainly, a measuring tape/digital caliper was used for measuring the distance of each location. Assuming the measuring tape has highest uncertainty, so uncertainty for measuring tape was deduced. The resolution and accuracy of the instrument is taking as precision error. Assuming the accuracy is 1% of the reading and the resolution is 1 mm, hence the bias error is calculated as

$$B_{\bar{F}} = B_{y_{tr}} = \pm \sqrt{1 \times 10^{-4} \times y_{tr}^2 + 0.25} \text{ mm} . \quad (A.81)$$

Due to clearance of the hole and measuring instrument, assuming the error 1% of the traversing for misalignment as

$$P_{align} = 0.01 y_{tr} \text{ mm}.$$

The instrument may not be inserted in proper location. Assume the traversing error could be 0.5 mm, hence the total error can be estimated as

$$E_{\bar{F}} = E_{y_{tr}} = \pm \sqrt{1 \times 10^{-4} \times y_{tr}^2 + 0.25 + 1 \times 10^{-4} \times y_{tr}^2 + 0.25} \text{ mm} . \quad (\text{A.82})$$

Sample calculation

For the traversing of last point of the duct (258 mm), the error is estimated as:

$$E_{\bar{F}} = E_{y_{tr}} = \pm \sqrt{2 \times 10^{-4} \times (258)^2 + 2 \times 0.25} = 3.72 \text{ mm} .$$

A.4.12 Uncertainty of the point velocity ($F = U$)

A.4.12.1 Uncertainty associated with velocity meter

The point velocity was calculated using velocity meter and Pitot-static tube (diameter = 2.38 mm, blockage ratio = 0.009). The pipe diameter is large compared to the probe diameter; hence the probe blockage effects can be neglected [ANSI/ASME, 1990; Coleman and Steele, 1989; Dally et al., 1984]; however, the boundary effects due to wall were considered. Due to the location of the probe, the velocity profile effects in radial direction can be accounted for within some acceptable uncertainty which is a function of the of traverse points [ANSI/ASME, 1990]. The averaging errors along the diameter were neglected, the average point velocity was measured from 3 to 4 traverses, and in each traverse 3-4 repeated measurements were recorded as discussed in section 4.

The sample mean for each position calculated by Equation (A.7) and the standard deviation of the sample calculated using Equation (A.8), then the precision index deduced by Equation (A.9) and the precision limit calculated by Equation (A.10). It is noted that the degrees of freedom was calculated using Equation (A.11). The results are summarized in Table A.1.

Table A.1 Mean point velocity and precision limit of Equal Area six-point traverse in uncertainty determination ($Re = 54800$).

Radial Position [mm]	Mean velocity [m/s]				Precision limit (m/s)			
	$\overline{U_{vel1}}$	$\overline{U_{vel2}}$	$\overline{U_{vel3}}$	$\overline{U_{vel4}}$	$\overline{P_{F1}}$	$\overline{P_{F2}}$	$\overline{P_{F3}}$	$\overline{P_{F4}}$
-122	2.78	2.78	2.82	2.82	0.0094	0.0120	0.0074	0.0054
-94	3.14	3.14	3.14	3.14	0.0068	0.0084	0.0087	0.0142
-54	3.53	3.53	3.59	3.53	0.0089	0.0087	0.0145	0.0089
54	3.53	3.59	3.53	3.59	0.0084	0.0172	0.0089	0.0115
94	3.07	3.07	3.07	3.07	0.0085	0.0098	0.0097	0.0126
122	2.78	2.70	2.78	2.78	0.0086	0.0089	0.0068	0.0095

The total bias error can be estimated for the velocity meter from Equation (A.35). The overall uncertainty for each point velocity can be estimated as

$$E_{\overline{F}} = E_{\overline{U}} = \pm \sqrt{B_{\overline{F}}^2 + P_{\overline{F}}^2} \quad (A.83)$$

Sample calculation

For the point velocity ($\overline{U_{vel1}} = 2.78 \text{ m/s}$), the uncertainty can be estimated as

$$\text{Absolute: } E_{\overline{U_{vel1}}} = \pm \sqrt{(0.0316 \times 2.78)^2 + (0.0094)^2} = 0.09 \text{ m/s}, \quad (A.84)$$

$$\text{Relative: } \frac{E_{\overline{U_{vel1}}}}{\overline{U_{vel1}}} = \frac{0.09}{2.78} = 0.0325 \approx 3.25\% \quad (A.85)$$

The uncertainty for the mean value calculated using Equal Area (U_{EQ}) or Log-Tchebycheff (U_{LT}) was calculated from the uncertainty of the individual mean velocity.

The obtained uncertainty was estimated 3.3% for the Equal Area method and 3.5% for the Log-Tchebycheff method using velocity meter.

The uncertainty associated with location was accounted with point velocity, the sample calculation is shown as

$$E_{location} = \pm \sqrt{\left(\frac{\partial y}{\partial x}\right)^2} = \frac{\partial y}{\partial x} . \text{ Assuming the last point have maximum error (i.e., } y_{tr} = 258$$

mm from the duct wall), which can be measured as 258 ± 3.72 mm and the point velocity can be estimated on that location as 2.78 ± 0.0094 m/s. Hence, the uncertainty for this location can be estimated as

$$E_{location} = \pm \frac{0.008}{0.2} = 0.04 = 4\%$$

The total uncertainty for the point velocity can be estimated as

$$E_U = \sqrt{(E_{U_{vel}}^2 + E_{location}^2)} = \pm \sqrt{(0.09)^2 + (0.04 \times 2.78)^2} = 0.14 \text{ m/s , which is } 5.15\%.$$

Hence, the uncertainty is varied from 5.15% to 6.15%.

A.4.12.2 Uncertainty associated with manometer

The absolute uncertainty was estimated using Equation (4.22) of Section 4.3 as

$$E_U = \left[\left(E_p \frac{\partial U}{\partial p} \right)^2 + \left(E_{p_v} \frac{\partial U}{\partial p_v} \right)^2 \right]^{1/2} . \quad (\text{A.86})$$

Similar to the Section (A.4.12.1), E_{p_v} was calculated. The uncertainty was obtained about (7.5% to 12.4%).

Similarly, the uncertainty for the locations in case of manometer can be estimated as

$$E_U = \sqrt{(E_{U_{vel}})^2 + E_{location}^2} = \pm \sqrt{(0.08 \times 2.78)^2 + (0.04 \times 2.78)^2} = 0.25 \text{ m/s}, \text{ which is } 9\%.$$

So the uncertainty was varied from 8.5% to 13.5%

A.4.13 Uncertainties of Q_{EQ} and Q_{LT}

The volumetric flow rate can be estimated as

$$\bar{Q} = \bar{U} \times \bar{A}, \quad (\text{A.87})$$

where \bar{Q} , volumetric flow rate deduced from mean velocity (\bar{U}), which deduced from the point velocity obtained using the traversing techniques times averaged area of the duct (\bar{A}). Hence, the absolute uncertainty can be deduced as

$$E_{\bar{Q}} = E_{\bar{Q}} = \left[\left(E_{\bar{U}} \frac{\partial \bar{Q}}{\partial \bar{U}} \right)^2 + \left(E_{\bar{A}} \frac{\partial \bar{Q}}{\partial \bar{A}} \right)^2 \right]^{1/2}, \quad (\text{A.88})$$

where $E_{\bar{U}}$ and $E_{\bar{A}}$ is the uncertainty components for the average velocity deduced by Equal Area or Log-Tchebycheff methods and area of the duct. The partial derivatives can be estimated from Equation (A.87). For ($\bar{U}_{EQ}=3.15 \text{ m/s}$), the uncertainty can be estimated as

$$\text{Absolute: } E_{\bar{Q}_{EQ}} = \left[\left(E_{\bar{U}_{EQ}} \frac{\partial \bar{Q}}{\partial \bar{U}} \right)^2 + \left(E_{\bar{A}} \frac{\partial \bar{Q}}{\partial \bar{A}} \right)^2 \right]^{1/2} \quad (\text{A.89})$$

$$= \left[(0.0325 \times 5.15 \times 0.056)^2 + (3.41 \times 10^{-4} \times 3.15)^2 \right] = 9.43 \times 10^{-3} \frac{\text{m}^3}{\text{s}},$$

$$\text{Relative: } \frac{E_{\bar{Q}_{EQ}}}{\bar{Q}_{EQ}} = \frac{9.43 \times 10^{-3}}{3.15 \times 0.056} = 0.0535 \approx 5.35\%. \quad (\text{A.90})$$

And similarly, the uncertainty for the Log-Tchebycheff method can be estimated as:

$$\text{Absolute: } E_{\bar{Q}_{LT}} = 9.55 \times 10^{-3} \frac{\text{m}^3}{\text{s}}$$

$$\text{Relative: } \frac{E_{\bar{Q}_{LT}}}{\bar{Q}_{LT}} = \frac{9.55 \times 10^{-3}}{3.06 \times 0.056} = 0.0557 \approx 5.57\%$$

It is noted that for the case $Re = 24400$ and 54800 , the velocity meter were used; which possessed the uncertainty for volumetric flow rate as 5.5% to 7%. The case $Re = 9400$, the manometer was used which possessed an uncertainty of 12%. All the results regarding the uncertainty analysis have been summarized in Table A.2.

Table A.2 Data for volumetric flow rate measurement with uncertainties

Parameters	Mean value	Uncertainties	Parameters	Mean value	Uncertainties
\bar{D} (mm)	266	± 1.5	\bar{P}_{sat} (Pa)	1702.25	± 70.82
\bar{P}_b (mm of Hg)	750	± 14.09	\bar{P}_{par} (Pa)	1502.27	± 91.3
\bar{T} ($^{\circ}\text{C}$)	18	± 0.61	$\bar{\rho}$ (kg/m^3)	1.19	± 0.023
$\bar{\Delta h}$ (in of H_2O)	0.265	± 0.0078	\bar{Q}_{ven} (m^3/s)	0.172	± 0.0079
\bar{U}_{vel} (m/s)	5	± 0.1	\bar{U}_{mean} (m/s)	3.08	± 0.146
$\bar{\rho}_{water}$ (kg/m^3)	998.6	± 0.11	\bar{Re}	54820	± 2810
\bar{A} (m^2)	0.056	$\pm 6.23 \times 10^{-4}$	\bar{U}_{EQ} (m/s)	3.15	± 0.16
$\bar{\Delta p}$ (Pa)	65.59	± 2.07	\bar{U}_{LT} (m/s)	3.06	± 0.17
\bar{Q}_{EQ} (m^3/s)	0.176	± 0.0094	\bar{Q}_{LT} (m^3/s)	0.172	± 0.0096

APPENDIX B**CALIBRATION OF A HOT WIRE PROBE**

Most calibrations are carried out in either a special calibration facility or in a flow field in which the magnitude and direction of the flow vector is known. In this investigation, a nozzle and automated air velocity calibrator supplied by TSI model 1129 with IFA 300 Constant Temperature Anemometer was used. The schematic of the calibration set-up is shown in Figure B.1.

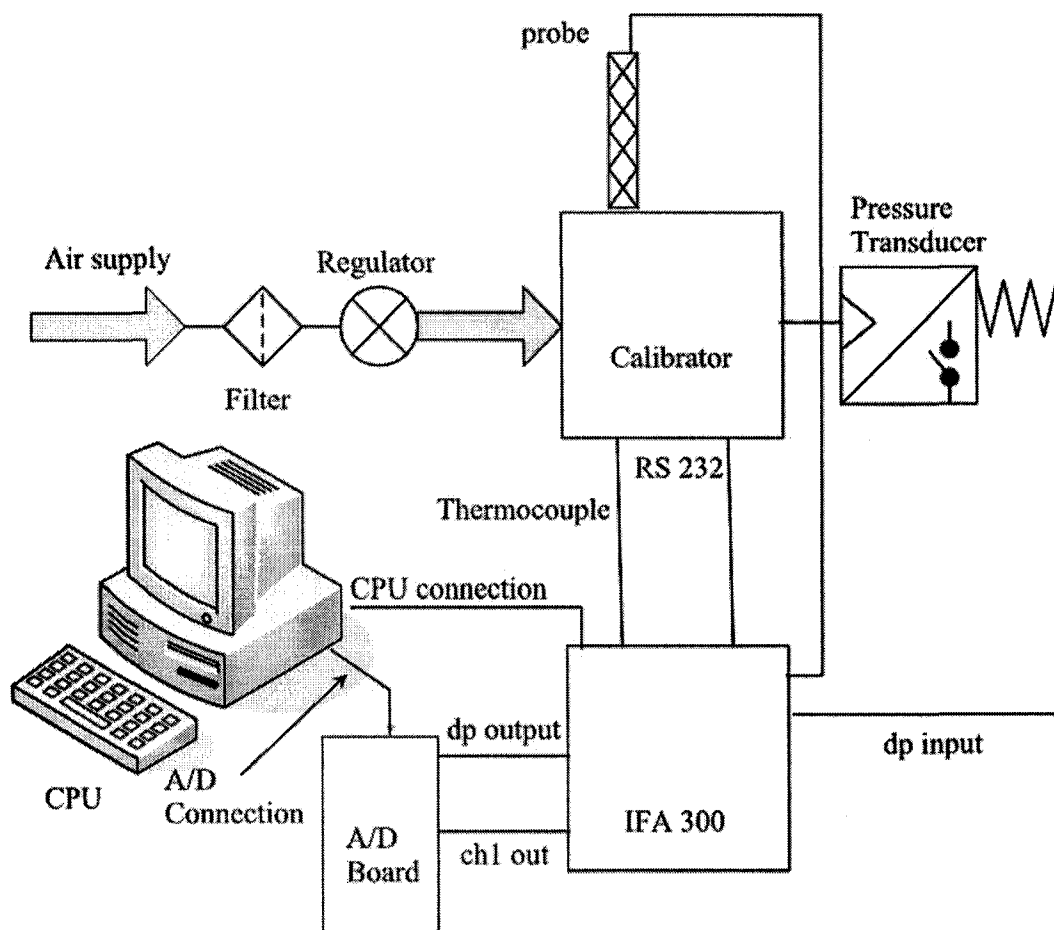


Figure B.1 Schematic of hot-wire calibration set-up.

B.1 Calibration principle

The calibration was performed for a specified velocity of 25 m/s. So the hot-wire was able to get the velocity from 0 to 25 m/s. Generally, calibration generates a relationship between the bridge voltage and a reference velocity. The acquisition program to convert raw data to velocity data uses calibration.

The response equation for the output voltage from an anemometer connected to a given hot-wire sensor can be expressed in the form of a simple power law [TSI, 2000]

$$V^2 = C_1 + C_2 U_{eff}^c, \quad (B.1)$$

where U_{eff} is an effective velocity, V is an output voltage from the anemometer. C_1 , C_2 is calibration constant and c is a calibration exponent. The effective velocity is defined by Jorgensen's equation as [Bruun, 1995]

$$U_e^2 = U_N^2 + k^2 U_T^2 + h^2 U_B^2, \quad (B.2)$$

where U_N , U_T and U_B are the normal, tangential and binormal velocity components, k and h are the sensor's yaw and pitch coefficients. However, for a single wire probe the relationship becomes:

$$V = f(U) \quad (B.3)$$

where U is the velocity component in the mean flow direction. The output of the anemometer is bridge voltage/raw voltage (V_{br}), which will convert to effective velocity by probe. The voltage is usually signal conditioned by A/D converter and deduced as [Bruun, 1995]

$$V_{con} = (V_{br} - \text{offset}) \times \text{Gain} \quad (B.4)$$

where V_{con} is the conditioned voltage, the offset and gain can be re-arranged from the default settings for different performance. A/D converter creates a 12-bit binary count, B_{count} , which can be deduced as follows [Bruun, 1995]

$$B_{count} = 4095 \frac{(V_{con} + 5)}{10}. \quad (B.5)$$

From Equation (B.4) and (B.5), the raw voltage is calculated as:

$$V_{br} = \frac{[(B_{count} \times 10/4095) - 5]}{\text{Gain}} + \text{offset} \quad (B.6)$$

The voltage is corrected by temperature as [Bruun, 1995]:

$$V = V_{br} \times \sqrt{\frac{(T_s - T_c)}{T_s - T_e}}, \quad (B.7)$$

where T_s is the hot-wire temperature, T_c is the temperature during calibration and T_e is the temperature during experiment. The calibration for effective velocity is a curve fit with a fourth order polynomial, which is a function of bridge voltage, V , deduced as [Bruun, 1995]:

$$U_e = B_{count} + C_1 \times V + C_2 \times V^2 + C_3 \times V^3 + C_4 \times V^4 \quad (B.8)$$

Finally, the velocity is corrected by density [Bruun, 1995], i.e.,

$$U_e(\text{corr}) = \frac{p_{bc}}{p_b} \times U_e, \quad (B.9)$$

where p_{bc} is barometric pressure during calibration, p_b is barometric pressure during test.

B.2 Components of auto calibration

The TSI supplied calibrator model 1129 has the following equipment to perform the calibration:

A settling chamber with a free jet diameter of 10 mm to settle the air from the supply, a in-line nozzles for increased sensitivity and accuracy at low velocity, a Filter/Regulator assembly which includes a pressure regulator, valve, filter, hose and fittings were connected. A probe support can be mounted and manipulated for velocity as well as yaw and pitch calibrations. A differential pressure transducer (0-10 mm of Hg) for measuring the pressure upstream of the free jet, an A/D converter (used with the Model IFA 300 Constant Temperature Anemometer) has an input of -5 volts to $+5$ volts was installed in a system; so a signal conditioner has been built into the IFA 300 that provides a 5 volt offset and a gain of 1 – 10 volt (for better resolution at low pressures). A copper constantan, T-type thermocouple is mounted in the settling chamber upstream of flow straightening screens located inside the settling chamber. The thermocouple cable that is furnished with the IFA 300 system can be used to connect the thermocouple to the IFA 300 back panel. Figure B.1 shows an automated air calibrator with all connected components.

B.3 Auto calibration procedure

For the calibration of the hot wire, the calibrator was attached to the air supply; the probe support was connected to one of the channel (channel 1) of the IFA 300 with a 5-meter probe cable, the output voltage from channel one of the IFA 300 was connected to channel 1 on the A/D board. The nozzle was set according to the desired velocity (Nozzle 1, Nozzle 2 or Nozzle 3). The pressure transducer output is connected to the dP input on the back panel of the IFA 300 and the signal from the differential output (dP OUT) on the IFA 300 was connected to channel 2 on the A/D board. The pressure

tube from the pressure transducer was attached to the appropriate location on the calibrator. A barometer is set up to measure the atmospheric pressure in the room. The thermocouple was installed in the calibrator and connected to the thermocouple connector of the IFA 300; see Figure B.1. It is noted that for this kind calibration setup (nozzle-calibration facility), where the nozzle is set inside the calibrator as shown in Figure B.1, the reference velocity can be determined from the pressure drop across the nozzle. The probe was placed about one diameter downstream from the nozzle exit. The mean flow velocity can be evaluated as

$$p_{st} - p_b = \frac{1}{2} \rho U^2, \quad (\text{B.10})$$

where p_{st} is stagnation pressure in the nozzle settling chamber and p_b is the barometric pressure. A set of calibration points was defined by software spaced evenly over the selected velocity range (U_{cmin} to U_{cmax}). Since, the CT anemometer is very high frequency response; the output voltage will usually correspond to the existing velocity. However, the velocity is normally varied stepwise, a significance difference can occur between the true value and the value obtained using Equation (B.10). The calibration was checked before and after the experiment.

Prior to the calibration, the IFA 300 Constant Temperature Anemometer system was started. After a certain period, the differential pressure switch was set to zero using the THERMALPRO software. It is specified that the software provided complete experiment documentation, automated calibration, traverse control, and data acquisition and analysis. The cable resistance using shorting probe and hot wire probe resistance was measured. In the screen of the THERMALPRO software, the parameters were set as

guidelines of the TSI supplied manual [TSI, 2003]. The TSI supplied auto cal file and auto calibration table was opened. Finally, the calibration was performed for 25 m/s velocity using the room conditions and the calibration file was saved as a different name, which was used in experimental measurement. The performance curve after calibration is shown in Figure B.2.

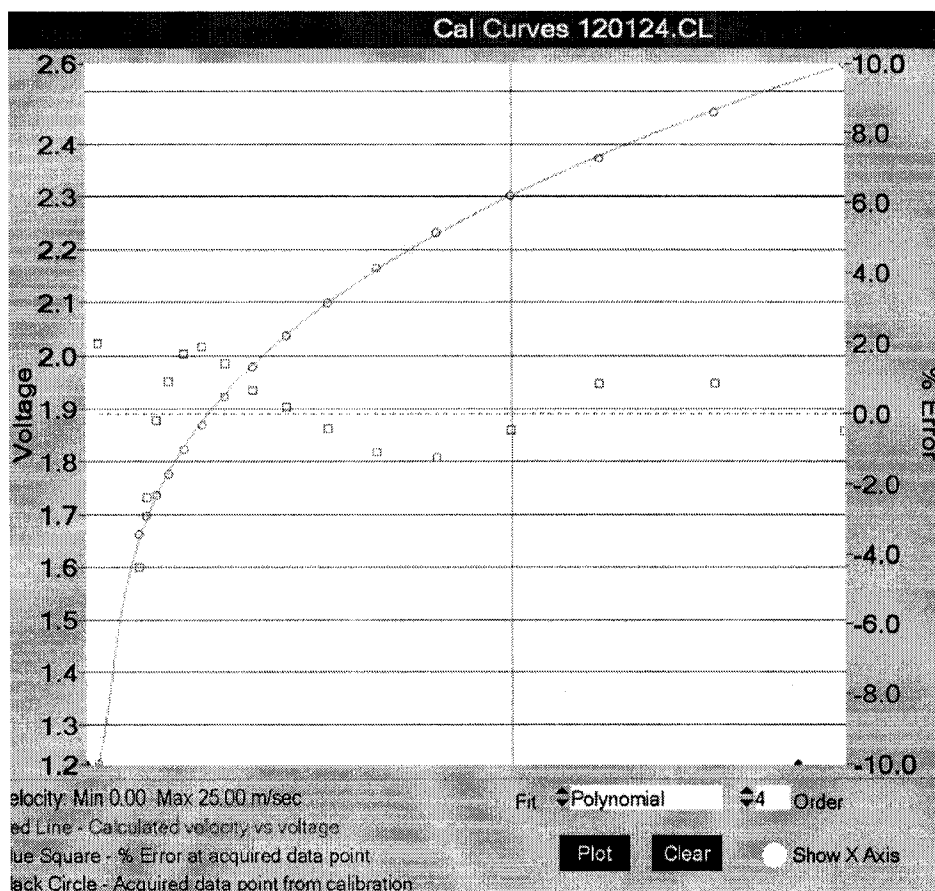


Figure B.2 Performance curve for calibration before experiment

The calibrated file was used in velocity measurement with the calibrated hot wire probe. It is noted that the hot-wire probe was recalibrated after the experiment and checked any significance difference with the previous calibration results. The

performance curve by calibration is shown in Figure B.3. It shows the calibration profile including the error percentage is almost identical. Hence, the data collection using the hot wire was sufficiently good.

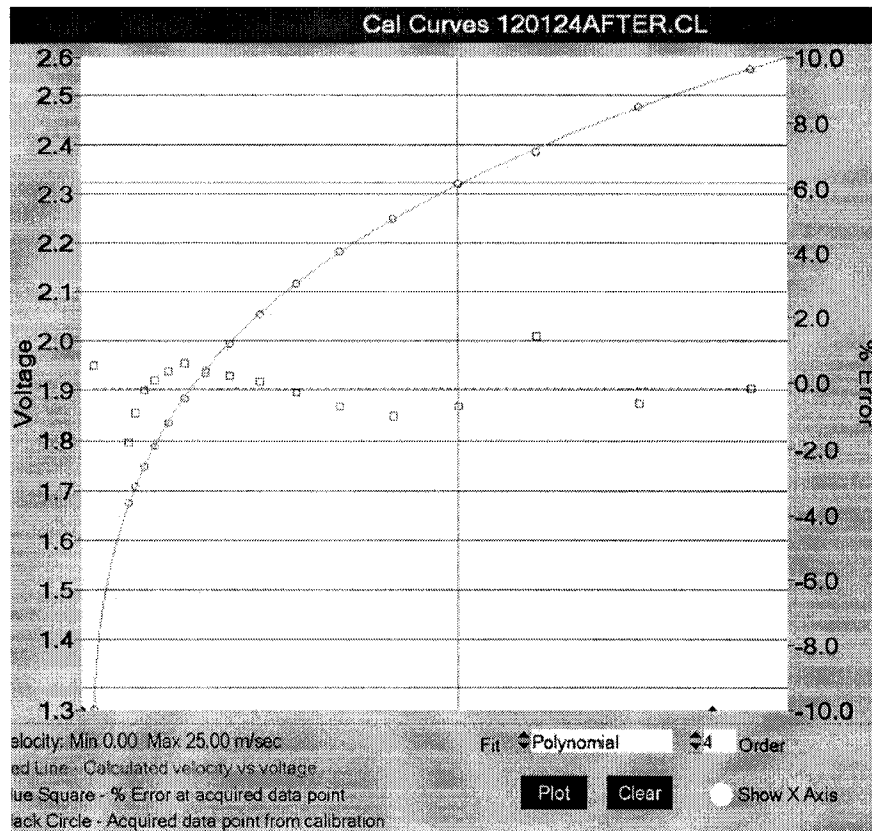


Figure B.3 Performance curve for calibration after experiment.

APPENDIX C

STANDARD κ - ε MODEL

The simplest “complete model” of turbulence is two-equation model in which the solution of two separate transport equations allows the turbulent velocity and length scale to be independently determined. The turbulent velocity scale (v_t) and length scale (Λ) is deduced as:

$$v_t = \kappa^{1/2} \quad (C.1)$$

and

$$\Lambda = \frac{\kappa^{3/2}}{\varepsilon} \quad (C.2)$$

In order to compute all mean flow properties of the turbulent flow, it need to compute the $\overline{u'v'}$; see momentum equation in section 3.1 for turbulent flow, which can be defined as [Wilcox, 1994]:

$$\tau_{ij} = -\rho \overline{u'v'} \quad (C.3)$$

where τ_{ij} is the stress Reynolds-stress tensor, which can be deduced:

$$\tau_{ij} = \mu \left(\frac{\partial u_i}{\partial x_j} + \frac{\partial u_j}{\partial x_i} \right) - \frac{2}{3} \mu \frac{\partial u_k}{\partial x_k} \delta_{ij} \quad (C.4)$$

where δ_{ij} is the Kronecker delta, which is a function of two variables i and j that equals 1 when $i = j$ and equals 0 otherwise.

In the stress tensor equation (Equation C.4), the second term of the right hand side is considered as dynamic pressure, will be ignored because it is small [Chen 1988]. The turbulent viscosity (μ_t) is calculated from

$$\mu_t = C_\mu \rho \frac{\kappa^2}{\varepsilon} \quad (\text{C.5})$$

Hence, the flow parameters (i.e., v_t , Λ , μ_t etc) in case of turbulent flow can be determined via κ and ε ; see Equations (C.1-C.5). The variables (κ and ε) can be determined using following relations

$$\frac{\partial}{\partial t}(\rho\kappa) + \frac{\partial}{\partial x_i}(\rho\kappa u_i) = \frac{\partial}{\partial x_j} \left[\left(\mu + \frac{\mu_t}{\sigma_\kappa} \right) \frac{\partial \kappa}{\partial x_j} \right] + G_\kappa + G_b - \rho\varepsilon - Y_M + S_\kappa \quad (\text{C.6})$$

$$\begin{aligned} & \frac{\partial}{\partial t}(\rho\varepsilon) + \frac{\partial}{\partial x_i}(\rho\varepsilon u_i) \\ &= \frac{\partial}{\partial x_j} \left[\left(\mu + \frac{\mu_t}{\sigma_\varepsilon} \right) \frac{\partial \varepsilon}{\partial x_j} \right] + C_{1\varepsilon} \frac{\varepsilon}{\kappa} (G_\kappa + C_{3\varepsilon} G_b) - C_{2\varepsilon} \rho \frac{\varepsilon^2}{\kappa} + S_\varepsilon \end{aligned} \quad (\text{C.7})$$

where G_κ is the generation of turbulence kinetic energy due to velocity gradients, which can be defined as

$$G_\kappa = -\overline{\rho u_i' v_j'} \frac{\partial u_j}{\partial x_i} \quad (\text{C.8})$$

G_b is turbulence kinetic energy due to buoyancy, Y_m is the components of dissipate rate due to compressible flow, S_κ and S_ϵ are user defined source terms [Fluent, 2003]. In this study, the effect of buoyancy (due to temperature gradient) and compressible flow ($M \gg 1$) was negligible, so G_b and Y_m were not considered. The default values were set for the constants ($C_{1\epsilon}$, $C_{2\epsilon}$ and C_μ) and for the turbulent Prandtl numbers (σ_κ , σ_ϵ) in Equations (C.6) and (C.7) based on experimental results [Fluent, 2003]. The implemented values are: $C_{1\epsilon} = 1.44$, $C_{2\epsilon} = 1.92$, $C_\mu = 0.09$, $\sigma_\kappa = 1.0$ and $\sigma_\epsilon = 1.3$ respectively. Nieuwstadt [1992] and Wilcox [1993] derived the above-mentioned equations (Equations C.6 and C.7) in details. In the derivation of the κ - ϵ model, it was assumed that the flow is fully turbulent, and the effects of molecular viscosity are negligible. The standard κ - ϵ model is therefore valid only for fully turbulent flows.

APPENDIX D

COPYRIGHT RELEASES

Copyright releases for:

- **Figure 3.3, with permission of Fluent Inc.**
- **Figure 4.4, with permission of Lambda Square Inc.**

From: Sharon Everts <se@fluent.com>
Subject: Re: Use of Fluent Figure
Date: Tue, 22 Feb 2005 11:37:36 -0500
To: Ahemad M <ahemad@uwindsor.ca>

FLUENT INC.

Yes you can use this figure. Please put a Courtesy of Fluent Inc. with the title.

Thank you for asking.

Ahemad M wrote:

*Dear Everts,
This figure is under chapter 10, title: "Modeling
turbulence" in Fluent Inc., January 28, 2003. Subtitle is
"Near wall treatments for wall-bounded flows" what is 10.8.*

*Please see the attachment of the Figure.
Thesis title is: "Evaluation of Equal Area and Log-Tchebycheff method
for circular duct flow."*

I am doing simulation in Fluent and experiment. Best regards

ramiz

*On Tue, 22 Feb 2005 07:50:21 -0500
Sharon Everts <se@fluent.com> wrote:*

Your email regarding use of Figure 10.8.1 Subdivision of
the Near-Wall Region.

I need to know where this figure is located and can you
tell me the title of your thesis.

Thank you

Sharon Everts
Marketing Administrator
Fluent Inc.
10 Cavendish Court
Lebanon, NH 03766
se@fluent.com
Phone: 603 643 2600 x645
Fax: 603 643 3967

From: "Rob Lang" <robatlsi@rcn.com>
Subject: Re: Permission for using figures
Date: Mon, 21 Feb 2005 14:07:17 -0500
To: "Ahemad M" <ahemad@uwindsor.ca>

Sure, by all means. Good Luck!

Rob Lang
Lambda Square Inc.
robl@lambdasquare.com
Phone (631) 587-1000 Ext #7
FAX (631) 587-1011
----- Original Message -----
From: "Ahemad M" <ahemad@uwindsor.ca>
To: "Rob Lang" <robatlsi@rcn.com>
Sent: Monday, February 21, 2005 1:14 PM
Subject: Permission for using figures

> Dear sir,
>
> For my thesis, I want to use couple of Figures from the
> document that you send to me for the respective venturi
> flow meter(Model 2300). One is ventur model 2300 and
> another is head loss curve.
>
> Would you please allow me to use the mentioned figures in
> my thesis.
>
> Best regards
>
>
> Ramiz
>
> University of Windsor
> ON, Canada
> N9B 3S8
>
>
> --
> No virus found in this incoming message.
> Checked by AVG Anti-Virus.
> Version: 7.0.300 / Virus Database: 266.2.0 - Release Date: 2/21/05
>
>

--
No virus found in this outgoing message.
Checked by AVG Anti-Virus.
Version: 7.0.300 / Virus Database: 266.2.0 - Release Date: 2/21/05

VITA AUCTOR

NAME	Md Ramiz Ahemad
PLACE OF BIRTH	Narayangonj, Dhaka, Bangladesh.
YEAR OF BIRTH	1968
EDUCATION	<p>1983: Completed 10-year schooling at Mograpara High School, Narayangonj, Bangladesh and passed the first compulsory public exam SSC (Secondary School Certificate) in 1st division.</p> <p>1985: Completed 2-year college at Notre-Dame College, Dhaka, Bangladesh and passed the second compulsory public exam HSC (Higher Secondary Certificate) in 1st division.</p> <p>1992: Obtained Bachelor of Science in Mechanical Engineering with first class from Bangladesh University of Engineering and Technology (BUET), Dhaka, Bangladesh.</p> <p>2002: Obtained Bachelor Degree in Computer Science (G) on April, from University of Windsor, Windsor, Canada.</p>
EXPERIENCE	1992 – 2001: Served as a Service Engineer in Utility Department of a Yarn Production Industry.
PRESENT	2005: A candidate for the degree of Master of Applied Science (M.A.Sc.) in Mechanical Engineering at the University of Windsor, Windsor, Ontario, Canada.